INTERIM REPORT

SAIC Analysis of Survey Data Acquired at Camp Sibert

ESTCP Project MM-0210

JULY 2008

Dean Keiswetter
SACI

Environmental Security Technology Certification Program

REPORT DOCUMENTATION PAGE

Form Approved
OMB No. 0704-0188

PLEASE DO NOT RETURN YOUR FORM TO THE ABOVE ORGANIZATION.

1. REPORT DATE *(DD-MM-YYYY)*	2. REPORT TYPE	3. DATES COVERED *(From - To)*
15-07-2008	Interim Report	

4. TITLE AND SUBTITLE
SAIC Analysis of Survey Data Acquired at Camp Sibert
Project MM-0210: Feature based UXO Detection and Discrimination

5a. CONTRACT NUMBER
Contract #: DACA72-02-C-0033

5b. GRANT NUMBER

5c. PROGRAM ELEMENT NUMBER

6. AUTHOR(S)
Dr. Dean Keiswetter

5d. PROJECT NUMBER

5e. TASK NUMBER

5f. WORK UNIT NUMBER

7. PERFORMING ORGANIZATION NAME(S) AND ADDRESS(ES)
Science Applications International Corporation
120 Quade Drive
Cary, NC 27513

8. PERFORMING ORGANIZATION REPORT NUMBER

9. SPONSORING/MONITORING AGENCY NAME(S) AND ADDRESS(ES)
ESTCP Program Office
901 North Stuart Street, Ste 303
Arlington, VA 22203-1821

10. SPONSOR/MONITOR'S ACRONYM(S)

11. SPONSOR/MONITOR'S REPORT NUMBER(S)

12. DISTRIBUTION/AVAILABILITY STATEMENT
Unclassified/Unlimited

13. SUPPLEMENTARY NOTES

14. ABSTRACT

An ESTCP sponsored demonstration was conducted at the Former Camp Sibert, Alabama, where the objective was to discriminate potentially hazardous 4.2-inch mortars from non-hazardous shrapnel, range, and cultural debris. Six different discrimination techniques were tested and used data from the MTADS magnetometer array, the MTADS time-domain electromagnetic induction array, the MTADS frequency-domain electromagnetic induction array, and a Geonics Limited EM61 commercial cart. Discrimination was achieved using either rule-based or statistical classification of feature vectors extracted from dipole or polarization tensor model fits to detected anomalies. Each of the EM methods used a size-base feature vector and some used shape indicators derived by comparing unconstrained and constrained fit results. Each of the methods successfully discriminated the 4.2-inch mortars from the clutter. The EMI and magnetometer classifications based on size estimates successfully identified all UXO without encountering a single false negative while eliminating over 45% of the native clutter.

15. SUBJECT TERMS

16. SECURITY CLASSIFICATION OF:			17. LIMITATION OF ABSTRACT	18. NUMBER OF PAGES	19a. NAME OF RESPONSIBLE PERSON
a. REPORT	b. ABSTRACT	c. THIS PAGE			Dean Keiswetter
U	U	U	Unlimited	112	19b. TELEPHONE NUMBER *(Include area code)* 919-653-0215

Reset

Contents

Figures

Tables

List of Acronyms

ASR	Archives Search Report
DGM	Digital Geophysical Mapping
DSB	Defense Science Board
EE/CA	Engineering Evaluation/Cost Analysis
EMI	Electromagnetic Induction
ESTCP	Environmental Security Technology Certification Program
FAR	False Alarm Rate
FUDS	Formerly Used Defense Site
GPO	Geophysical Prove Out
GPS	Global Positioning System
HE	High Explosive
IDA	Institute for Defense Analyses
IMU	Inertial measurement unit
M&F	Mag and Flag
MR	Munitions Response
MTADS	Multisensor Towed Array Detection System
NRL	Naval Research Laboratory
Pdet	Probability of Detection
Pdisc	Probability of Correct Discrimination
Pfa	Probability of False Alarm
QA	Quality Assurance
QC	Quality Control
ROC	Receiver Operating Characteristic
RTK	Real time kinematics
SNR	Signal to Noise Ratio
TOI	Target(s) of Interest
UXO	Unexploded Ordnance

GLOSSARY

Discrimination	Determination that a detected object is (1) high confidence clutter (and need not be dug), or (2) munitions or unknown (and must be removed)
Detection	Determination of the presence of a target, typically by observation of a signal level crossing a threshold set to limit the probability that a crossing would be caused by noise or interference.
False Alarm (Detection) False Alarm (Discrimination)	Declaration of a target that is actually caused by noise, interference, or geology Declaration of an item that could safely be left in the ground as munitions or unknown
Target of Interest	For this study, defined to be intact munitions, both HE and practice; sizeable pieces of munitions (on the order of half a round); and items that look like munitions (e.g., pipes of similar size)
Characterization	Determination of parameters that are intrinsic to a target and can be used to make a discrimination decision.
Classification	Formally, determination that an object belongs to a particular class of ordnance (i.e., is a 155 as opposed to an 81). Classification, by its formal definition, will not be explored in this study. Instead, in this document we will use the term classification as a synonym for discrimination.

DISCRIMINATION PILOT PROGRAM

1. Introduction

1.1. Background

The FY06 Defense Appropriation contained funding for the "Development of Advanced, Sophisticated, Discrimination Technologies for UXO Cleanup" in the Environmental Security Technology Certification Program. In 2003, the Defense Science Board observed: "The … problem is that instruments that can detect the buried UXOs also detect numerous scrap metal objects and other artifacts, which leads to an enormous amount of expensive digging. Typically 100 holes may be dug before a real UXO is unearthed! The Task Force assessment is that much of this wasteful digging can be eliminated by the use of more advanced technology instruments that exploit modern digital processing and advanced multi-mode sensors to achieve an improved level of discrimination of scrap from UXOs." [1]

Significant progress has been made in discrimination technology. To date, these technologies have primarily been tested at constructed test sites, with only limited application at live sites. The routine implementation of discrimination technologies will require demonstrations at real UXO sites under real world conditions. Any attempt to declare detected anomalies to be harmless and requiring no further investigation will require demonstration to regulators and project managers of not only individual technologies, but an entire decision making process. This discrimination study will be the first phase in what is expected to be a continuing effort that will span several years.

1.2 Objective of the Demonstration

1.2.1 ESTCP Discrimination Pilot Program at Camp Sibert

As outlined in the Environmental Security Technology Certification Program Unexploded Ordnance Discrimination Study Demonstration Plan, the objectives of the study were to (i) test and validate UXO detection and discrimination capabilities of currently available and emerging technologies on real sites under operational conditions, and (ii) investigate how UXO discrimination technologies can be implemented in cleanup operations.

The broad study was designed to test and evaluate the capabilities of various UXO discrimination processes which each consist of a selected sensor hardware, a survey mode, and a software based processing step. These advanced methods will validate the pilot technologies for the (i) detection of UXO; (ii) identification of features that can help distinguish scrap and other clutter from UXO; (iii) reduction of false alarms (items that could be safely left in the ground that are incorrectly classified as UXO) while maintaining P_ds acceptable to all; and (iv) quantify the cost and time impact of advanced methods on the overall cleanup process as compared to existing practices.

Additionally, the study aimed to understand the applicability and limitations of the selected technologies in the context of project objectives, site characteristics, and suspected munitions contamination. Finally, high-quality, well documented data were collected to support the next generation of signal processing research.

1.2.2 Specific Objectives of the Demonstration

The demonstration objective of our analysis was to determine the discrimination capability and reliability of magnetometer array data, EM61 Mk2 array data, GEM array, and EM61 Mk2 cart data using analysis procedures initially developed for MM-0210, *Feature based UXO Detection and Discrimination*, and MM-0033, *Enhanced UXO discrimination using Frequency-domain Electromagnetic Induction*.

After analyzing each of the four data sets independently, we created six prioritized dig lists. Prioritized dig lists were provided for the EM61 Mk2 Cart data, the GEM array data, and the magnetometer array data. Two prioritized dig lists were generated from the EM61 Mk2 array data. The first EM61 array dig list was generated using a solver that compares fit results from a constrained, two-β target of interest (TOI) library with an unconstrained three-β model. The second EM61 array dig list was generated using a solver embedded in UX-Analyze that inverts using a non-constrained, three-β model only. Finally, we combined inversion results from the EM61 Mk2 array data and magnetometer data to produce a sixth, and final prioritized dig list.

1.3 Regulatory Drivers and Stakeholder Issues

ESTCP assembled an Advisory Group to address the regulatory, programmatic and stakeholder acceptance issues associated with the implementation of discrimination in the Munitions Response (MR) process.

The advisory group focused on exploring UXO discrimination processes that will be useful to regulators and site managers in making decisions by determining:

- What information is required to support a discrimination decision?
- What does the pilot project need to demonstrate for the community to consider not digging every anomaly as a viable alternative?
- For implementation beyond the pilot project, how should proposals to implement discrimination be evaluated?

2. Technology Description

2.1 Technology Development and Application

We analyzed MTADS magnetometry data, MTADS EM61 MK2 array data, MTADS GEM array, and standard cart EM61 MK2 survey data. The standard cart EM61 MK2 survey data were collected by Parsons Incorporated using a standard cart platform. Typical industry standard equipment and procedures for navigation, geolocation using global positioning systems (GPS), data recording, and reduction were used. Details of the MTADS acquisition systems and plans are presented in Technology Demonstration Plan entitled *MTADS Demonstration at Camp Sibert, Magnetometer / EM61 MK2 / GEM-3 Arrays*, ESCTP MM-0533. Because the MTADS data acquisition systems are custom and not industry standard, a brief summary description follows.

2.1.1 Data Acquisition Systems

The MTADS hardware consists of a low-magnetic-signature vehicle that is used to tow the different sensor arrays over large areas (10 - 25 acres / day) to detect buried UXO (Figure 2-1). Spatial registration is provided using high performance Real Time Kinematic (RTK) Global Positioning System (GPS) receivers with position accuracies of ~5 cm.

2.1.1.1. Magnetometer Array

The MTADS magnetometer array is a linear array of eight Cs-vapor magnetometer sensors (Geometrics, Inc., G-822ROV/A). The sensors were sampled at 50 Hz and with a nominal survey speed of 6 mph; resulting, in a sampling density of ~6 cm along track. The horizontal spacing between sensors is 25 cm. A single GPS antenna placed directly above the center of the sensor array measured the sensor positions in real-time (5 Hz). All navigation and sensor data were time-stamped with Universal Coordinated Time derived from the satellite clocks and recorded by the data acquisition computer in the tow vehicle.

Figure 2-1 MTADS tow vehicle and magnetometer array

2.1.1.2. EM61 MK2 Array

The EM61 MK2 MTADS array is an overlapping array of three pulsed-induction sensors specially modified by Geonics, Ltd. based on their EM61 MK2 sensor with 1x1m sensor coils. The sensors employed by MTADS were modified to make them more compatible with vehicular speeds and to increase their sensitivity to small objects. The timing of the gates has been altered (Table 2-1). Differential mode was used for this demonstration. Nominal survey speed is 3 mph and the sensor readings were recorded at 10 Hz. This results in a down-track sampling of ~15 cm and a cross-track interval of 50 cm. In order to obtain sufficient "looks" at the anomalies, or to insure illumination of all three principal axes of the anomaly with the primary field, data is collected in two orthogonal surveys. The EM61 array being pulled by the MTADS tow vehicle is shown in Figure 2-2.

Individual sensors in the EM61 MK2 array were spatially registered using a three-receiver RTK GPS system. An Inertial Measurement Unit (IMU) is also included on the sensor array to provide complementary platform orientation information. The IMU is a Crossbow VG300 running at 30 Hz. A close-up view of the sensor platform is shown in Figure 2-3 which shows the three GPS antennae and the IMU (black box under the aft port GPS antenna).

Table 2-1 NRL EM61 MK2 Gate timing parameters

Channel	4 Gate Mode		Differential Mode	
	Coil	Delay (μs)	Coil	Delay (μs)
1	Bottom Coil	307	Bottom Coil	307
2	Bottom Coil	508	Top Coil	307
3	Bottom Coil	738	Bottom Coil	738
4	Bottom Coil	1000	Bottom Coil	1000

Figure 2-2 MTADS EM61 array pulled by the MTADS tow vehicle

Figure 2-3 Close-up of MTADS EM61 array with GPS and IMU

2.1.1.3. GEM-3 Array

The MTADS GEM-3 array consists of three, 96-cm diameter Geophex, Limited GEM-3 sensors in a triangular configuration with two sensors across the front of the array and one centered in the rear. The roughly 2-m square array was mounted on a rigid support which is attached to the MTADS EM cart using non-metallic fasteners (Figure 2-4). The GPS / IMU telemetry equipment used for GEMTADS is the same as that used for the EM61 MK2 array and described in the previous section.

The standard GEM-3 sensor drive electronics were modified to produce a substantially higher transmit moment for this array. Each individual sensor transmits a composite waveform of one to ten frequencies in the frequency range of 30 to 20,010 Hz with a base period of 1/30 sec. A composite transmitter waveform of nine frequencies log-spaced from 90 to 20010 Hz was used. Two additional base periods were required for signal deconvolution and to output the response from each sensor. The array operates continuously with one sensor actively transmitting while the other two sensors are processing data at any given time. Allowing for a short coil settling time between the transmissions from each sensor, an effective array sampling rate of just over 9 Hz was achieved. Sequential transmitter operation also alleviates the need for the orthogonal survey mode employed for the EM61 MK2 array. Coupled with our standard survey speed of 3 mph, the result is a down-track sampling spacing of ~15 cm. The cross-track spacing is 50 cm. An interleaved survey pattern was used to decrease the cross-track spacing to 25 cm.

Figure 2-4 MTADS GEM array mounted on the EM sensor cart. In addition to the three GEM sensors (false colors to identify coils), note the three GPS antennae and the inertial measurement unit (under GPS receiver near back left tire) for platform motion measurement.

The GEM sensors are controlled by a custom electronics package designed and built by Geophex, Ltd. Overall control of data collection was accomplished with a custom version of the standard GEM sensor control software, WinGem2KArr, which logged the data from the GEM sensors, the three GPS NMEA sentences, the time of the GPS 1-PPS pulse, the GPS UTC time stamp, and the IMU data in separate files with a common base survey name. The data are periodically transferred to the data analyst for immediate QC checks and for further processing.

2.1.2 Data Analysis Methodology

Our discrimination approach uses a model-based estimation procedure to determine whether or not an unknown target is likely to be a UXO item. It entails estimating the size and shape of the target from the spatial pattern of the induced field above the target [2, 3]. The EMI signal is a linear function of the flux through the receiving coil. In our model, the flux is assumed to originate from an induced dipole moment at the target location given by:

$$\mathbf{m} = \mathrm{UBU}^{\mathrm{T}}\mathbf{H}_0$$

where $\mathbf{H}_0$ is the peak primary field at the target, U is the transformation matrix between the coordinate directions and the principal axes of the target, and B is an empirically determined, effective magnetic polarizability matrix [4, 5]. For an arbitrary compact object, this matrix can be diagonalized about three primary body axes and written as:

$$B = \begin{bmatrix} \beta_X & 0 & 0 \\ 0 & \beta_Y & 0 \\ 0 & 0 & \beta_Z \end{bmatrix}.$$

The relative magnitudes of the β's are determined by the size, shape and composition of the object as well as the transmit waveform and time gate or frequency. The transformation matrix contains the angular information about the orientation of these body axes.

For cylindrical objects like most UXO, B is a diagonal matrix with only two unique coefficients, corresponding to the longitudinal (β_T) and transverse (β_L) directions:

$$B = \begin{bmatrix} \beta_L & 0 & 0 \\ 0 & \beta_T & 0 \\ 0 & 0 & \beta_T \end{bmatrix}.$$

Discrimination is based on target β's estimated from spatially mapped data. Specific ordnance items have specific β values, while clutter items generally have different β values.

We received the final geo-positioned, demedianed magnetometer, EM61 MK2, and GEM-3 data from NRL and the standard cart EM61 data acquired by Parsons. For each anomaly in each data set, we use UX-Analyze to extract a subset of data, taking care to limit competing signatures, noise spikes, and the like, and invert using a dipole model. Fitted model parameters include anomaly size (based on the moment for magnetic data and the trace of the polarizability tensor for EMI), shape (EMI only), XY position, depth, orientation, and fit error statistics. In addition to presenting the results of the inversion in spreadsheet form, UX-Analyze generated an anomaly summary sheet that shows the measured data, inversion results, and model data for QC purposes.

2.2 Previous Testing of the Analysis Technology

By virtue of our involvement in a variety of projects, we (formerly AETC Incorporated) have developed forward models and inversion procedures for total field and vector magnetometers and gradiometers, and all of the major EMI sensors (EM31, EM61, EM61-HH, EM63, EM73, nanoTEM, GEM-3). Furthermore, as part of several SERDP and ESTCP projects we have catalogued target parameters for an extensive inventory of UXO and clutter items. During the Congressionally-mandated Jefferson Proving Ground Advanced Technology Demonstrations, AETC processing consistently provided outstanding buried UXO detection performance, and only the AETC-supported demonstrations correctly classified more than half of both the munitions and clutter targets. Our analysis framework and procedures, described in a number of publications [6-13], have been, or are being, successfully demonstrated in a variety of ESTCP Projects, listed below.

199811	Portable UXO Detection System Adjunct to *MTADS*
199812	Electromagnetic Induction and Magnetic Sensor Fusion for Enhanced UXO Target Classification
199526	Multi-Sensor Towed Array Detection System
199812	Electromagnetic Induction & Magnetic Sensor Fusion for Enhanced UXO Target Classification

199918	Matched Filter Processor for Detection and Discrimination of Unexploded Ordnance
200031	Airborne UXO Surveys Using Magnetometer Arrays
200033	Enhanced UXO Discrimination Using Frequency-Domain Electromagnetic Induction
200034	Demonstration of Advanced UXO Detection and Discrimination Technologies
200108	Handheld Sensor for Unexploded Ordnance Discrimination

2.3 Factors Affecting Cost and Performance

Implementation of the demonstrated analysis method requires additional time compared to that required for detection only. This is due to the fact that the analyst must not only identify and locate the anomaly, but also must extract signal responses while excluding background or overlapping signatures to the extent possible, re-level the extracted data if needed, and invert data around the anomaly for model parameters.

2.4 Advantages and Limitations of the Technology

This Demonstration technology uses spatially referenced geophysical data to estimate model parameters. This has an inherent advantage over analysis methods based on non-quantitative schemes. Non-quantitative analysis methods frequently base the declaration on anomaly amplitude, half width, spatial footprint, or overall 'look'. These characterization methods are, however, sensitive to the targets' orientation and depth of burial. The methodology demonstrated here separates the measured signatures into that which is inherent to the target, and that which is related to the geometry of the problem (such as distance to sensor and orientation).

Known limitations to the data analysis approach adopted here result from (i) non-unique inversion results, and (ii) overlapping, or non distinct, signatures in feature space. The former limitation, one in which multiple sets of model parameters explain the vast majority of the observed data, is well known. The second, while perhaps not as widely appreciated, is equally problematic. Inverting EMI data using our dipole models, results in three eigenvalues of the magnetic polarizability tensor, each corresponds to a principal axis of object. Discrimination is possible only to the degree that the derived eigenvalues are different for different objects and stable for similar classes of objects. In other words, even with ideal data, the estimated burial depth, apparent size, and shape features may not separate UXO and clutter signatures into distinct, non-overlapping classes. This is because the anomaly features derived from EMI and magnetic data are not unique to UXO. Clutter items that have similar shapes and burial attributes to munitions can have geophysical signatures that are indistinguishable from UXO signatures and, as such, will have similar eigenvalues and therefore likely be classified as munitions. Examples include items such as pipes, post sections and axial symmetrical fragments.

3. Demonstration Design

3.1 Performance Objectives

Performance objectives for the demonstration are given in Table 3-1 to provide a basis for evaluating the performance and costs of the demonstrated technology.

3.2 Selecting the Test Site

ESTCP selected Camp Sibert as the demonstration site. Camp Sibert is located within the boundaries of Site 18 of the former Camp Sibert. The land is under private ownership and is used as a hunting camp.

The criterion that drove the site selection process were (i) a single use artillery or mortar range, (ii) simple clutter environment, (iii) benign geology, (iv) live munitions used, and (v) benign topography and vegetation. Additional considerations were size (20-25 acres was desired), anomaly density (mostly isolated anomalies; 100-200 per acre), total anomaly count (2,500 to 5,000 anomalies were desired), and access/authorization to seed site with inerted targets.

3.3 Test Site History/Characteristics

Information on the former Camp Sibert is available in the archival literature such as an Archives Search Report (ASR) developed in 1993. The former Camp Sibert is located in the Canoe Creek Valley between Chandler Mountain and Red Mountain to the northwest, and Dunaway Mountain and Canoe Creek Mountain to the southeast. Camp Sibert is comprised of mainly sparsely inhabited farmland and woodland and encompasses approximately 37,035 acres. The City of Gadsden is growing towards the former camp boundaries from the north. The Gadsden Municipal Airport occupies the former Army airfield in the northern portion of the site. The site is located approximately 50 miles northwest of the Birmingham Regional Airport or 86 miles southeast of the Huntsville International Airport. The site is near exit 181 off of Interstate 59 in Gadsden and located approximately 8 miles southwest of the City of Gadsden, near the Gadsden Municipal Airport.

Table 3-1 Performance Objectives for the Discrimination Study

Type of Performance Objective	Primary Performance Criterion	Expected Performance (Metric)	Actual Performance Objective Met?
Quantitative	Correct characterization parameters	Radial Distance: <25 cm mean and < 20 cm standard deviation Depth: <25 cm mean and <20 cm standard deviation Size: (COV <0.2)	Yes – excluding the EM61 Cart data set
	Maximize correct determinations of non-munitions	Discrimination eliminates >20% of the detections corresponding to items not of interest at the no-dig threshold	Yes
	Maximize correct determinations of munitions	Discrimination retains target of interest above the no-dig threshold (>0.95Pd)	Yes
	Demonstrate effect of data quality (line spacing, location error, signal/noise levels, etc) on the ability to correctly extract parameters and classify munitions versus non-munitions	Data quality effects can be isolated and understood	Yes - With the exception of human error (poor definition of the spatial footprint of two targets), the false negative failures were caused by positioning problems

*coefficient of variation (COV) – standard deviation / mean

3.4 Present Operations

The site is no longer in active use by the military. The demonstration area is owned by a single landowner who uses the area for a hunting camp. The field portion of the demonstration study was conducted after January 31st, the end of the hunting season.

3.5 Pre-Demonstration Testing and Analysis

No pre-demonstration testing and analyses were performed against which the performance of this demonstration was compared.

3.6 Testing and Evaluation Plan

3.6.1 Scope of the Demonstration

The site is approximately 25-acres and contains the following number of anomalies, by sensor type:

a) GEM Array 1039
b) EM61 MK2 Array 870
c) EM61 MK2 Cart 663
d) Magnetic 969
e) Magnetic or EM61 MK2 Array 1165

3.7 Management and Staffing

Dr. Dean Keiswetter was the project's lead for SAIC. Dr. Tom Bell was the Quality Assurance Officer. Dr. Bruce Barrow, Mr. Jonathan Miller, and Mr. Tom Furuya served as Data Analysts.

4. Performance Assessment

4.1 Performance Criteria and Confirmation Methods

TOIs were defined to include (i) intact munitions, both HE and practice, (ii) sizeable pieces of the munitions of interest, on the order of half a round, and (iii) items that look like munitions (i.e., pipes of similar size).

Items that may be safely left in the ground included HE fragments, single fins, cultural debris, geology, and small arms rounds (if present).

Our focus was on identifying items that may be safely left in the ground. *The main failure, therefore, was misclassifying a TOI as an item that can be left in the ground*. Individual targets were scored as indicated in Table 4-1. These discrimination labels were then used to calculate the rolled up performance measures presented in §4.2.

Table 4-1 Discrimination Labels (Categories)

Category	**Comment**	**Recommended Action: (Dig or Leave in Place)**
1	High confidence clutter	Leave in Place
2	Low confidence clutter	Dig
3	Can't Analyze	Dig
4	Low confidence TOI	Dig
5	High confidence TOI	Dig

The 'Can't Analyze' Category 3 label was used to identify targets that (i) could not be inverted (i.e., the inversion did not converge) or (ii) could be inverted but the fit error statistics indicated that the results could not be trusted. We determined the threshold for the later case for each dataset individually using labeled data.

4.2 Performance Criteria and Confirmation Methods

Our prioritized dig lists were scored against the emplaced targets by analysts from the Institute for Defense Analyses (IDA). Performance results for each of our six prioritized dig lists are shown in Table 4-2 through Table 4-7.

In the tables below, the ROC calculation excludes Category 3 items because they were, by default, recommended to be removed and therefore do not contribute any gains due to the discrimination process. Also, the metric used for the estimation of size is the coefficient of variation (COV), which is simply the standard deviation divided by the mean value of the size parameter. It essentially reports variability in the estimated size parameter. We used this normalized metric to compare performance because different EMI solvers return polarization estimates that vary in absolute magnitude and it allows comparisons of magnetic as well.

Table 4-2 Performance and the Confirmation Methods: **EM61 MK2 Cart**

Performance Metric	**Expected Performance (pre demo)**	**Performance Confirmation Method**	**Actual Performance (post demo)**
Pdisc (emplaced) at Pthreshold	> 0.95	Comparison to seeded items	0.992
Pfa at Pthreshold	< 0.80	Validation Digging	0.409
Pfa at 100% Pdisc	< 0.80	Validation Digging	0.495
ROC	0.4	Gains over chance diagonal Validation Digging	0.465
Accuracy of Parameter Estimation	Radial Distance (XY): <25cm Depth: <15 cm SIZE (UXO ONLY): COV < 0.2	Comparison to truth data Comparison to truth data Comparison to truth data	32cm (15cm σ) 15cm (17cm σ) 0.18

σ = standard deviation

Table 4-3 Performance and the Confirmation Methods: **EM61 MK2 Array** (Approach 1 - Library Based)

Performance Metric	**Expected Performance (pre demo)**	**Performance Confirmation Method**	**Actual Performance (post demo)**
Pdisc (emplaced) at Pthreshold	>0.95	Comparison to seeded items	0.983
Pfa at Pthreshold	< 0.80	Validation Digging	0.278
Pfa at 100% Pdisc	< 0.80	Validation Digging	0.385
ROC	0.4	Gains over chance diagonal Validation Digging	0.489
Accuracy of Parameter Estimation	Radial Distance (XY): <25cm Depth: <15 cm SIZE (UXO ONLY): COV < 0.2	Comparison to truth data	22cm (16cm σ) 13cm (14cm σ) 0.17

Table 4-4 Performance and the Confirmation Methods: **EM61 MK2 Array** (Approach 2 - Size Based)

Performance Metric	**Expected Performance (pre demo)**	**Performance Confirmation Method**	**Actual Performance (post demo)**
Pdisc (emplaced) at Pthreshold	>0.95	Comparison to seeded items	1.0
Pfa at Pthreshold	< 0.80	Validation Digging	0.421
Pfa at 100% Pdisc	< 0.80	Validation Digging	0.270
ROC	0.4	Gains over chance diagonal Validation Digging	0.470
Accuracy of Parameter Estimation	Radial Distance (XY): <25cm Depth: <15 cm SIZE (UXO ONLY): COV < 0.2	Comparison to truth data	18cm (12cm σ) 20cm (17cm σ) 0.28

Table 4-5 Performance and the Confirmation Methods: **GEM-3 Array**

Performance Metric	**Expected Performance (pre demo)**	**Performance Confirmation Method**	**Actual Performance (post demo)**
Pdisc (emplaced) at Pthreshold	>0.95	Comparison to seeded items	0.992
Pfa at Pthreshold	< 0.80	Validation Digging	0.389
Pfa at 100% Pdisc	< 0.80	Validation Digging	0.461
ROC	0.4	Gains over chance diagonal Validation Digging	0.482
Accuracy of Parameter Estimation	Radial Distance (XY): <25cm Depth: <15 cm SIZE (UXO ONLY): COV < 0.2	Comparison to truth data	17cm (10cm σ) 15cm (16cm σ) 0.10

Table 4-6 Performance and the Confirmation Methods: **Magnetic Array**

Performance Metric	Expected Performance (pre demo)	Performance Confirmation Method	Actual Performance (post demo)
Pdisc (emplaced) at Pthreshold	>0.95	Comparison to seeded items	1.0
Pfa at Pthreshold	< 0.80	Validation Digging	0.490
Pfa at 100% Pdisc	< 0.80	Validation Digging	0.487
ROC	0.4	Gains over chance diagonal Validation Digging	0.416
Accuracy of Parameter Estimation	Radial Distance (XY): <25cm Depth: <15 cm SIZE (UXO ONLY): COV < 0.2	Comparison to truth data	14cm (10cm σ) 10cm (12cm σ) 0.24

Table 4-7 Performance and the Confirmation Methods: **Combined EM61 + Magnetic Array**

Performance Metric	Expected Performance (pre demo)	Performance Confirmation Method	Actual Performance (post demo)
Pdisc (emplaced) at Pthreshold	>0.95	Comparison to seeded items	1.0
Pfa at Pthreshold	< 0.80	Validation Digging	0.305
Pfa at 100% Pdisc	< 0.80	Validation Digging	0.286
ROC	0.4	Gains over chance diagonal Validation Digging	0.487
Accuracy of Parameter Estimation	Radial Distance (XY): <25cm Depth: <15 cm SIZE (UXO ONLY): COV < 0.2	Comparison to truth data	NA

4.3 Data Analysis, Interpretation, and Analysis

We received sensor data and anomaly information (ID & location) from the ESTCP Program Office. Table 4-8 presents data sets and analysis details with regard to training, model features, and classifier for the various data types. Each data set is discussed individually in the sections that follow.

Table 4-8 Detailed demonstration approach.

		Training Data	Model Features	Features used for Discrimination	Classifiers	Gate or Frequency
Individual Sensor Data	**EM61 MK2 CART (IDL)**	GPO & ESTCP directed digging	x,y,z, 3 response coefficients for each time gate, inclination, declination, roll, fit error	Coherence Ratio (library/unconstrained normalized by fitted Sdev(SMAX))	GLRT	Both Coils All three time gates (relative weighting)
	EM61 MK2 ARRAY (IDL)	GPO & ESTCP directed digging	x,y,z, 3 response coefficients for each time gate, inclination, declination, roll, fit error, unconstrained, constrained	Coherence Ratio (library/unconstrained)	Proximity measure relative to fitted line six sigma below mean of TOI	Lower coil All three Time Gates
	GEM ARRAY (IDL)	GPO & ESTCP directed digging	x,y,z, 3 response coefficients for each frequency, inclination, declination, roll, fit error, unconstrained, constrained	Coherence Ratio (Library/unconstrained normalize by fitted Sdev (SMAX))	Proximity measure relative to fitted line three sigma below mean of TOI	Quadrature Only (570Hz, 1230Hz, 2610Hz)
	EM61 MK2 ARRAY (UX-ANALYZE)	GPO & ESTCP directed digging	x,y,z, 3 response coefficients for each time gate, inclination, declination, roll, fit error	Apparent Size	GLRT	Bottom Coil Gate 1
	MAG ARRAY (UX-ANALYZE)	GPO & ESTCP directed digging	x,y,z, dipole moment, inclination, declination, fit error	Magnetic moment (size)	Rank	NA
Combined	**EM61 MK2 ARRAY PLUS MAG ARRAY**	GPO & ESTCP directed digging	see MTADS EM61 MkII and MTADS Mag (above)	EM Coherence Ratio Magnetic Size	GLRT	Lower Coil All Three Time Gates Mag

4.3.1 EM61 MK2 CART

4.3.1.1. Data Presentation, Description, and Pre-processing

Data from the EM61 MK2 (Figure 4-1) is shown in Figure 4-2 thru Figure 4-4. The circles identify anomalies selected for analysis by the ESTCP Program Office.

Summary of preprocessing steps for EM61 MK2 Cart data:

1) De-median filter applied to remove long wavelength drift
2) inverted data from both coils and all three time gates (0.217, 0.366, and 0.660ms)
3) used tools developed in Oasis montaj to select polygons (spatial footprint) about anomalies
4) no IMU data (assigned roll and pitch to be zero)

One day's worth of EM61 cart data exhibited unpredictable and unexpected discontinuities with regard to the time stamps and spatial positions (Figure 4-5). In the figure, this behavior is evident by the spatial jumps in travel path and gaps in time, which were often on the order of 11seconds between neighboring data samples.

After preprocessing, we ran inversions in batch and generated custom diagnostic plots for quality assurances purposes. A parameter was added to the solver to automatically account for variable time lag.

Figure 4-1 Photograph of the EM61 MK2 Cart

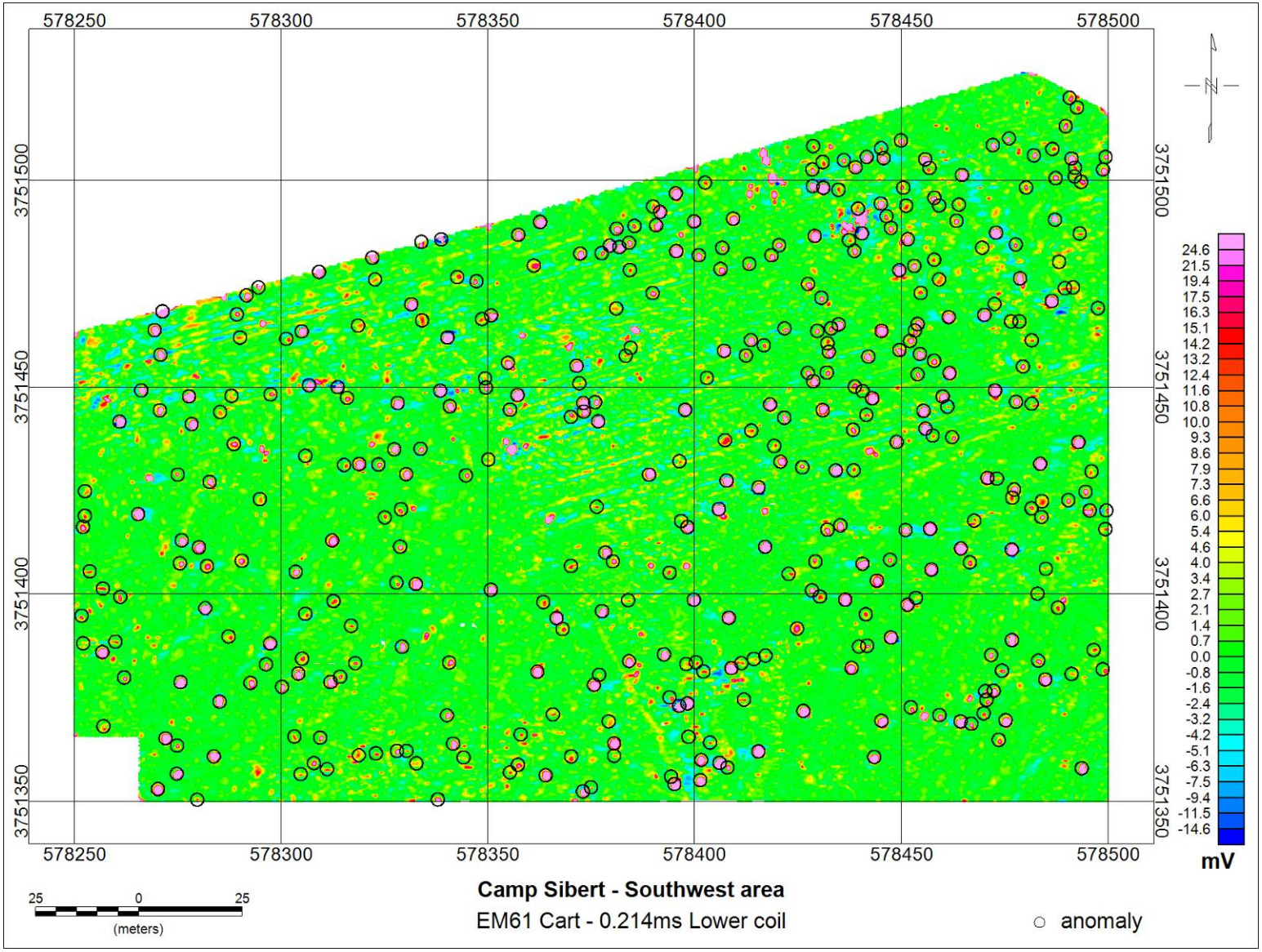

Figure 4-2 EM61 MK2 Cart data; Southwest area.

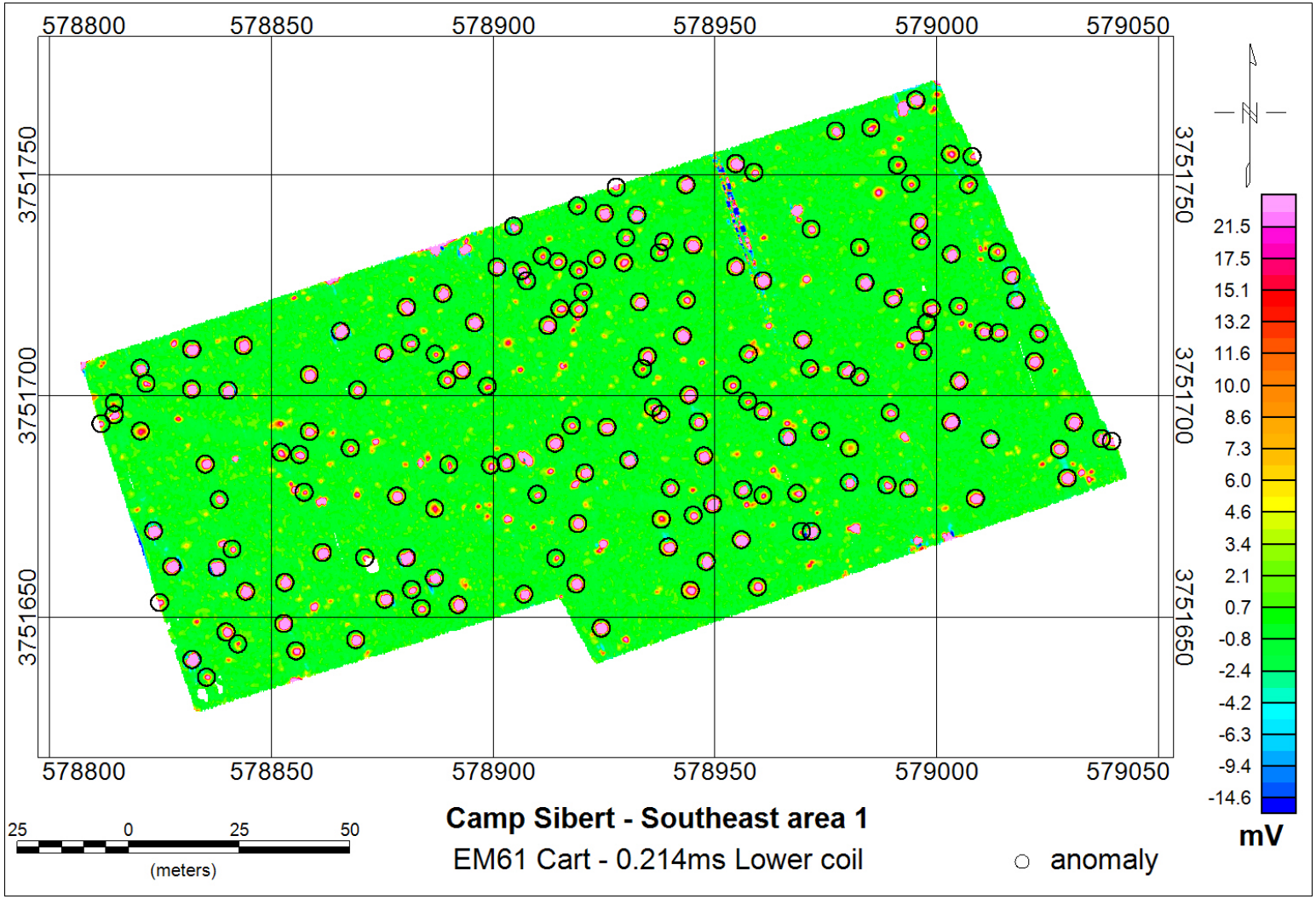

Figure 4-3 EM61 MK2 Cart data; Southeast area 1.

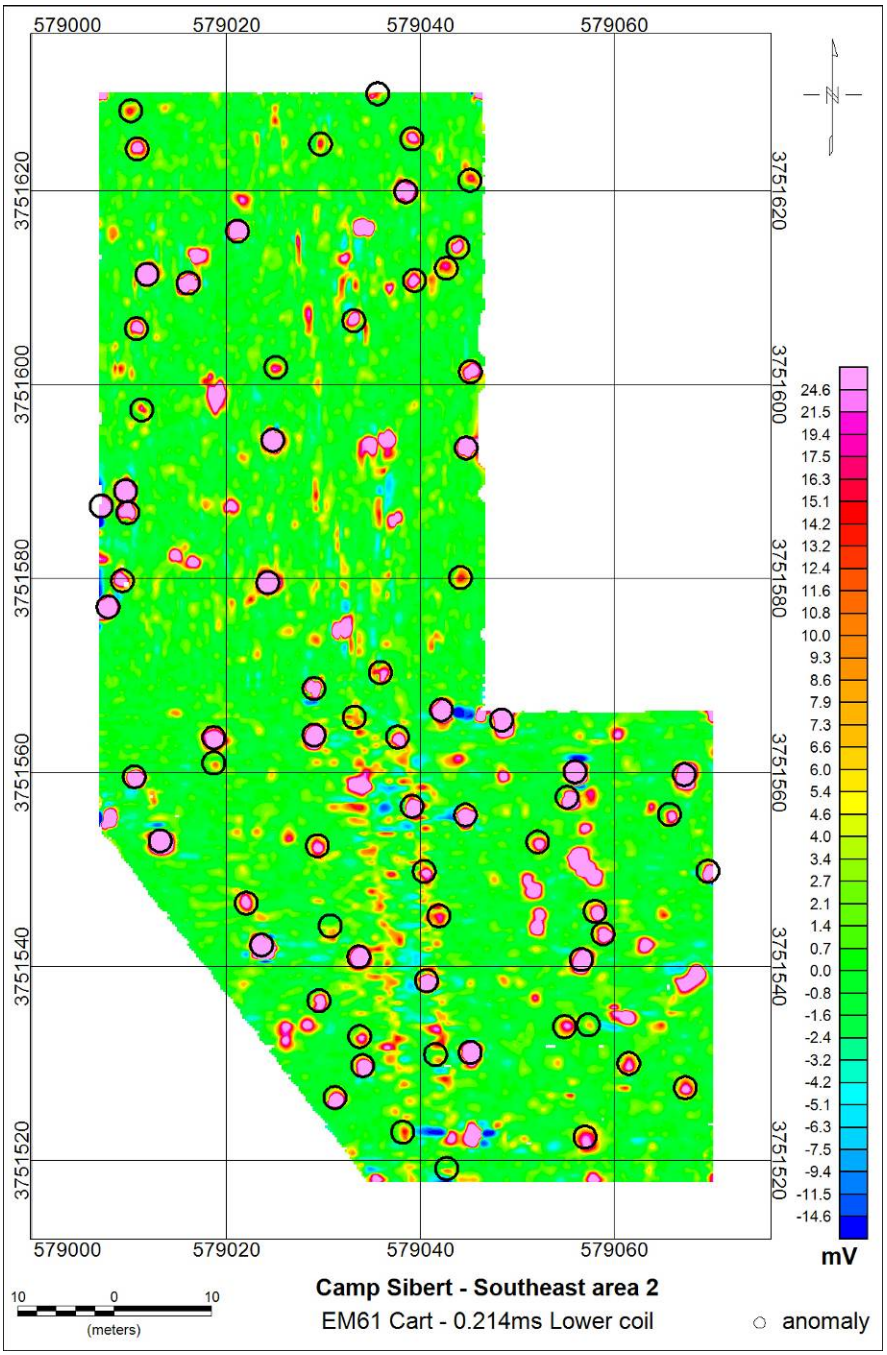

Figure 4-4 EM61 MK2 Cart data; Southwest area 2.

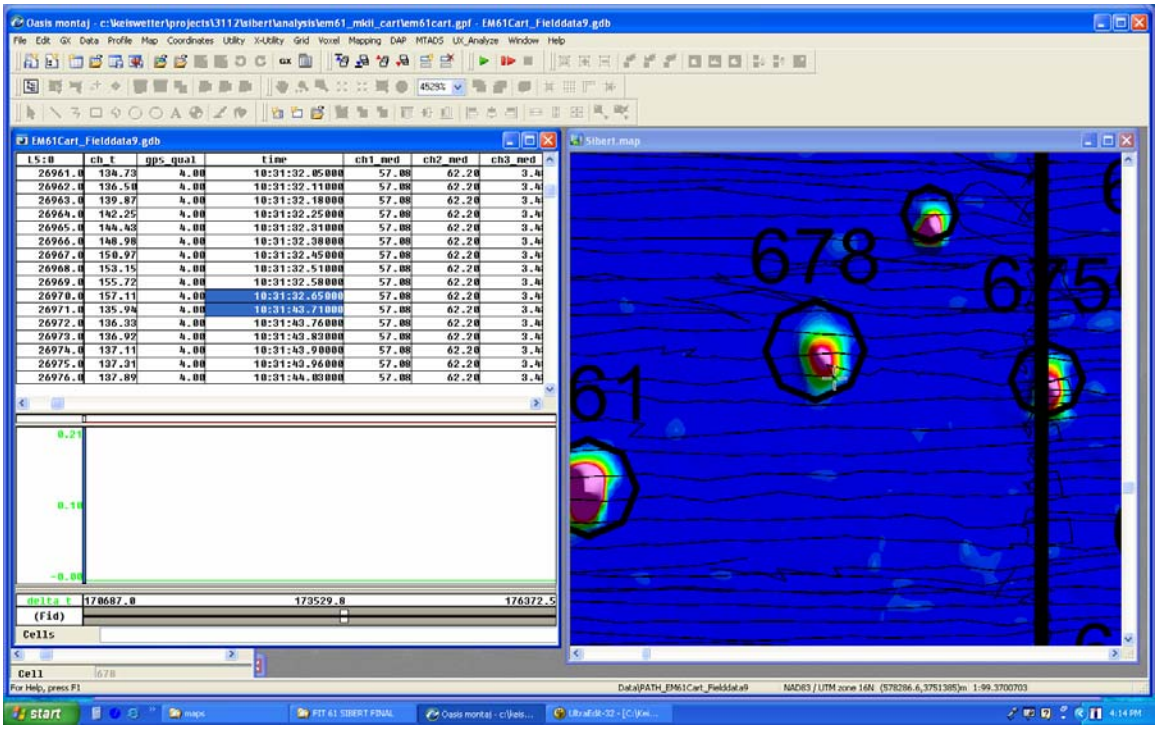

Figure 4-5 One day's worth of EM61 cart data exhibited unpredictable and unexpected discontinuities with regard to the time stamps and spatial positions. This behavior is evident from the spatial jumps in travel path (right) and gaps in time, often on the order of 11seconds between neighboring data samples, as shown on the left (highlighted fields).

4.3.1.2. Inversion Approach

Inversion of EM61 cart data is based on a standard dipole model. The algorithm finds seven (7) fitted parameters: x,y,z,lag,ph,th,ps, where x,y,z, are the target coordinates (m), lag is an offset between sensor and GPS clocks (Figure 4-6), and ph,th,ps are the Euler angles (deg). The associated best-fit betas, three polarizations for each frequency, are also recovered and values for the chi-squared error and coherence are calculated. Follow-on fits are made with betas constrained to match given values from a library. Associated chi-squared and coherence values are found for each library item, and ratios of (constrained coherence) / (un-constrained coherence) are calculated.

To avoid being trapped in local minima, the unconstrained inversion operates in two stages. The first stage steps through fixed z values from ground surface down to 1.75m depth in 5cm intervals. At each z step, the best-fit target x,y position is found using the a method in which elements of the response tensor are found through linear regression. This permits fast run times and experience has shown it is robust against local minima. No restrictions are placed on the tensor values. Each time channel was treated independently, so each will have a different apparent target orientation.

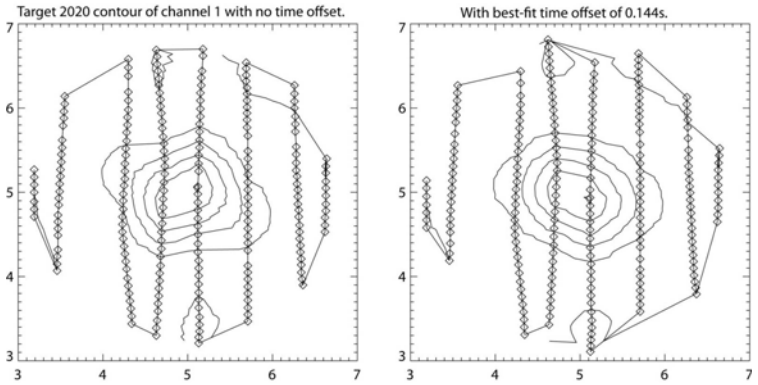

Figure 4-6 The EM61 MK2 solver was modified to solve for a constant time lag between sensor and GPS clock.

The 10 best solutions, judged by chi square value, are used as starting points in the 2nd stage. Before submitting these data, Euler angles must be found. It was discovered that using arbitrary angles can lead to failure of the solver due to local minima, so a special optimization step was performed separately on each of the 10 solutions. In this step, "best-fit" Euler angles are found through minimization of off-diagonal elements in the response tensor, across all channels. Starting points for this optimization are the apparent Euler angles from each channel's tensor.

The second stage searches all 6 fitted parameter values: x,y,z,ph,th,ps, through downhill simplex minimization. After cycling through all 10 of the startpoints from the 1st stage, the best-ever solution is saved.

Summary of solver steps used for EM61 cart data:

- Standard Dipole Magnetic Polarization Model
- First stage:
  - Step through Z (distance below array) in 5cm increments.
  - Time lag added as fit parameter to compensate for dynamic response.
  - Search target X,Y,Lag nonlinearly, find tensor elements linearly.
  - Find Euler angles to minimize off-diagonals across all gates.
  - Save 10 best fits judged by chi-square (different Z values & lags).
    These are start points for following stages.
- Second stage:
  - Search x,y,z,phi,theta,psi all non-linearly, find axial betas linearly.
  - Axial-symmetry not assumed.
- Third stage:
  - Library of fixed beta values from 21 UXO in GPO with high SNR.
  - Search x,y,z,phi,theta non-linearly (axial symmetry imposed).
  - Fresh fit with each library item using 10 restarts.
  - Ratio of best library fit coherence / unconstrained fit coherence used in discrimination. This ratio is always < 1.

4.3.1.3. Decision Metric: threshold selection and mitigating factors

Classification of the EM61 cart data was based on results shown in Figure 4-7. Here, we plot the coherence ratio (constrained/unconstrained) versus fit mismatch, or fit error. The fit mismatch is defined as the square root of (1-correlation coefficient^2). The solid black line limits to the mean value of the fit ratio for high SNR 4.2-inch mortars. The dashed line is shifted down by ten standard deviations.

We used a generalized likelihood ratio test (GLRT) to classify the inverted model features. The two features used as input to the classifier include the (i) coherence ratio distance from the solid line representing the 4.2-inch mortars, and (ii) a size estimate (the principal polarization, all three time gates). The decision metric is based the GLRT output, and set using labeled data as follows (Figure 4-8):

Category 1: <-6.2 (Probability UXO < 0.01)
Category 2: -6.2 to 1 (Probability UXO = 0.01 to 0.5)
Category 3: fit error greater than 25%
Category 4: 1 to 2 (Probability UXO = 0.5 to 0.74)
Category 5: >2 (Probability UXO > 0.74)

The threshold between categories 2 and 4 set based on first UXO encountered. The thresholds between 1 and 2 and between 4 and 5 were set to accommodate observed uncertainty.

Mitigating factors included the following: (1) if the inversion failed, the anomaly was declared Category 3, and (2) if fitted depth was greater than 0.75m, it could not be declared high confidence clutter (Category 1).

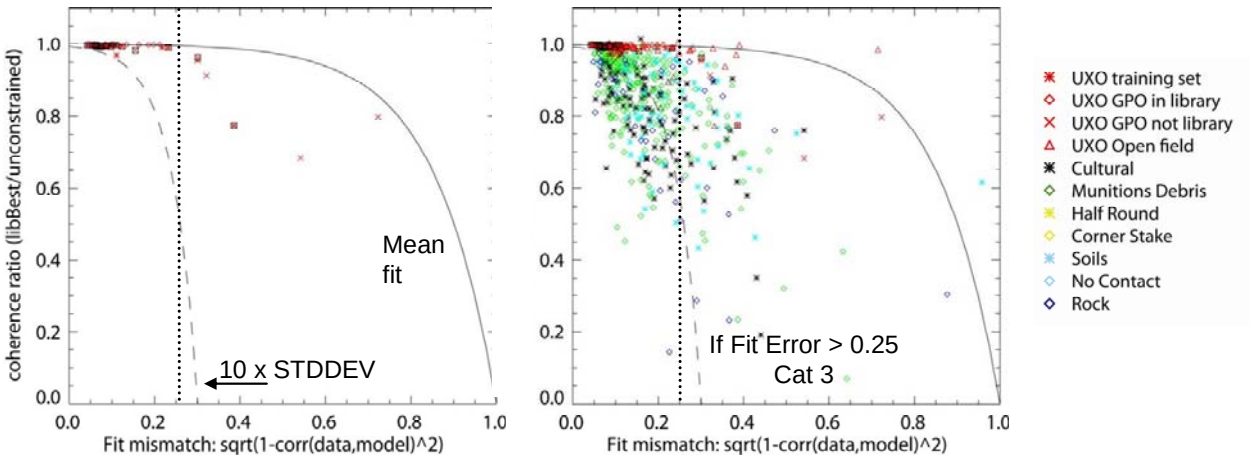

Figure 4-7 EM61 MK2 cart training data.

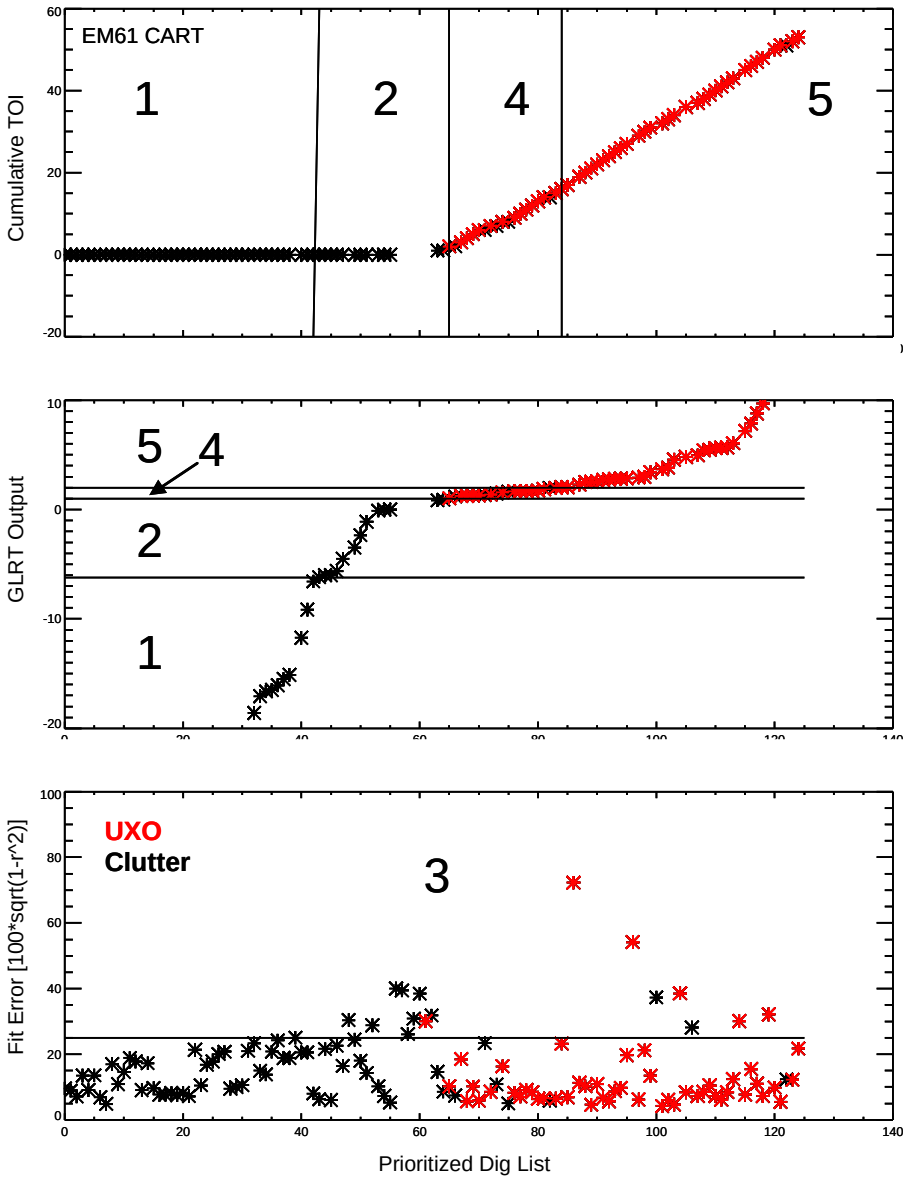

Figure 4-8 EM61 MK2 cart training data and selected thresholds. Bold numbers indicate classification category.

4.3.1.4. Performance Scores from IDA

Scoring performances for the EM61 MK2 cart analysis are reported in Table 4-9 and shown graphically in Figure 4-9. A ROC chart is shown in Figure 4-10, where we plot the number of false positives (FP) versus the probability of detection (Pd). From a declared-category perspective, the Category 3 targets are plotted first, followed by categories 5 (red), 4 (orange), 2 (yellow), and finally 1 (green). The colored dots on the ROC curves indicate the operating point for a Pd=0.95 (red), the demonstrator's threshold point (blue) and the lowest FP_{disc} for Pd=1.0

(green), and that the gray lines indicate a 95% confidence interval around each point on the ROC curvely.

Using the thresholds adopted for this analysis, there was one false negative. Anomaly #1171, which was in fact a seeded 4.2-inch mortar, was classified as high confidence clutter (Category 1).

Table 4-9 Performance Summary: EM61 MK2 Cart Constrained/Unconstrained Analysis

EM61 CART

	Cultural	Munition Debris	No Contact	Rock	Soil	UXO
1	61	150	3	19	19	1
2	6	31	0	3	7	3
3	18	32	1	19	23	18
4	0	19	0	0	2	9
5	0	14	0	0	1	87
TOTAL	**85**	**246**	**4**	**41**	**52**	**118**

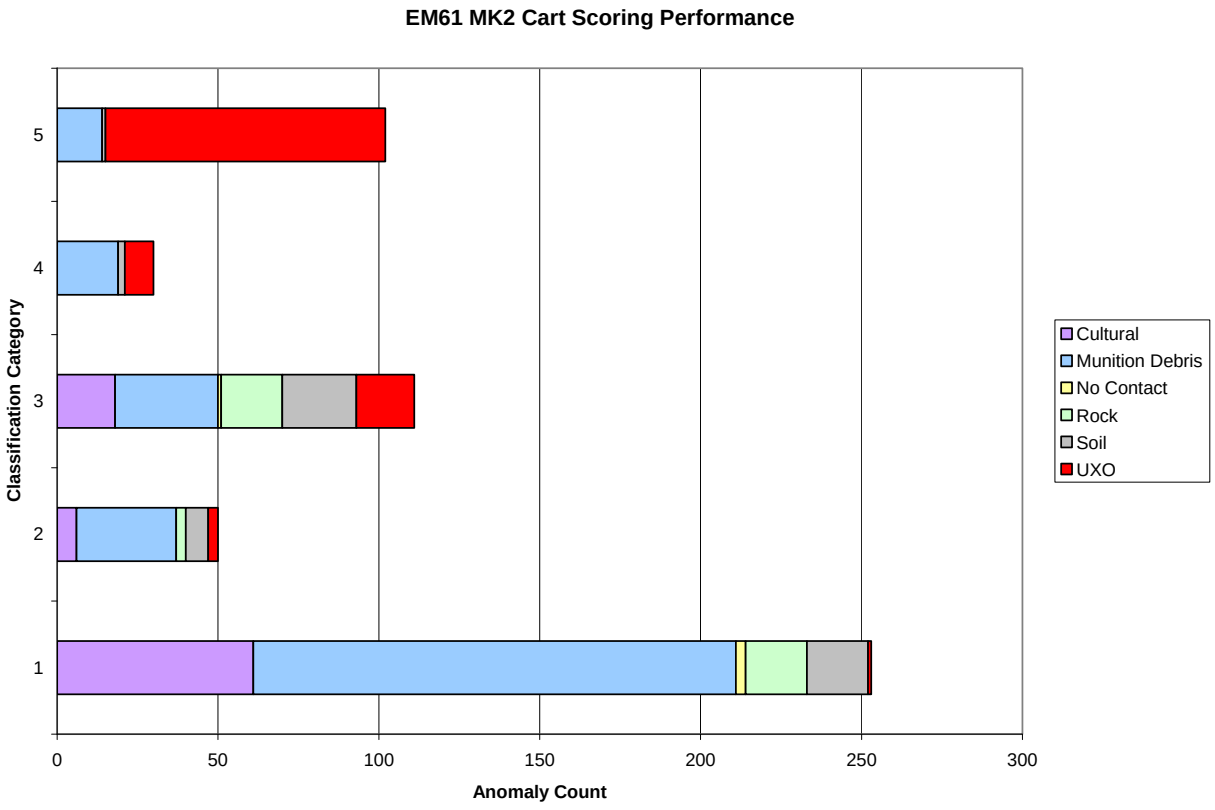

Figure 4-9 EM61 MK2 Cart performance as a function of classification category.

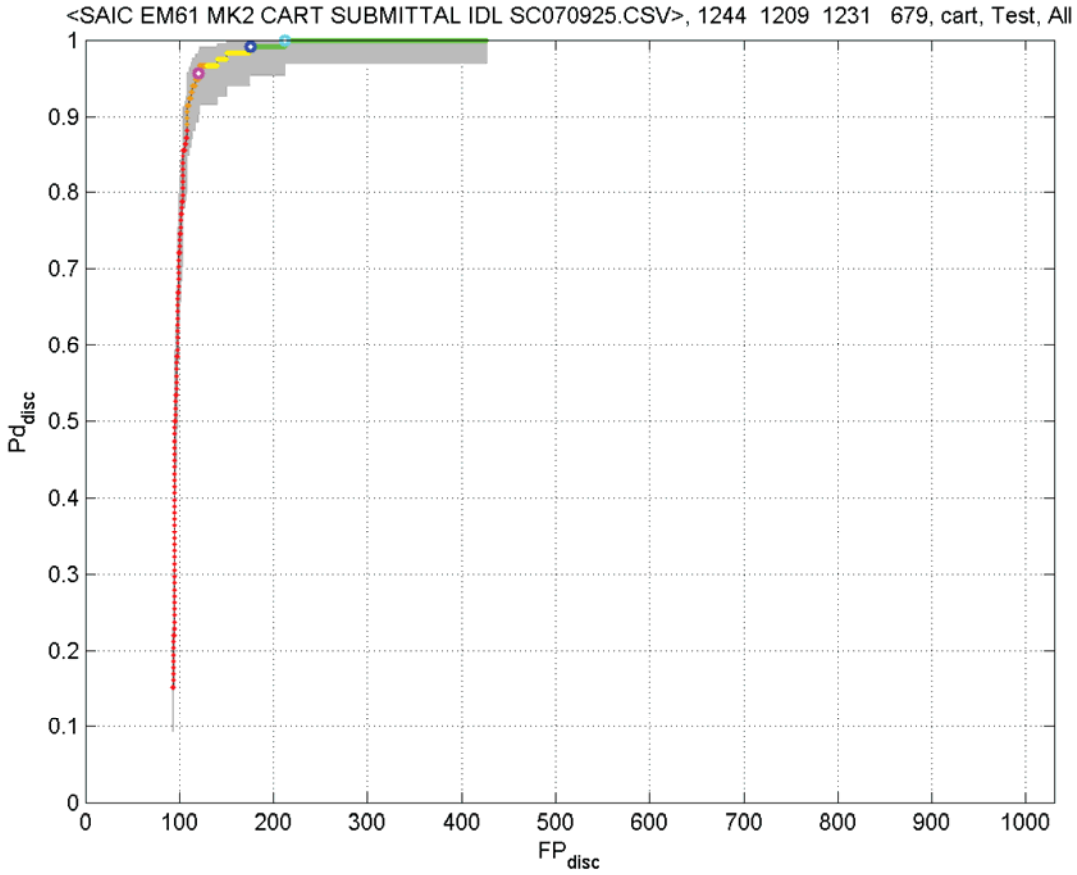

Figure 4-10 EM61 MK2 Cart ROC chart; analyzed comparing library-constrained and unconstrained inversions.

4.3.1.5. Characterization Plots

The mean error between the fitted and measured XY locations for seeded 4.2-inch mortars, based on EM61 MK2 cart inversion, is 0.32m (standard deviation of 0.15m; Figure 4-11).

The RMS depth error for seeded 4.2-inch mortars, based on EM61 MK2 cart inversion, is 0.15m (standard deviation of 0.17m; Figure 4-12).

Figure 4-13 plots the net polarizability, defined as the sum of the three principal polarizations ($\Sigma\log(\beta)$) for the first time gate (0.217 ms), for each of the 119 seeded 4.2in mortars. The seeded mortars were nearly identical in size and shape and we expect their net polarizabilities to be similar. For the EM61 MK2 cart data, the mean net polarizability was 1.886 with a standard deviation of 0.339. The COV for net polarizability is 0.179.

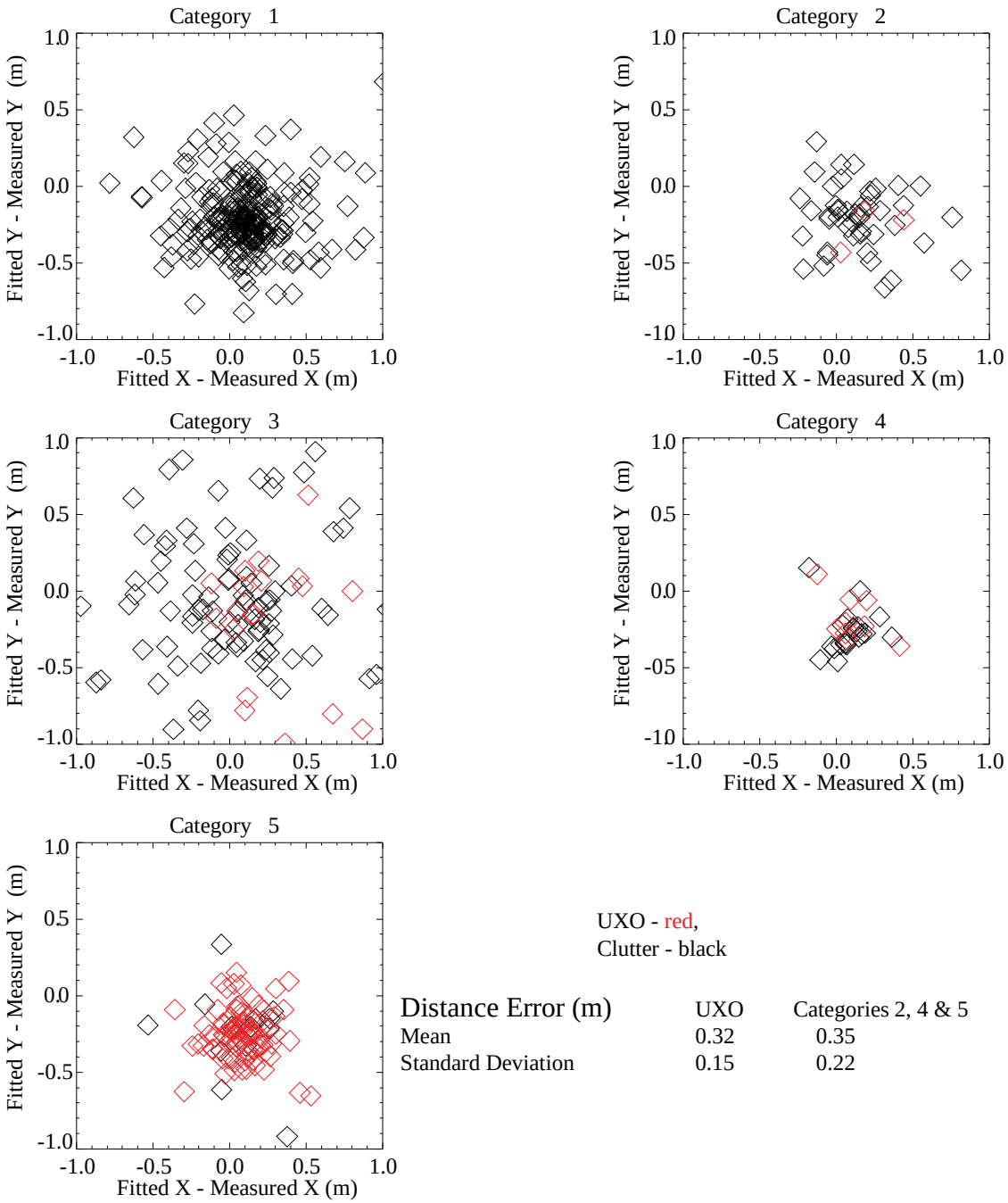

Distance Error (m)	UXO	Categories 2, 4 & 5
Mean	0.32	0.35
Standard Deviation	0.15	0.22

Figure 4-11 Differences between fitted and measured XY locations; EM61 MK2 cart

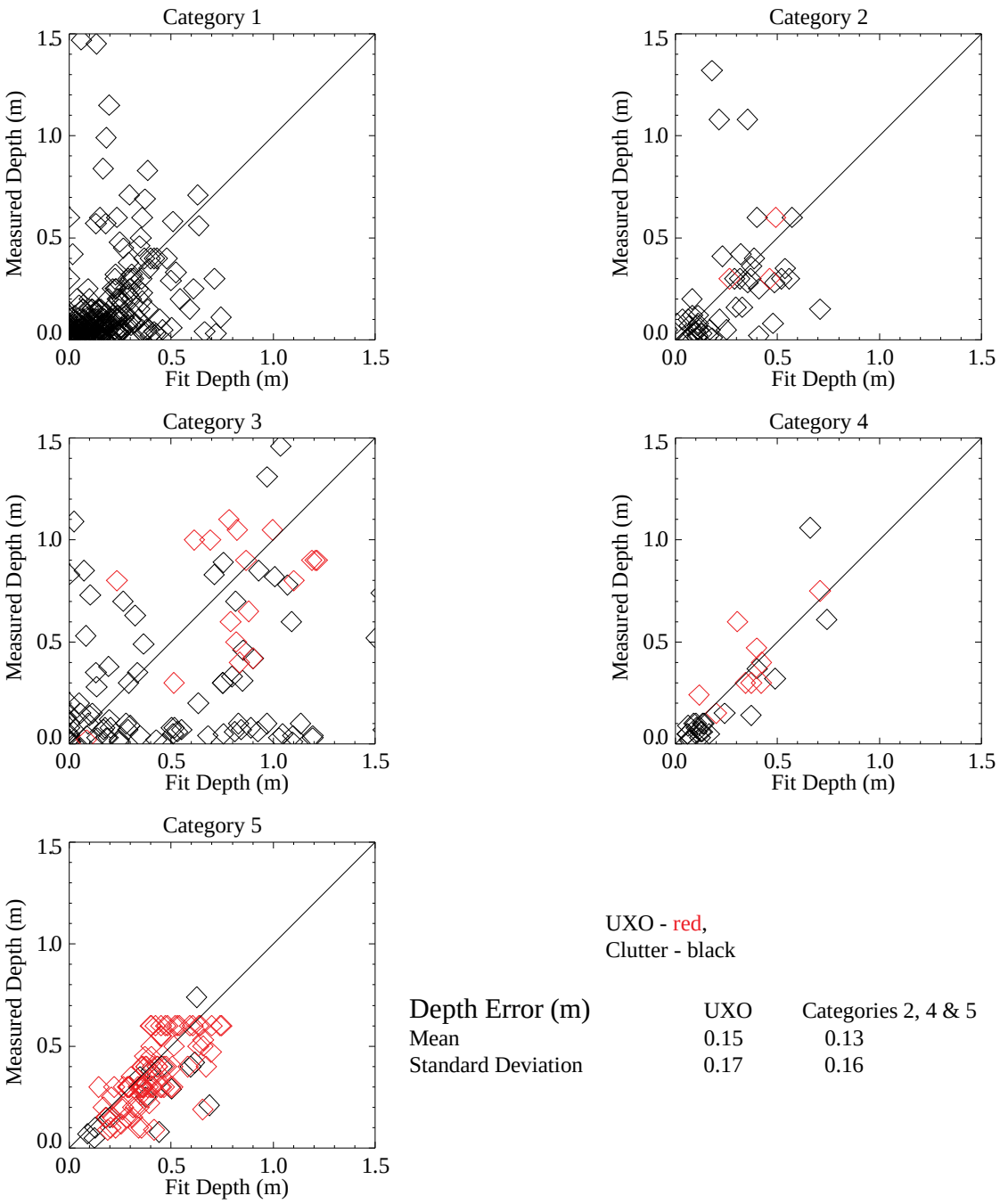

Depth Error (m)	UXO	Categories 2, 4 & 5
Mean	0.15	0.13
Standard Deviation	0.17	0.16

Figure 4-12 Fitted versus measured depth of burial; EM61 MK2 cart

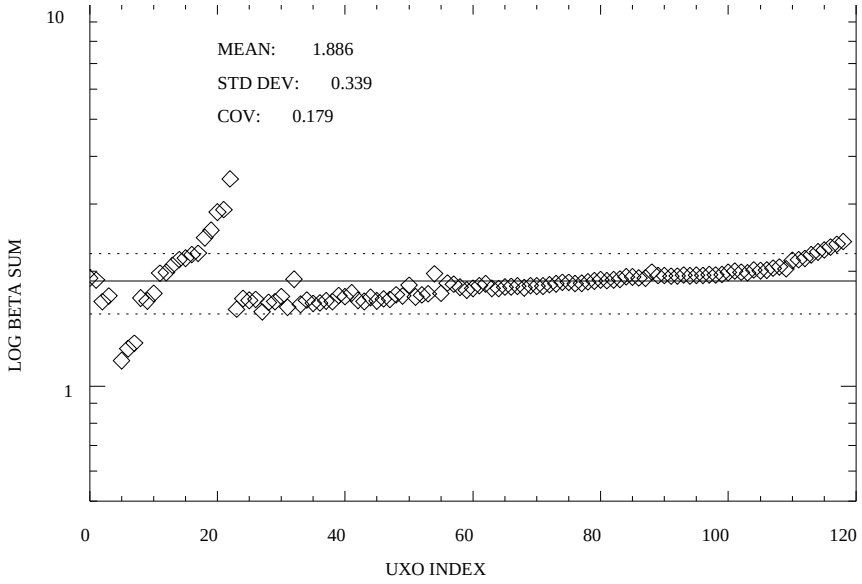

Figure 4-13 Raster of the Σβ, which is a measure of size, for 4.2in mortars, EM61 MK2 cart

4.3.1.6. Failure Analyses

Anomaly #1171 was a seeded 4.2-inch mortar but was classified high confidence clutter (Category 1) using the constrained/unconstrained approach detailed here. A reexamination of the anomaly data revealed that the polygon used to define the spatial footprint of the anomaly was inappropriate and did not include the entire anomaly. The decision metric for these analyses was the output of a GLRT classifier that used coherence ratios and principal polarization magnitude as inputs. These two inputs were chosen because they produced the best performance for the labeled data. Our post mortem analysis revealed, however, that if we had not added the principal polarization magnitude, anomaly #1171 would not have been assigned Category 1 (high confidence clutter; Figure 4-14).

Anomaly #506 was a seeded 4.2-inch mortar but was classified low confidence clutter (Category 2). Our follow-on analysis discovered poor spatial coverage (3 transects over anomaly, 0.4m and 0.7m between adjacent lanes).

Anomaly #8 was a seeded 4.2-inch mortar but was classified low confidence clutter (Category 2). It too had irregular spatial sampling and conflicting measured values. At the intersection of two transects, for example, the first transect recorded a 70.4mV response while the second recorded only 44mV.

There were 18 seeded mortars assigned to Category 3 (i.e., Can't Analyze). Of these, nine (9) had fit errors above the 25% threshold. The other nine (9) had acceptable fit errors but their fitted depths were greater than 0.75m. These later nine were misclassified. Our post mortem analysis uncovered that all targets with fitted depth greater than 0.75m were assigned Category 3. This was a mistake, because our intent was to simply not allow targets with fitted depths greater

than 0.75m to be Category 1 (high confidence clutter). We intended to assign Category 2 or 4 for deeply buried targets depending on their final discrimination metric value from the GLRT classifier.

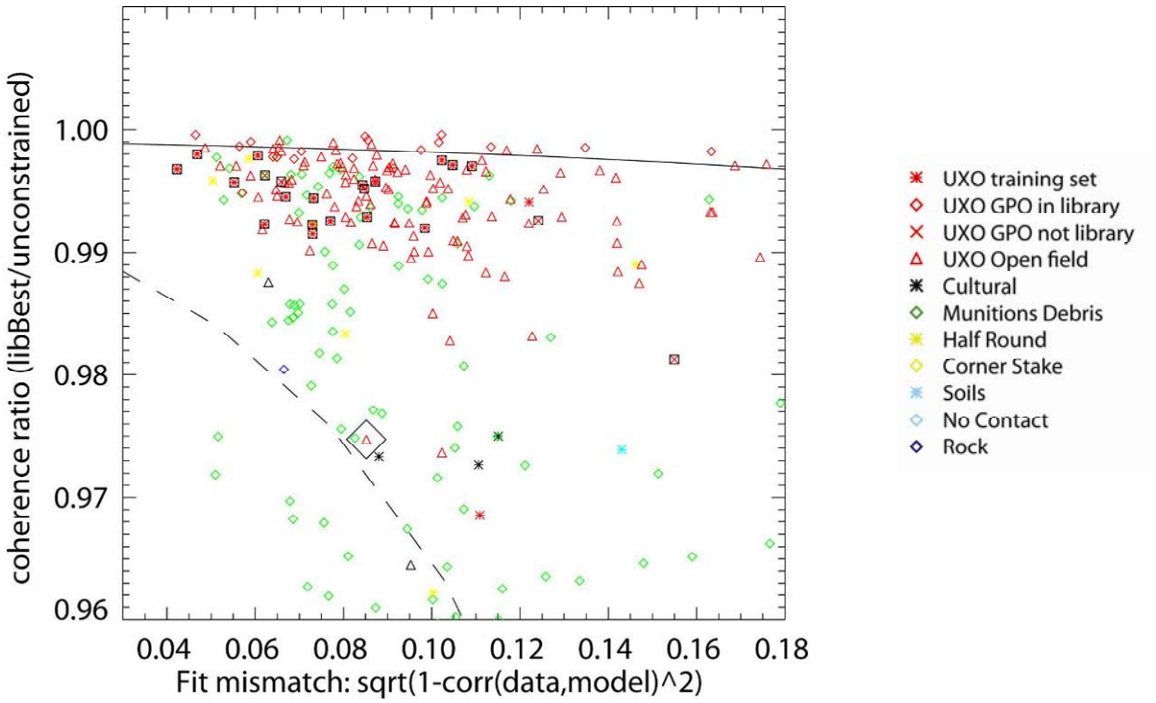

Figure 4-14 Target #1171, identified by the black diamond, was just above our coherence ratio threshold that was established as Category 1-2 boundary.

4.3.2 EM61 MK2 ARRAY

The EM61 MK2 Array data were analyzed independently using two different inversion approaches and implemented in different environments. The first approach utilized Interactive Data Language (IDL) routines to perform unconstrained and library-constrained inversions. The second approach utilizes UX-Analyze to perform unconstrained 3β model fits. Each approach is described below.

4.3.2.1. Inversions using a Constrained/Unconstrained Approach

4.3.2.1.1. Data Presentation, Description, and Pre-processing

Data from the EM61 MK2 array (Figure 4-15) is shown in Figure 4-16 thru Figure 4-18. The circles identify anomalies selected for analysis by the ESTCP Program Office.

The MTADS MK2 array platform consists of three modified Geonics's EM61 MK2 sensors. Data collected by the platform can be modeled with the standard dipole response model, but there are several issues that must be considered: anomalous negative spikes, time varying transmit currents, inter-calibration of the three sensors, and the sensor's dynamic response.

The negative spikes in the MTADS array data result from an unfixed problem in Geonic's electronics. The electronics covers a large dynamic range by switching the gain in the A-to-D conversion; the raw data is stored as counts from the A-to-D and the current gain factor. Normally, as signals become large, the gain factor switches automatically. The MTADS system has a delay in this switching. As signals get large (over most items of interest), the A-to-D counts, stored as integers, wrap from a very large number to a negative one. This occurs for one or two data values and then the gain switches and the data proceeds with normal values. Most of these spikes were fixed in pre-processing by correcting any large negative integer count values. Any remaining spikes were edited out of the final data set. This has left small gaps in the data over some of the anomalies of interest.

The three EM61 Mk2 sensors have time varying transmitter currents. As the power supply batteries slowly go down in voltage, the sensors transmit smaller currents. To maintain a constant sensor output, each sensor measures the transmit current and applies a gain based on the measurement to boost the outputted signal. Hooked into an array, these measured currents oscillate in time as shown in Figure 4-19. Independent measurements with a calibrated current probe have shown that these oscillations are not real. To correct for this, the data presented here has been normalized by a linear fit to the current.

Figure 4-15 MTADS EM61 MK2 array

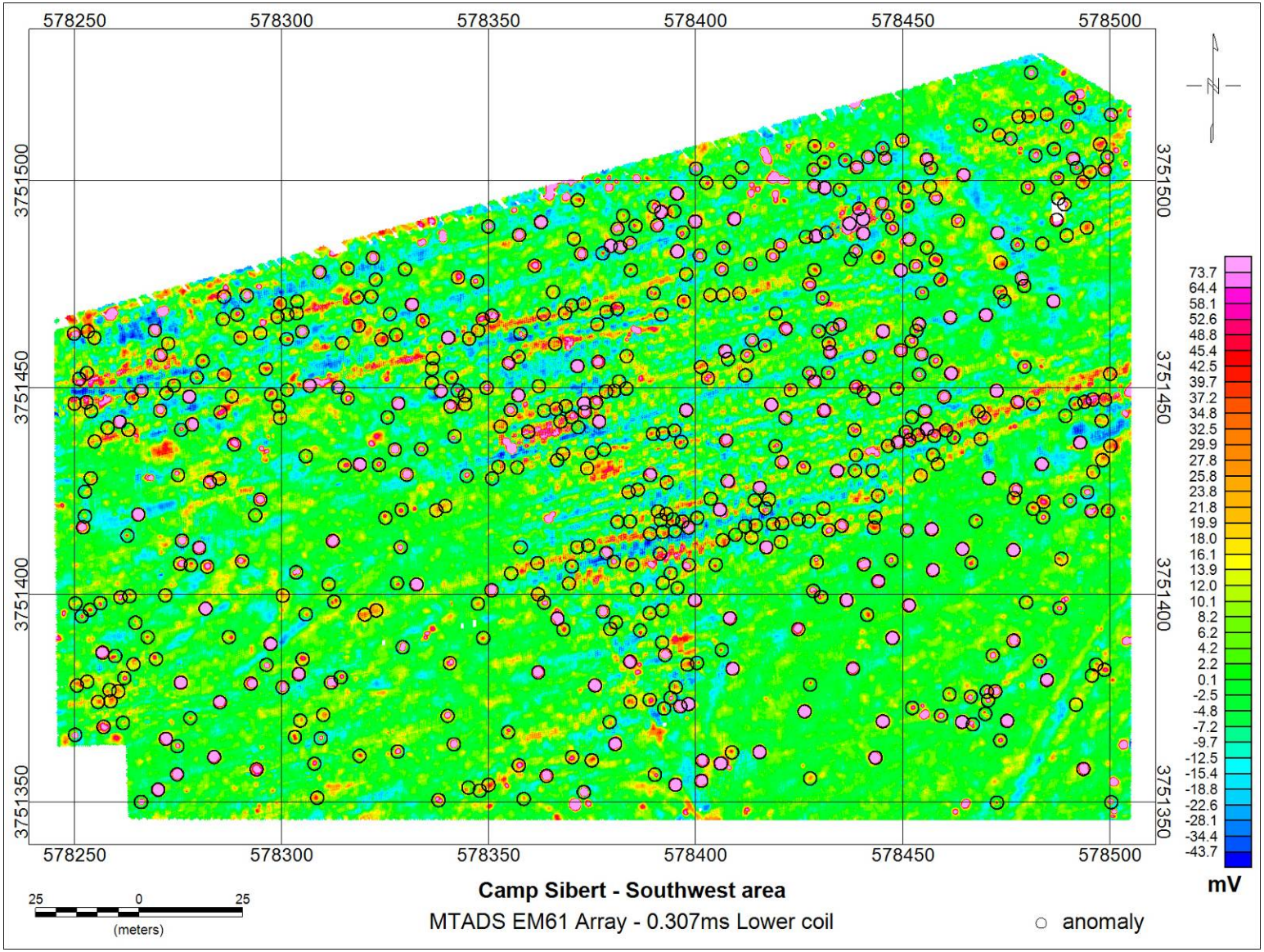

Figure 4-16 EM61 MK2 Array data; Southwest area.

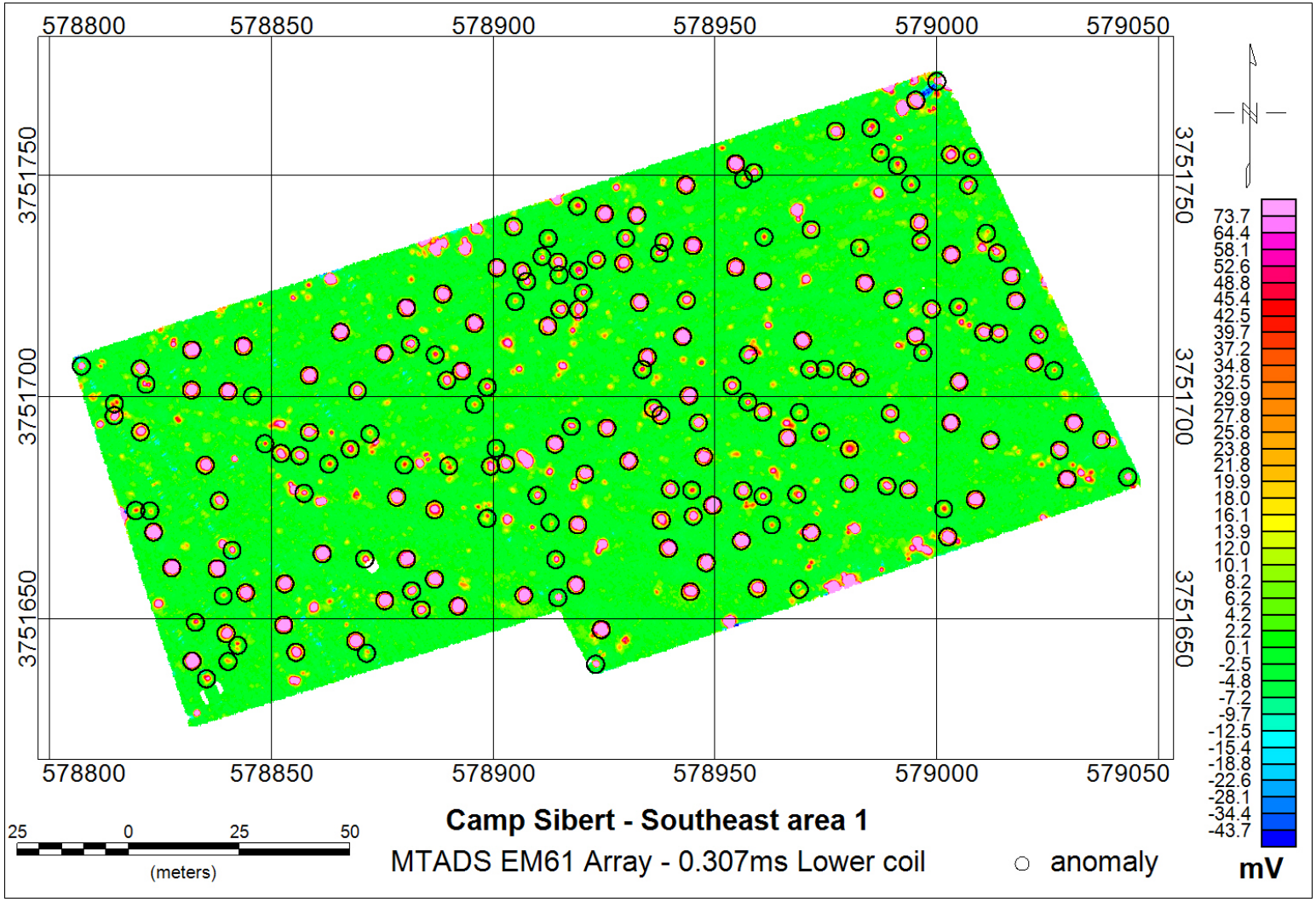

Figure 4-17 EM61 MK2 Array data; Southeast area 1.

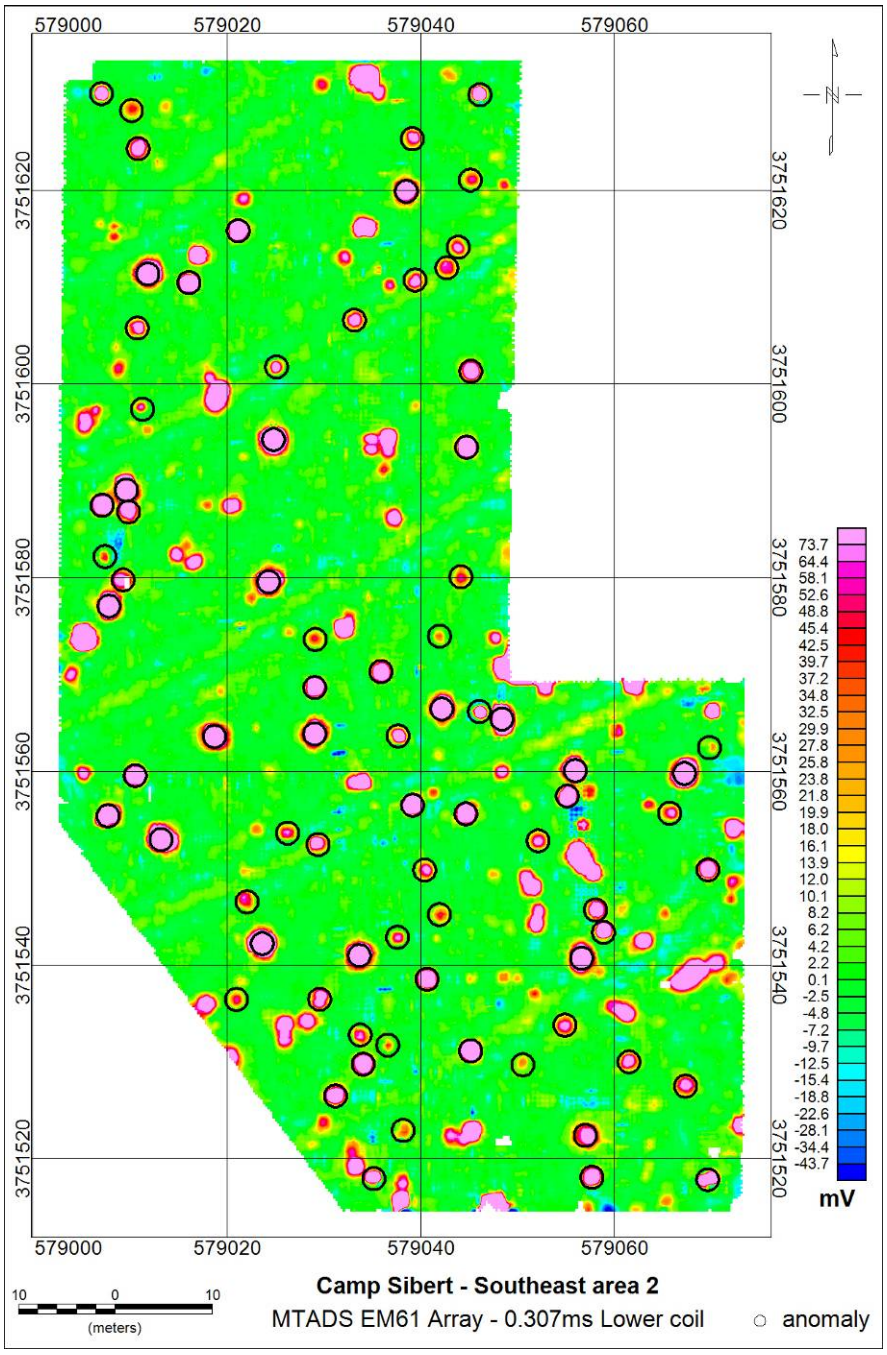

Figure 4-18 EM61 MK2 Array data; Southeast area 2.

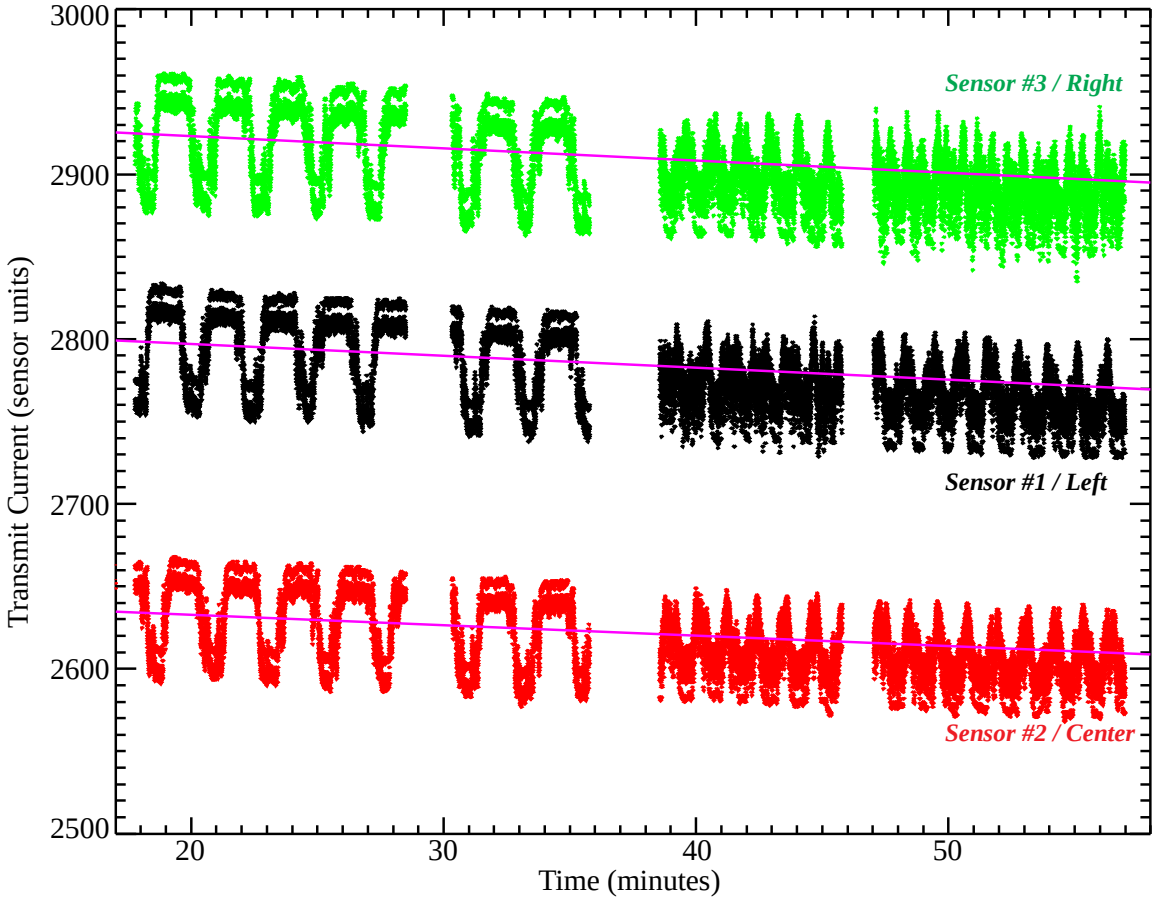

Figure 4-19 Measured EM61 Mk2 array transmit currents.

After correcting for different transmit currents, the three array sensors still do not have equal responses. Figure 4-20 plots the results of moving a metal sphere over the array. By symmetry, the left and right sensors should have equal peaks. The red dashed lines indicate the expected signal peaks relative to the center sensor. Based on this calibration data and the relative amplitudes predicted from the model, a set of relative, inter-array calibration factors were calculated and applied to the data.

Lastly, Geonics EM61 sensors analog integrate the receive coil output and have a dynamic time response because of this. The filter characteristics of this response can be modeled and Geonics publishes the time constant parameters for this filter. The MTADS array has a very short time constant. To first order, the filter simply shifts the data by roughly 0.2 seconds. The distributed data has had this time shift applied. At vehicle speeds of 1.5 to 2.0 m/s, the filter also distorts the measured signal. We have attempted to include this dynamic response in the inversion model, but to date, have not had much success in doing so. The inversion algorithm has trouble converging to the correct solution when this filter is included. If it does converge, the fit to the data is often improved. None of the work presented here accounts for the sensors time response.

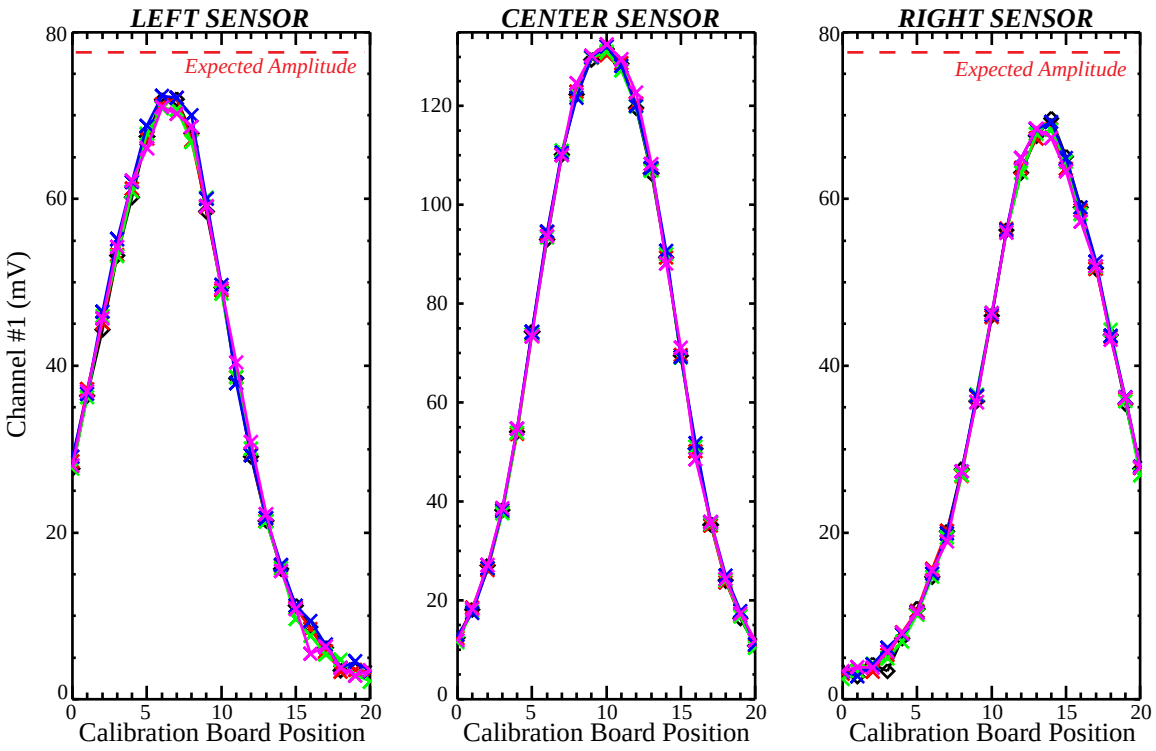

Figure 4-20 Calibration measurements of metal sphere over EM61 MK2 array.

The EM61 MK2 array data shows a great deal of structure in the noise signal across the site. Figure 4-21 shows contours of the low signal levels in the North-South (NS) and East-West (EW) data sets across the GPO. The NS survey shows long east-to-west structures which are not as apparent in the EW survey. Presumably, this noise is a result of the array crossing east-to-west furrows in the ground. It is the result of the array bouncing up and down relative to the ground surface. Figure 4-22 and Figure 4-23 graph data along single tracks over the GPO (black lines in Figure 4-21). Figure 4-22 shows the first two channels (lower/upper coil, first time gate). The NS raster shows the up/down variation of crossing the presumed furrows. The EW raster shows a surprising amount of jittering noise on the upper coil. Presumably, the ground surface is rough and the platform is shaking a great deal. Figure 4-23 plots the same data for channels three and four (two later time gates on the lower coil). Similar noise characteristics are apparent at smaller amplitudes. Figure 4-24 shows comparison NS and EW contours over a section of the "South West" site. The furrow structures are even more apparent. Figure 4-25 plots sample tracks for the first two channels and Figure 4-26 plots the other two channels. The noise levels are significantly worse than the GPO across this area. There are spikes on the order of +/- 40 mV. Based on these observations, it is difficult to distinguish actual detection signals from structured noise with any signal less than 100 mV.

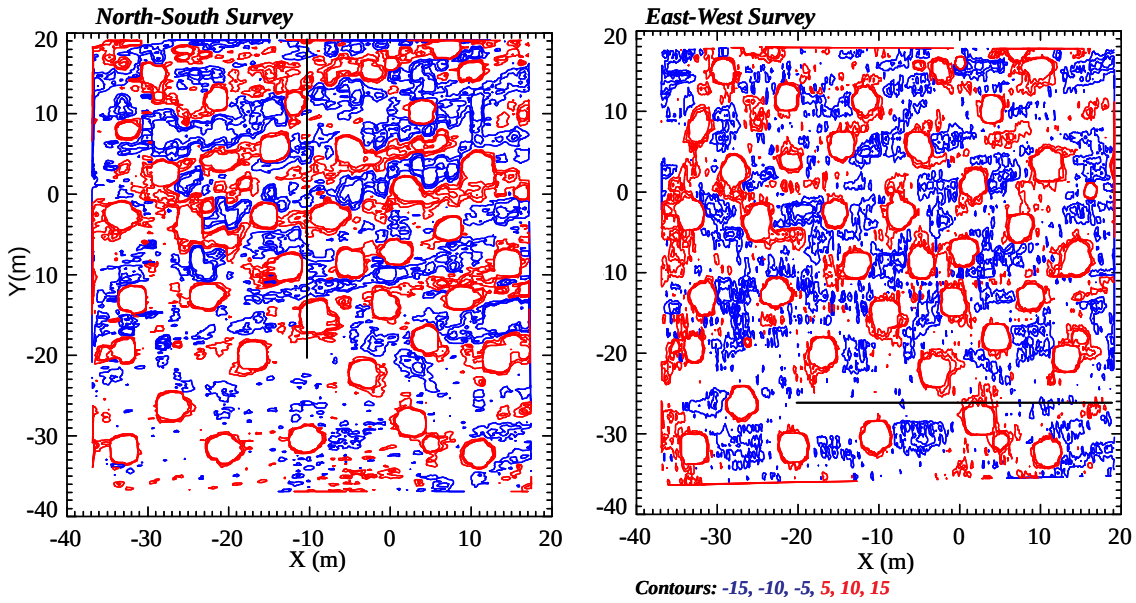

Figure 4-21 EM61 MK2 array contours over GPO site.

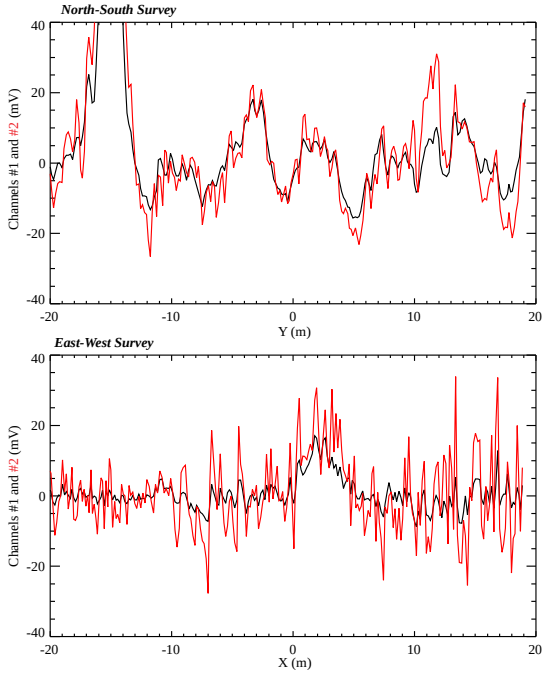

Figure 4-22 Rasters of channels #1 and #2 over track samples on GPO.

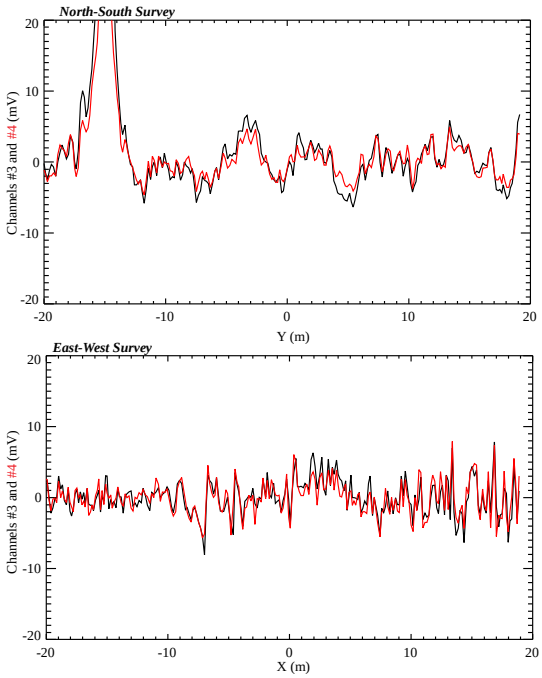

Figure 4-23 Rasters of channels #3 and #4 over track samples on GPO.

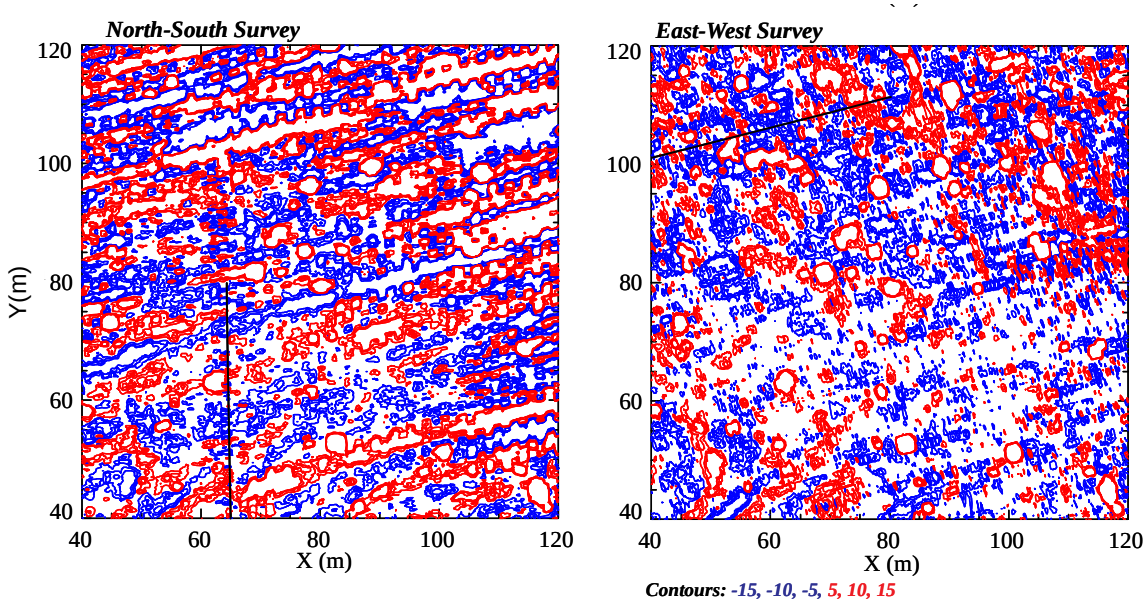

Figure 4-24 EM61 MK2 contours of noise over South West site.

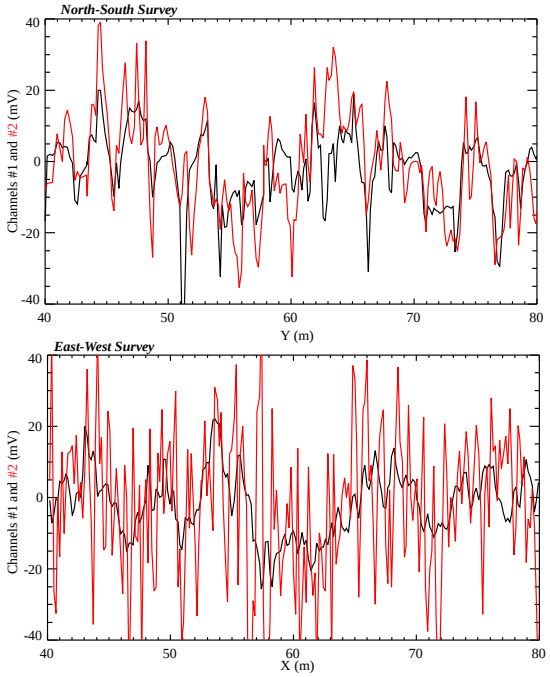

Figure 4-25 Rasters of channels #1 and #2 over track samples on South West site.

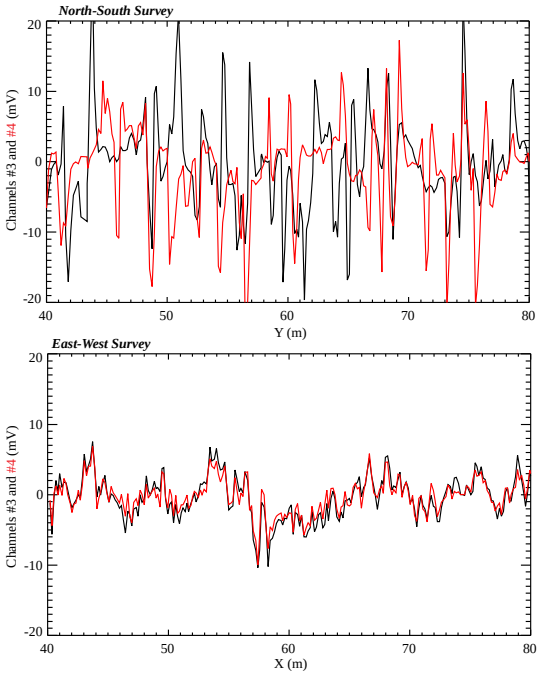

Figure 4-26 Rasters of channels #3 and #4 over track samples on South West site.

Summary of preprocessing steps for EM61 MK2 data:

1) current normalization
2) inter-sensor calibration
3) inverted data from lower coils only, all three time gates (0.307, 0.738, and 1.0ms; we discarded data from upper coil due to noise)
4) used tools developed in Oasis montaj to select polygons (spatial footprint) about anomalies
5) automated routines in IDL to carve out data for each anomaly, keeping data collected along NS and EW transects separate

After preprocessing, we ran inversions in batch and generated custom diagnostic plots for quality assurances purposes.

4.3.2.1.2. Inversion Approach

The dipole response model for the EM61 MK2 array inverted the model parameters of: location (X_0, Y_0, Z_0), magnetic polarization response terms (β_x, β_y, β_z), and orientation angles (*yaw, pitch, roll*). The model used here applied a non-linear Marquardt-Levenberg search for the location parameters and did a linear inversion for the general response tensor. The eigenvalues of the tensor are the three response terms and the eigenvectors are the orientation angles. Data over a given anomaly was carved out separately from each survey (N-S and E-W) and then combined for the fit process.

In an attempt to classify objects in the < 500 mV range, a second strategy was tried. The quality of the fit results was compared between the previous unconstrained 3β fits with that generated assuming fixed β values. The second set of fits was "library fits" with fixed response parameters representing the UXO item of interest. The library values were based on the mean of the log of the best unconstrained fits (β's = 3, 2, 2 for the first time gate) from the GPO. The discrimination parameter becomes the ratio of the fit qualities between the two fits. As this ratio approaches 1.0, there is high confidence that the source of the anomaly under interrogation is munitions.

4.3.2.1.3. Decision Metric: threshold selection and mitigating factors

Classification of the EM61 array data was based on results shown in Figure 4-27. Here, we plot Fit Ratio versus Fit Error. The Fit Ratio is defined as (library coherence) / (unconstrained coherence) and the Fit Error is the square root of (1-correlation coefficient^2). The solid black line limits to the mean value of the fit ratio for high SNR 4.2-inch mortars. The dashed line is shifted down from the mean by six standard deviations of the fit ratio for high SNR mortars. At higher values of fit error, these lines are arbitrarily curved down to match the higher fit error, low SNR 4.2-inch mortar data. Objects that are above the dashed line are categorized UXO and objects below the dashed line are categorized as non-UXO, each ranked according to their distance from the dashed line. Distances above the line are positive and distances below the line

are negative. The decision metric is based on the distance from dashed line, in units of coherence ratio, and set using labeled data as follows (Figure 4-28):

Category 1: <-0.01
Category 2: -0.01 to 0
Category 3: fit error greater than 0.3
Category 4: 0 to 0.01
Category 5: >0.01

The threshold between categories 2 and 4 was set based on first UXO encountered. The thresholds between categories 1 and 2 and between 4 and 5 were set to accommodate observed uncertainty.

Mitigating factors included the following: (1) if no appreciable signal was observed in either the NS or EW data set, the anomaly was declared a Category 3, (2) if the inversion failed, the anomaly was declared Category 3, and (3) if an anomaly was present in the NS transects only (viz., no appreciable signal in the EW transects; Figure 4-29), it was declared Category 1.

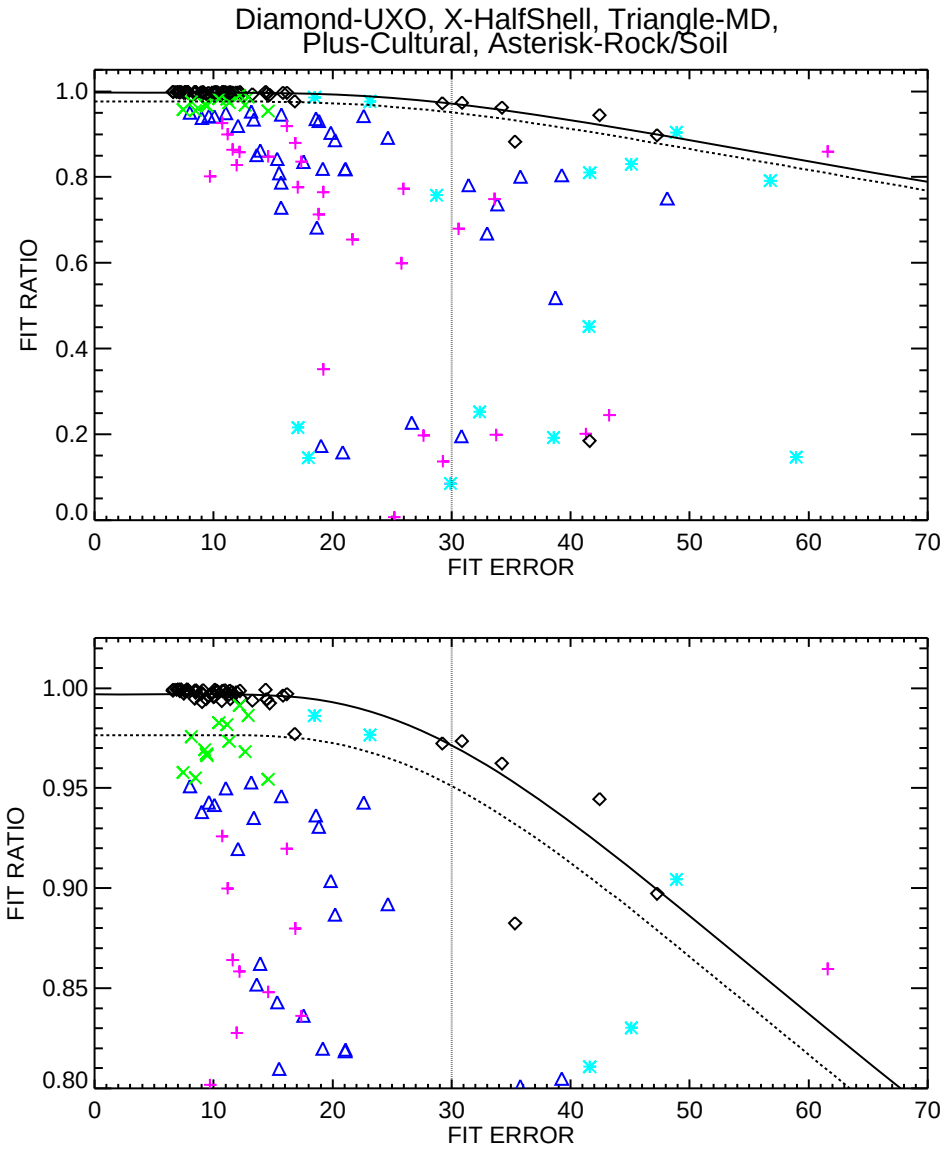

Figure 4-27 Coherence fit ratio versus fit error: EM61 MK2 Training + GPO data

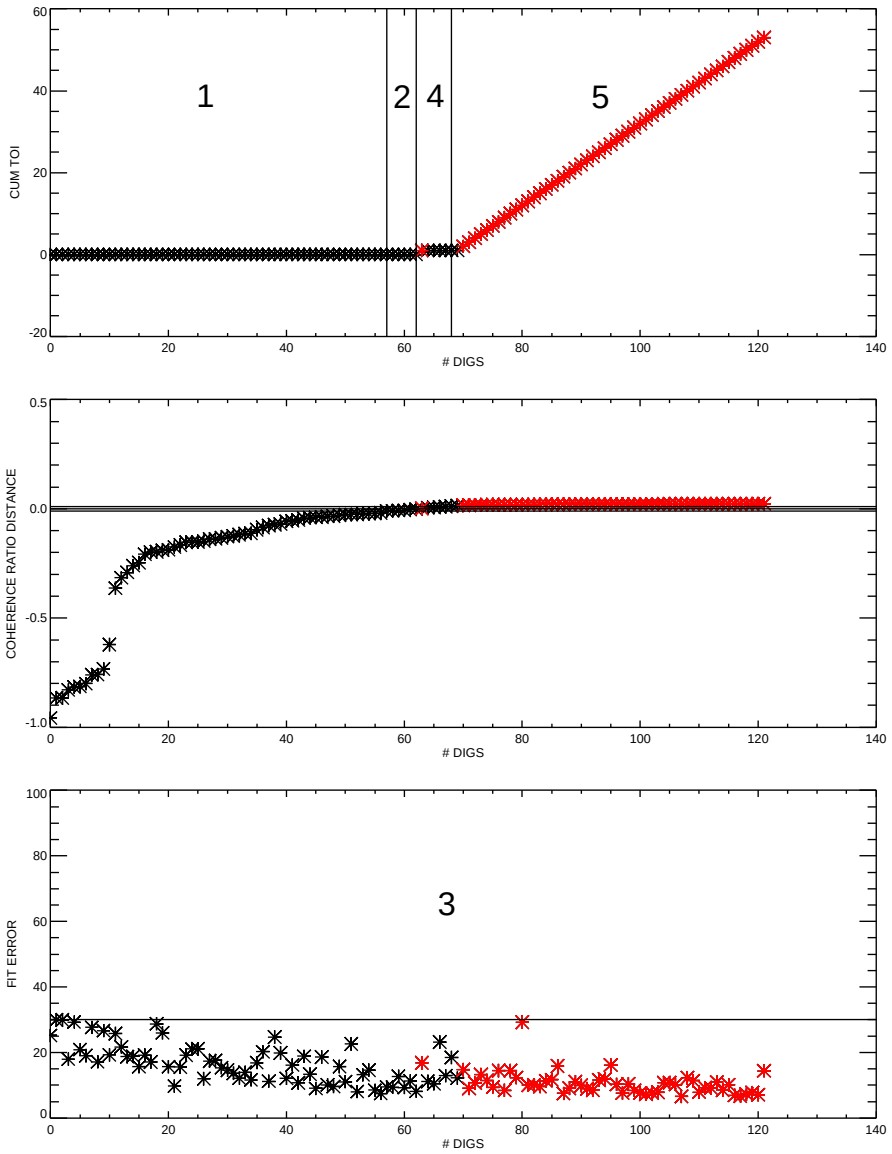

Figure 4-28 EM61 MK2 Array training data and selected thresholds.

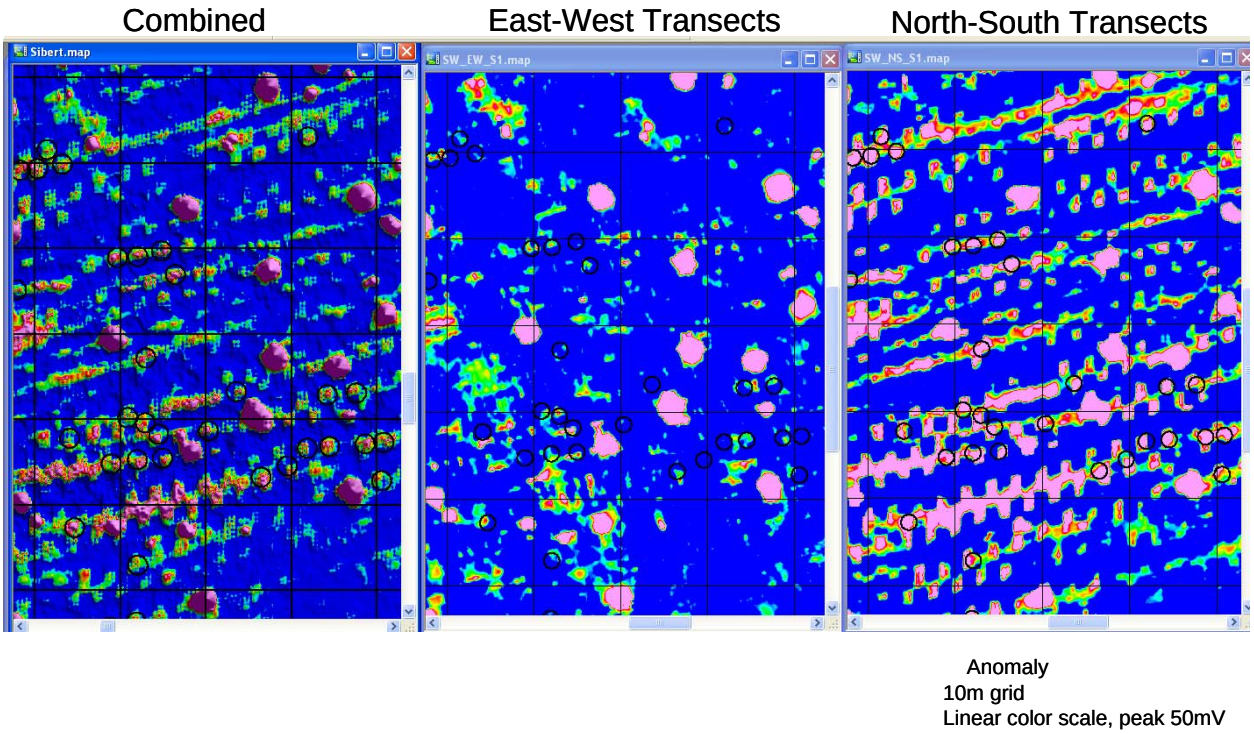

Figure 4-29 EM61 MK2 Array heading dependent noise

4.3.2.1.4. Performance Scores from IDA

Scoring performances for the constrained versus unconstrained analysis approach are reported in Table 4-10 and shown graphically in Figure 4-30. A ROC chart is shown in Figure 4-31, where we plot the number of false positives (FP) versus the probability of detection (Pd).

Anomaly #420, which was in fact a seeded 4.2-inch mortar, was classified as high confidence clutter (Category 1).

Table 4-10 Performance Summary: EM61 MK2 Constrained/Unconstrained Analysis

EM61 Array IDL

CAT	Cultural	Munition Debris	No Contact	Rock	Soil	UXO
1	79	211	4	26	124	1
2	0	12	0	0	3	1
3	27	35	0	19	34	0
4	0	23	1	0	4	8
5	0	11	0	0	2	109
TOTAL	**106**	**292**	**5**	**45**	**167**	**119**

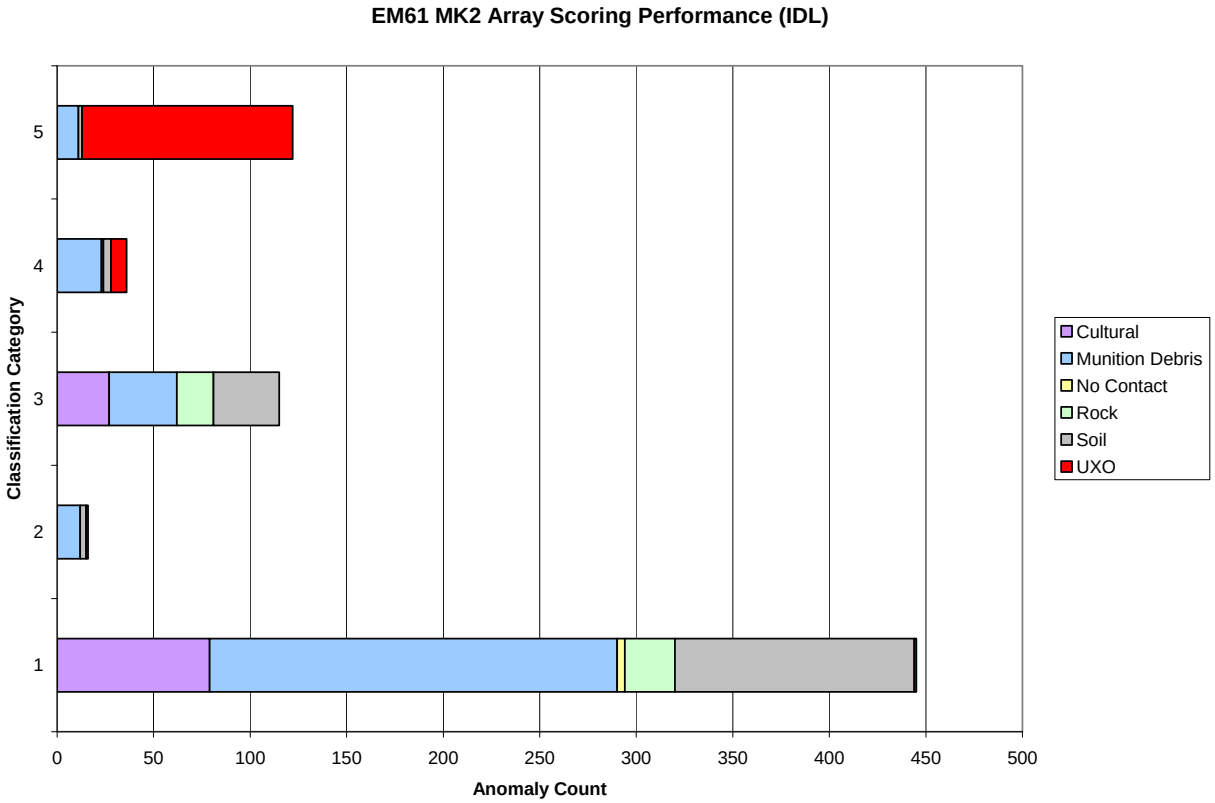

Figure 4-30 EM61 MK2 Array performance as a function of classification category.

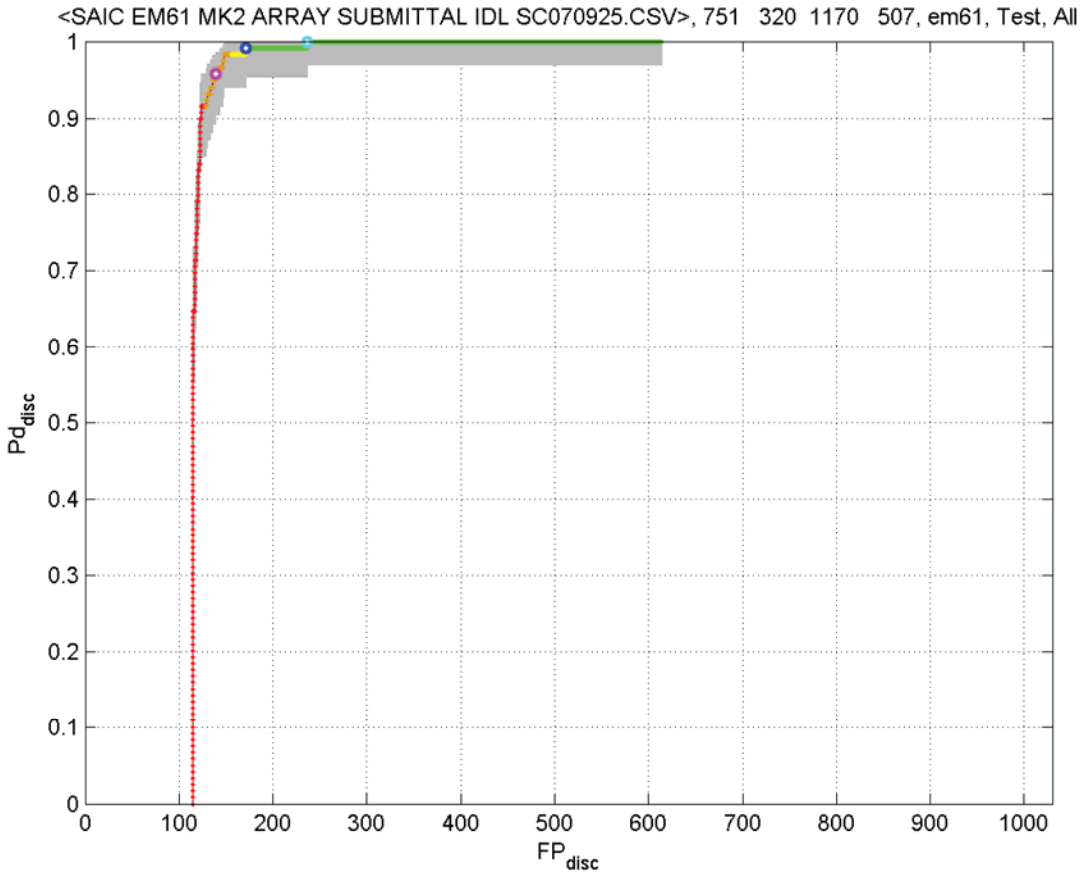

Figure 4-31 EM61 MK2 Array ROC chart; analyzed comparing library-constrained and unconstrained inversions.

4.3.2.1.5. Characterization Plots

The mean error between the fitted and measured XY locations for seeded 4.2-inch mortars, based on EM61 MK2 array inversion results, is 0.22m with a standard deviation of 0.16m. Figure 4-32 plots the distance between inverted and measured locations for UXO and clutter, segmented by discrimination ranking.

The RMS depth error for seeded 4.2-inch mortars is 0.13m with a standard deviation of 0.14m. Figure 4-33 plots the fitted depth versus measured depth for UXO and clutter, segmented by discrimination ranking.

Figure 4-34 plots the net polarizability for the first time gate (0.217 ms) bottom coil, for each of the 119 seeded 4.2in mortars. The seeded mortars were nearly identical in size and shape and we expect their net polarizabilities to be similar. For the EM61 MK2 array data and solver

employed for this analysis, the mean net polarizability was 0.682 with a standard deviation of 0.118. The corresponding COV is 0.174.

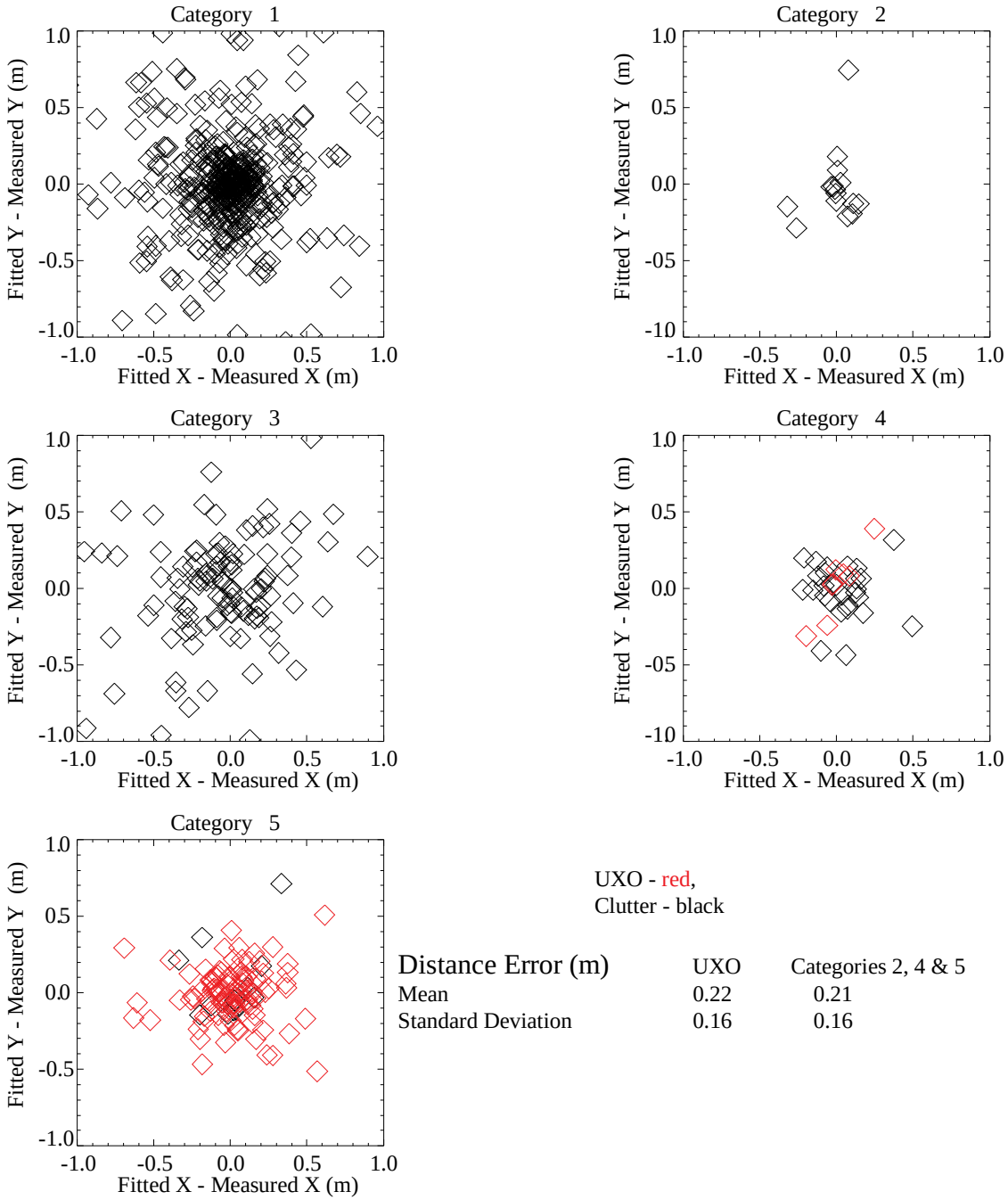

Figure 4-32 Differences between fitted and measured XY locations; EM61 MK2 array

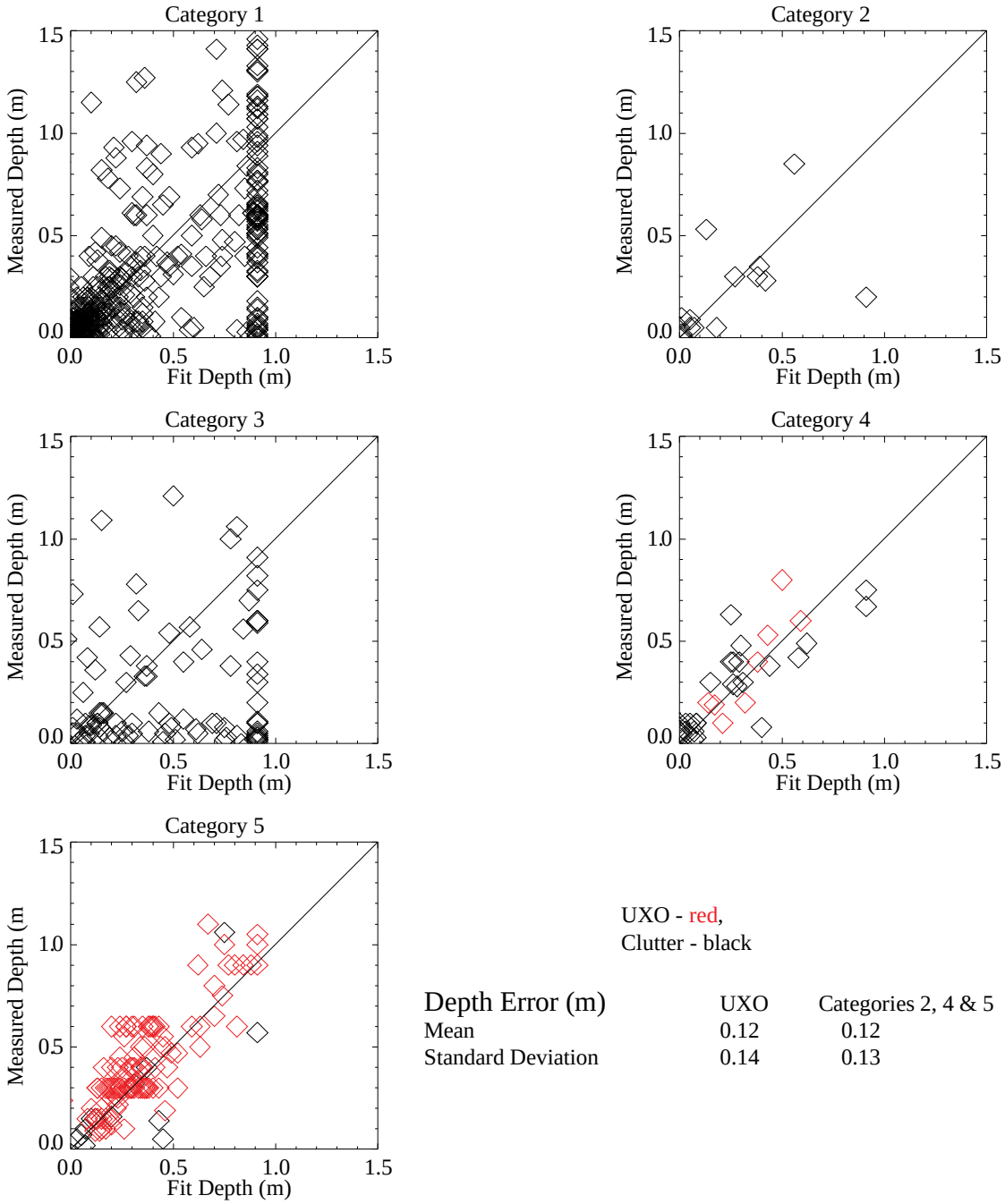

Figure 4-33 Fitted versus measured depth of burial; EM61 MK2 array

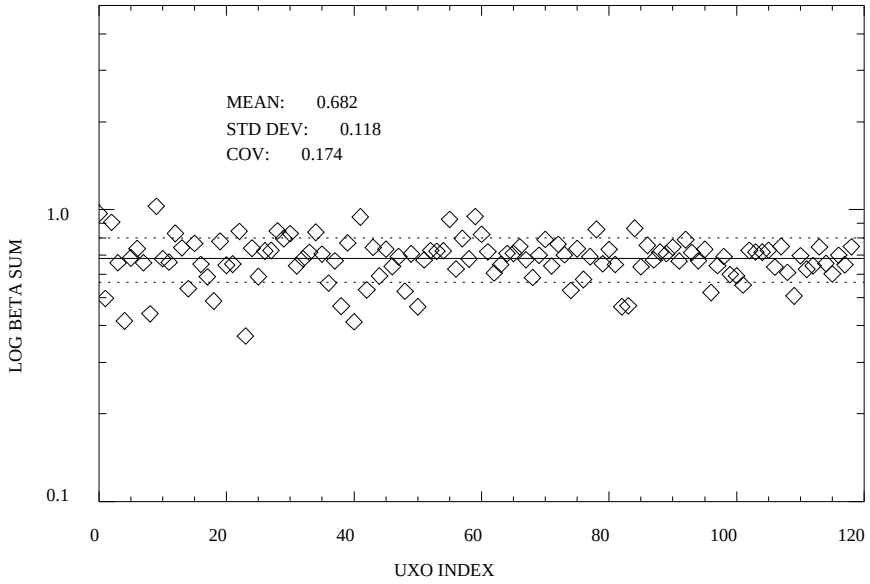

Figure 4-34 Raster of the Σβ, which is a measure of size, for 4.2in mortars, EM61 MK2 array

4.3.2.1.6. Failure Analyses

Anomaly #420 was a seeded 4.2-inch mortar but was classified high confidence clutter (Category 1) using the constrained/unconstrained approach. A reexamination of the anomaly data revealed that one sensor transect had inconsistent elevation measurements relative to nearby transects (Figure 4-35). The poor z positioning of this single track of data altered the inverted polarizations such that it was not fit well using our library representing 4.2-inch mortars.

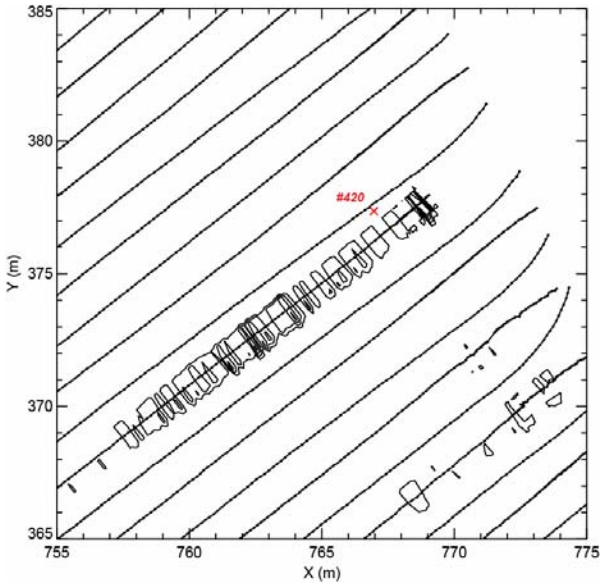

Figure 4-35 Contours of measured elevation (z) show poor consistency for one transect near anomaly #420.

Anomaly #192 was also a seeded mortar but classified as low confidence UXO (Category 2). Upon inspection, we found that our search algorithm did not search deep enough in the depth parameter. Extending the range of our search algorithm changed the classification of this anomaly to high confidence UXO (Category 5).

4.3.2.1.7. Summary and Comments

Analyzing the EM61 MK2 array data using a library-constrained versus unconstrained coherence metric resulted in one false negative. The analysis failure was caused by poor elevation (z) positioning along one of transects.

Data glitches and timing problems degraded some of our inversions. A number of anomalies acquired during a single sortie, for example, possessed timing errors and chevron signals. Of the 19 fits from this sortie, six high amplitude anomalies were classified Category 4. In another case, #421) there are three samples at identical spatial positions, but the EM signal is changing. Still others (#331 and #342) possess timing irregularities.

4.3.2.2. Inversions using an Unconstrained Approach only (UX-Analyze)

4.3.2.2.1. Data Presentation, Description, and Pre-processing

The EM61 MK2 Array data were presented and discussed in §4.3.2.1 above.

The preprocessing steps for EM61 MK2 data, prior to analysis using UX-Analyze, included:

1) current normalization
2) inter-sensor calibration
3) inverted data from lower coil only, first time gates (0.307 msec)
4) used tools developed in Oasis montaj to select polygons (spatial footprint) about anomalies
5) automated UX-Analyze tools to carve out data for each anomaly, keeping data collected along NS and EW transects separate.

After preprocessing, we ran inversions in batch and generated custom diagnostic plots for quality assurances purposes.

4.3.2.2.2. Inversion Approach

The dipole response model for this analysis method inverts the model parameters of: location (X_0, Y_0, Z_0), magnetic polarization response terms (β_x, β_y, β_z), and orientation angles (*yaw, pitch, roll*). The model used here applied a non-linear Marquardt-Levenberg search for all nine parameters. For the Southeast 1 and 2 areas, data from NS and EW transects were merged prior to fitting. For the Southwest area, inversions were preformed on data collected along EW transects only due to noise issues with the NS data. The goodness of fit metric, ε, is the squared correlation of data and model. By definition, the dipole fit error metric is equal to $\sqrt{1-\varepsilon}$.

4.3.2.2.3. Decision Metric: threshold selection and mitigating factors

Using UX-Analyze, classification of the EM61 array data was based on the sum of the polarizations ($\Sigma\beta$). Figure 4-36 presents fitted results for all labeled data. In the figure, the data are prioritized according to apparent size and color coded according to the actual labels. Based upon these labeled data, we established the following thresholds:

Category 1: <0.04
Category 2: 0.04 to 0.05
Category 3: fit error greater than 45%
Category 4: 0.05 to 0.07
Category 5: >0.07

The threshold between categories 2 and 4 was set based on first UXO encountered. The thresholds between categories 1 and 2 and between 4 and 5 were set to accommodate observed uncertainty.

Mitigating factors included the following: (1) if no appreciable signal was observed in either the NS or EW data set, the anomaly was declared a Category 3, (2) if the inversion failed, the anomaly was declared Category 3, and (3) if an anomaly was present in the NS transects only (viz., no appreciable signal in the EW transects), it was declared Category 1.

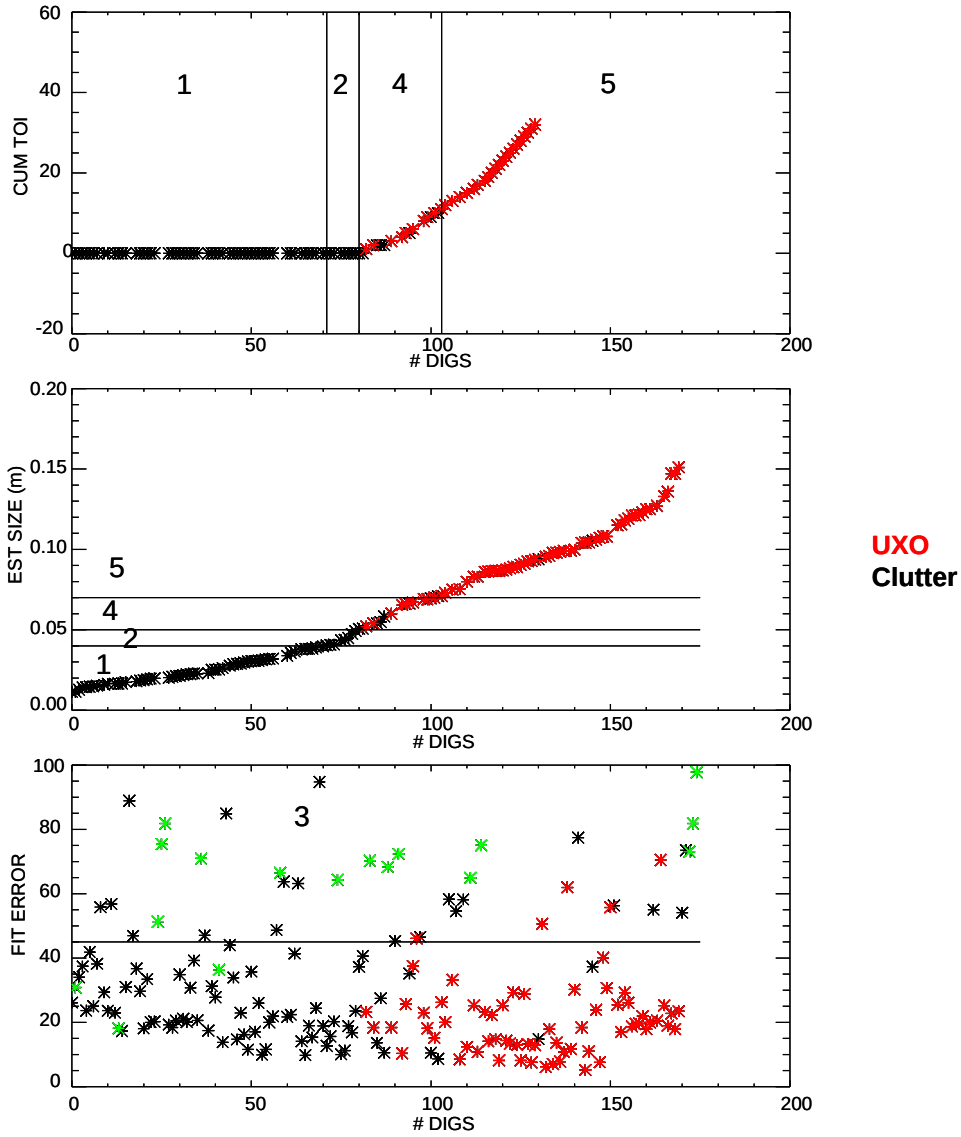

Figure 4-36 EM61 MK2 Array training data and selected thresholds; UX-Analyze analysis. The anomalies shown in green were classified Category 1 based on a comparison between data collected along NS and EW transects.

4.3.2.2.4. Performance Scores from IDA

Scoring performances for the size-based analysis approach are reported in Table 4-11 and shown graphically in Figure 4-37. A ROC chart is shown in Figure 4-38. From a declared-category perspective, the category 3 targets are plotted first, followed by categories 5 (red), 4 (orange), 2 (yellow), and finally 1 (green).

Using the established thresholds, there were no classification failures. All UXO were categorized medium or high confidence UXO (Category 4 or Category 5).

Table 4-11 Performance Summary: EM61 MK2 size-based Analysis

EM61 Array UXA

	Cultural	Munition Debris	No Contact	Rock	Soil	UXO
1	75	155	2	22	101	0
2	8	59	1	3	11	0
3	17	16	0	18	44	0
4	4	28	1	1	7	6
5	2	34	1	1	4	113
TOTAL	**106**	**292**	**5**	**45**	**167**	**119**

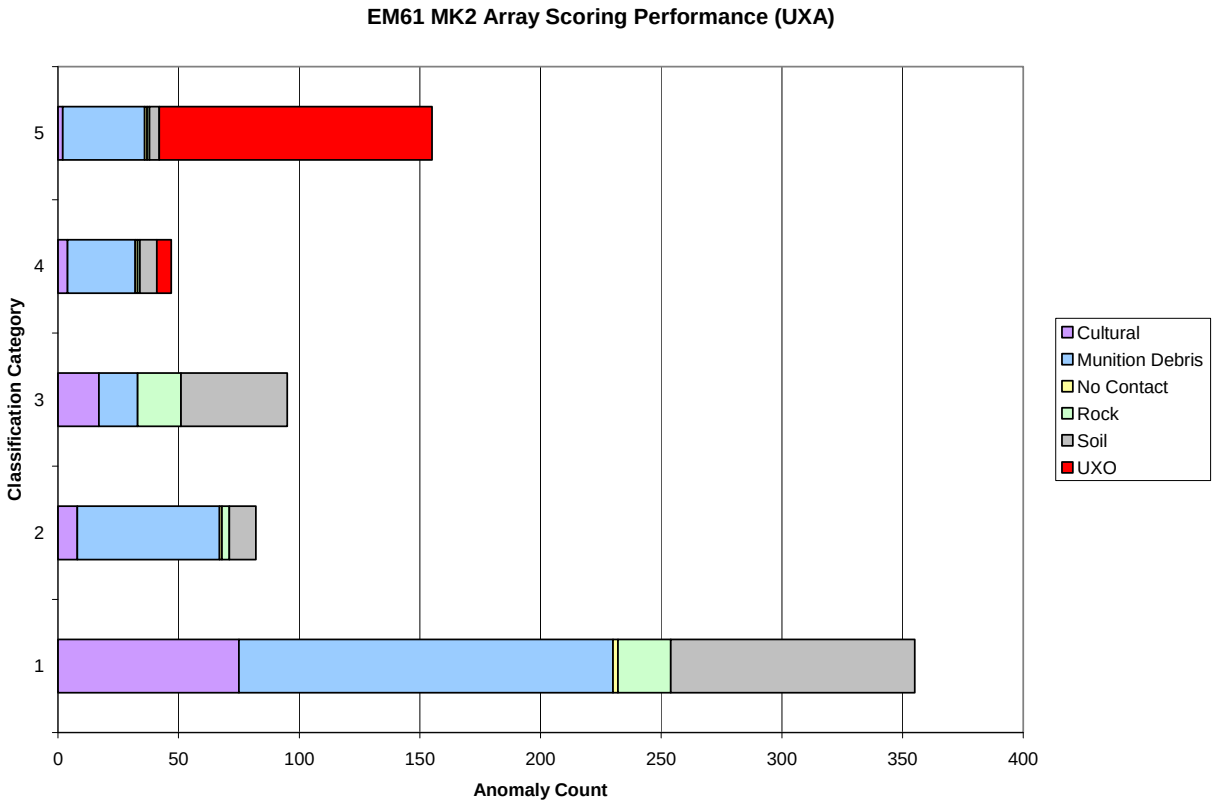

Figure 4-37 EM61 MK2 Array performance as a function of classification category.

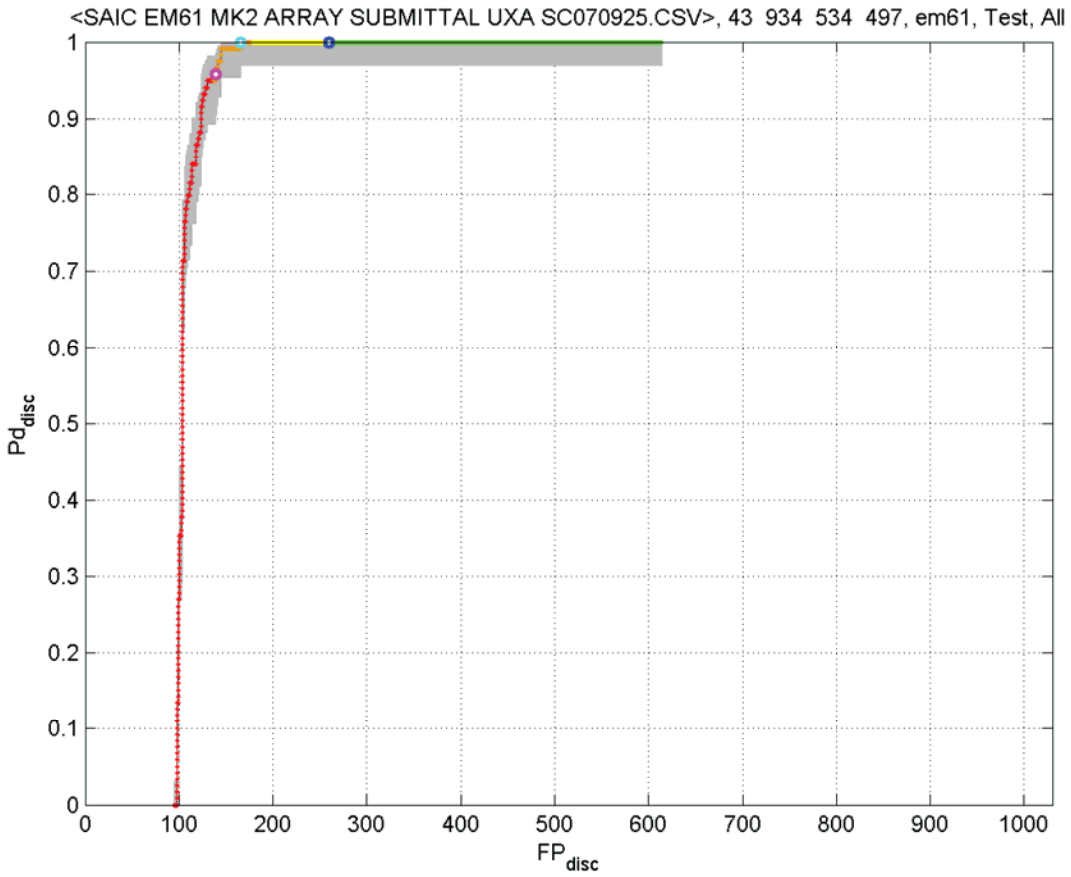

Figure 4-38 EM61 MK2 Array ROC chart; analyzed based on size metric.

4.3.2.2.5. Characterization Plots

The RMS error between the fitted and measured XY locations for seeded 4.2-inch mortars, based on UX-Analyze EM61 MK2 array inversion results, is 0.18m with a standard deviation of 0.12m. Figure 4-39 plots the distance between inverted and measured locations for UXO and clutter, segmented by discrimination ranking.

The RMS depth error for seeded 4.2-inch mortars is 0.20m with a standard deviation of 0.17m. Figure 4-40 plots the fitted depth versus measured depth for UXO and clutter, segmented by discrimination ranking.

Figure 4-41 plots the net polarizability for the first time gate (0.217 ms) bottom coil, for each of the 119 seeded 4.2in mortars. For the EM61 MK2 array data and UX-Analyze solver, the mean net polarizability was 0.751 with a standard deviation of 0.211. The corresponding COV is 0.282.

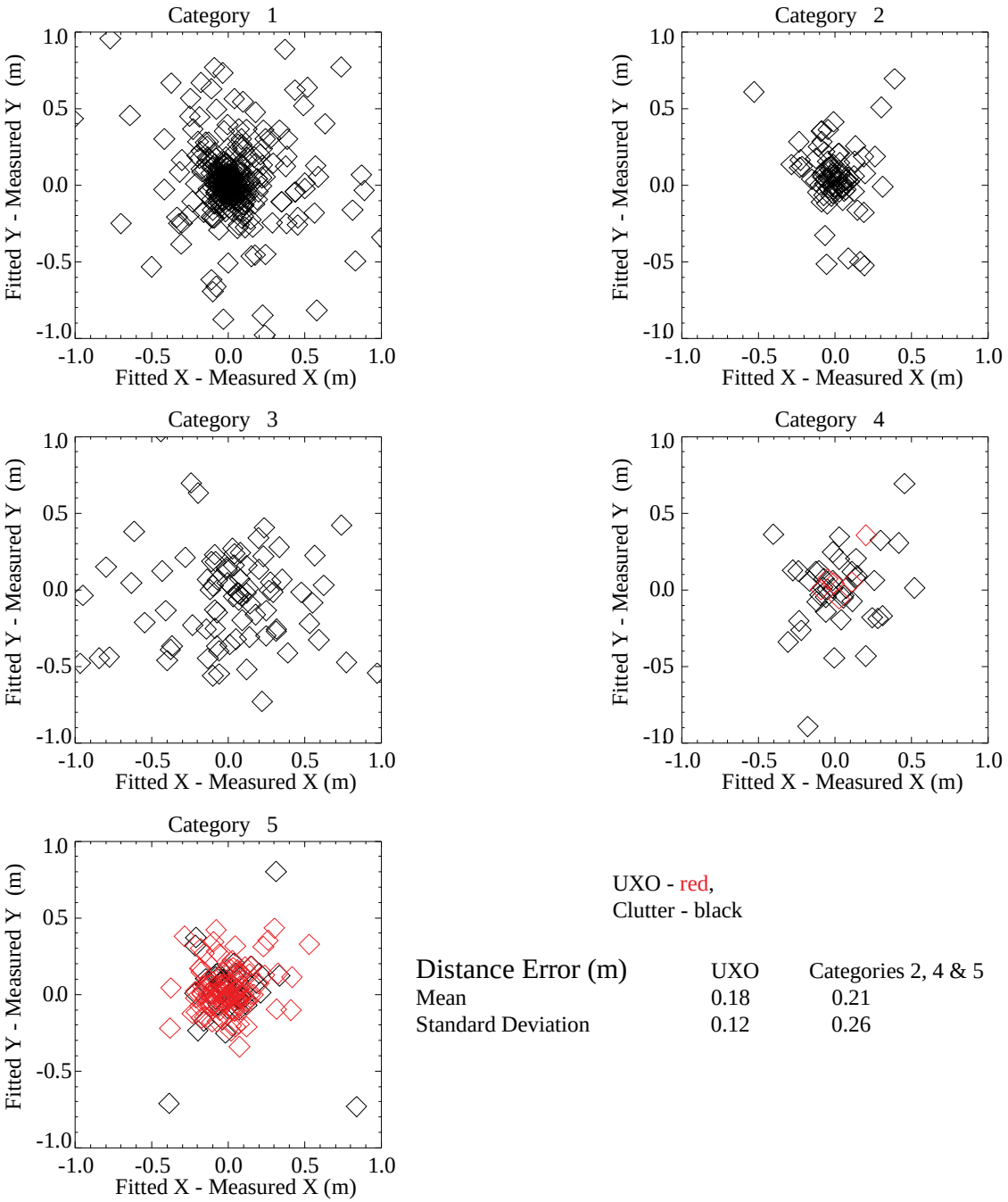

Distance Error (m)	UXO	Categories 2, 4 & 5
Mean	0.18	0.21
Standard Deviation	0.12	0.26

Figure 4-39 Differences between fitted and measured XY locations; EM61 MK2 array with size based analysis

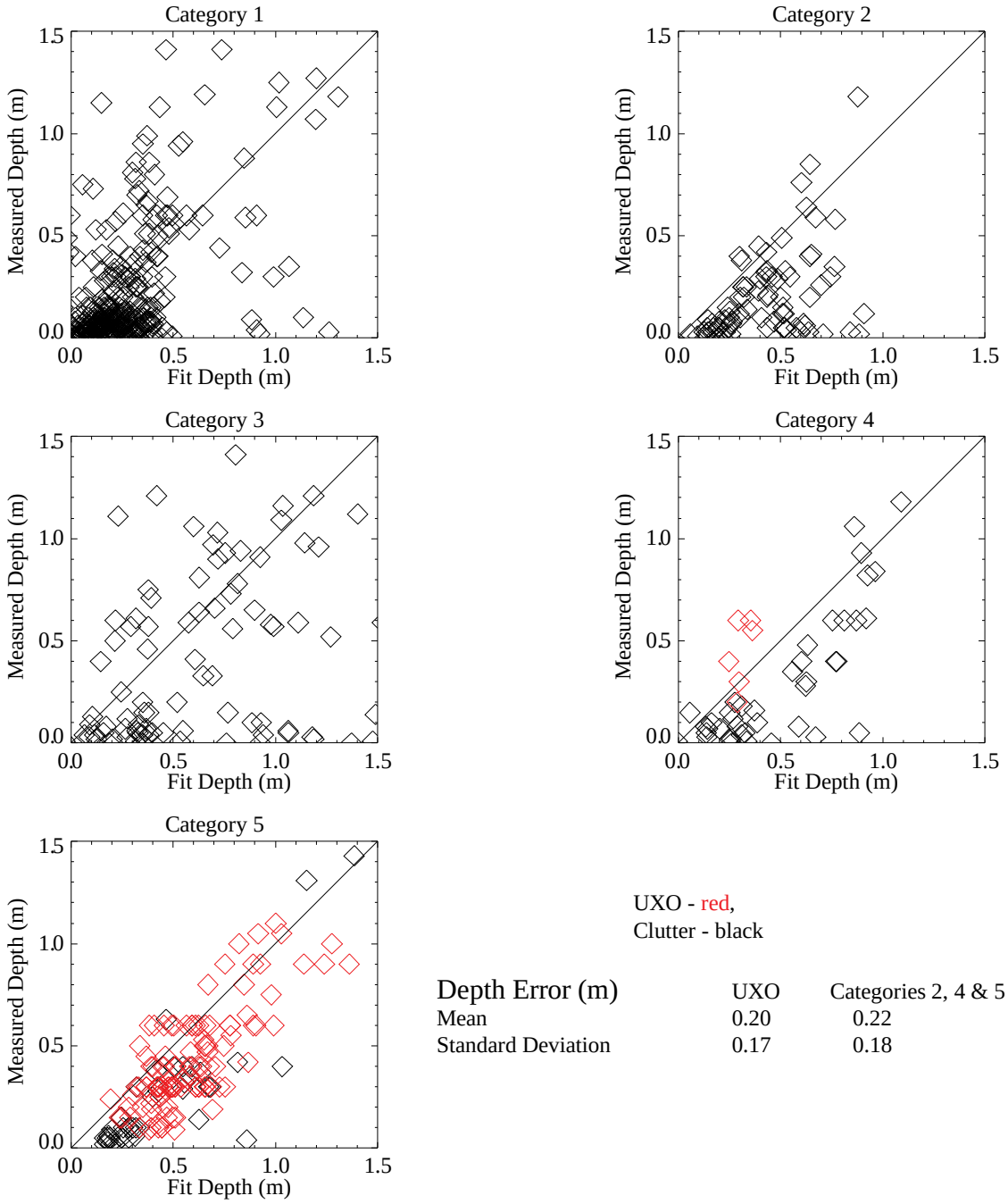

Depth Error (m)	UXO	Categories 2, 4 & 5
Mean	0.20	0.22
Standard Deviation	0.17	0.18

Figure 4-40 Fitted versus measured depth of burial; EM61 MK2 array with size based analysis

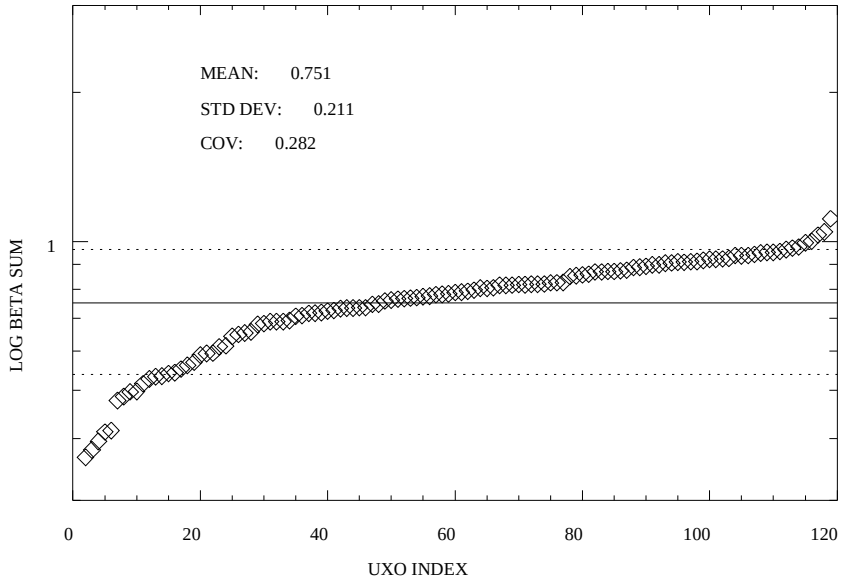

Figure 4-41 Raster of the Σβ, which is a measure of size, for 4.2in mortars, EM61 MK2 array with size based analysis

4.3.2.2.6. Failure Analyses

Using the thresholds adopted for this analysis, there were no false negatives.

4.3.2.2.7. Comments

Analyzing the EM61 MK2 array data with a size-based (Σβ) metric resulted in zero false negatives while eliminating 49% of the potential targets.

Geolocation errors and noise contributed to overlap in size estimates.

Although the size-based metrics generated by UX-Analyze were able to separate the 4.2-inch mortars from clutter at this site, the IDL-based solver produced tighter polarizations. Figure 4-42 compares primary versus secondary polarizations for UXO, halfshells, and baseplates. The data are grouped based on labels received post demonstration. In the figure, symbols and color show the declared categories. Diamonds identify UXO, X are halfshells, triangles are munitions debris, plus symbols are cultural and asterisk are used to identify rock/soil classifications.

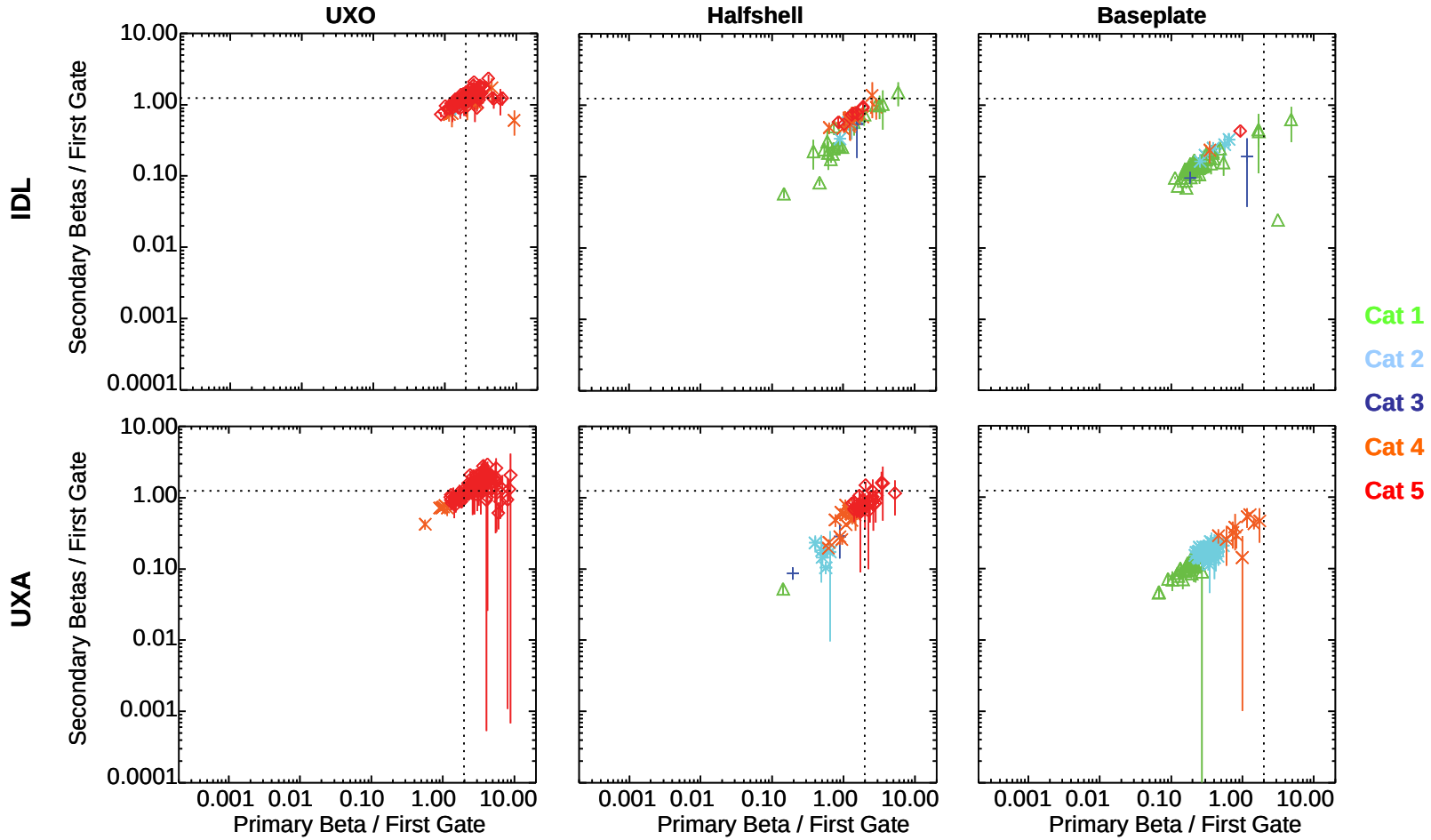

Figure 4-42 Type discrimination as a function of inversion approach.

4.3.3 GEM-3 ARRAY

4.3.3.1. Data Presentation, Description, and Pre-processing

Data from the GEM-3 array (Figure 4-43) is shown in Figure 4-44 thru Figure 4-46. The circles identify anomalies selected for analysis by the ESTCP Program Office.

Summary of preprocessing steps for GEM-3 Array data:

1) Sensor cross-calibration using ferrite rods;
2) De-median filter applied to data to remove long wavelength drift;
3) Inverted data from three mid-rage frequencies, quadrature only (in-phase, three lowest quadrature, and three highest quadrature components discarded due to high levels of noise) (Figure 4-47);
4) Used tools developed in Oasis montaj to select polygons (spatial footprint) about anomalies;
5) Automated routines in IDL to carve out data for each anomaly.

After preprocessing, we ran inversions in batch and generated custom diagnostic plots for quality assurances purposes.

Figure 4-43 GEM-3 array of three coils

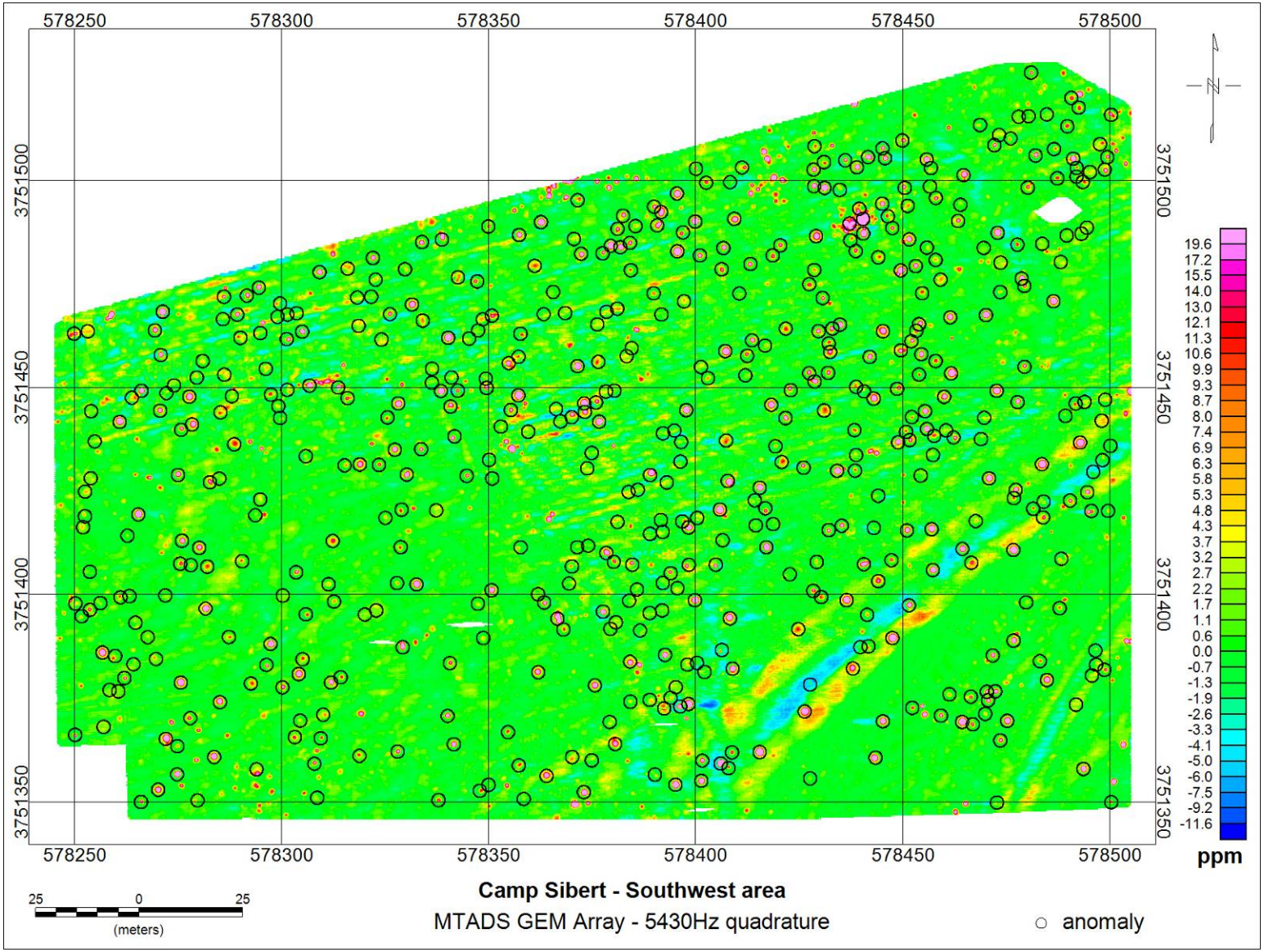

Figure 4-44 GEM Array data; Southwest area.

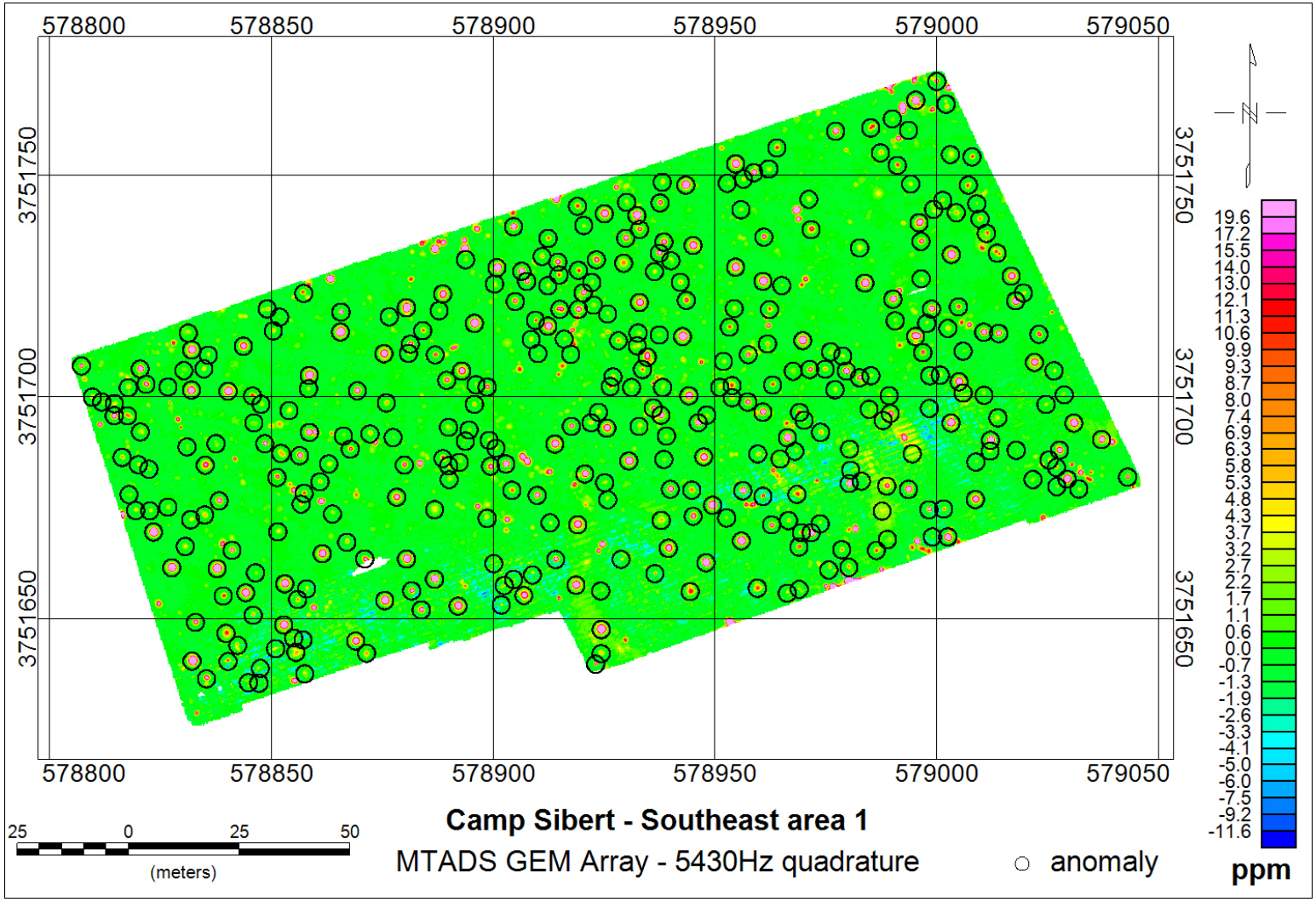

Figure 4-45 GEM Array data; Southeast area 1.

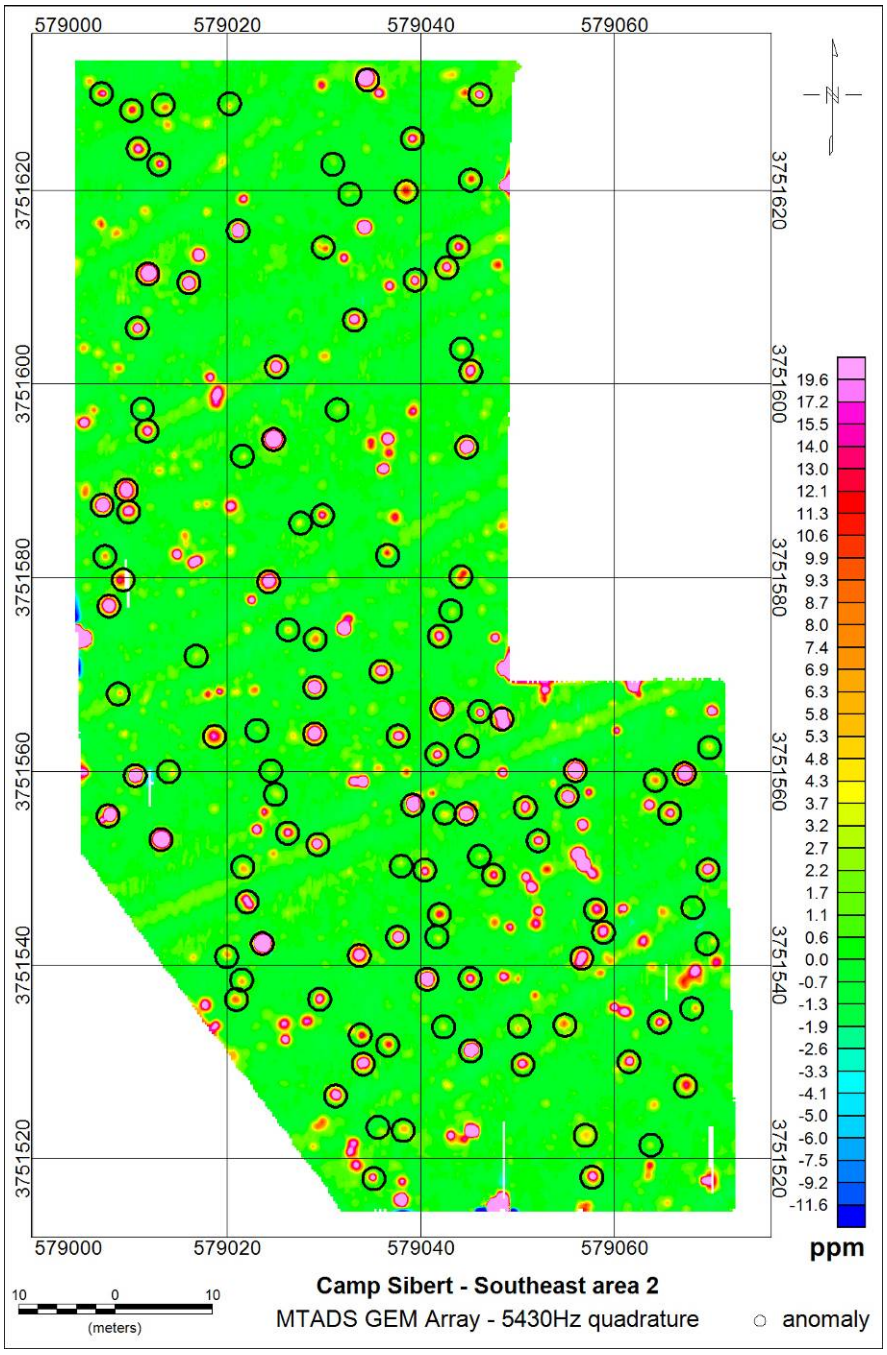

Figure 4-46 GEM Array data; Southeast area 2.

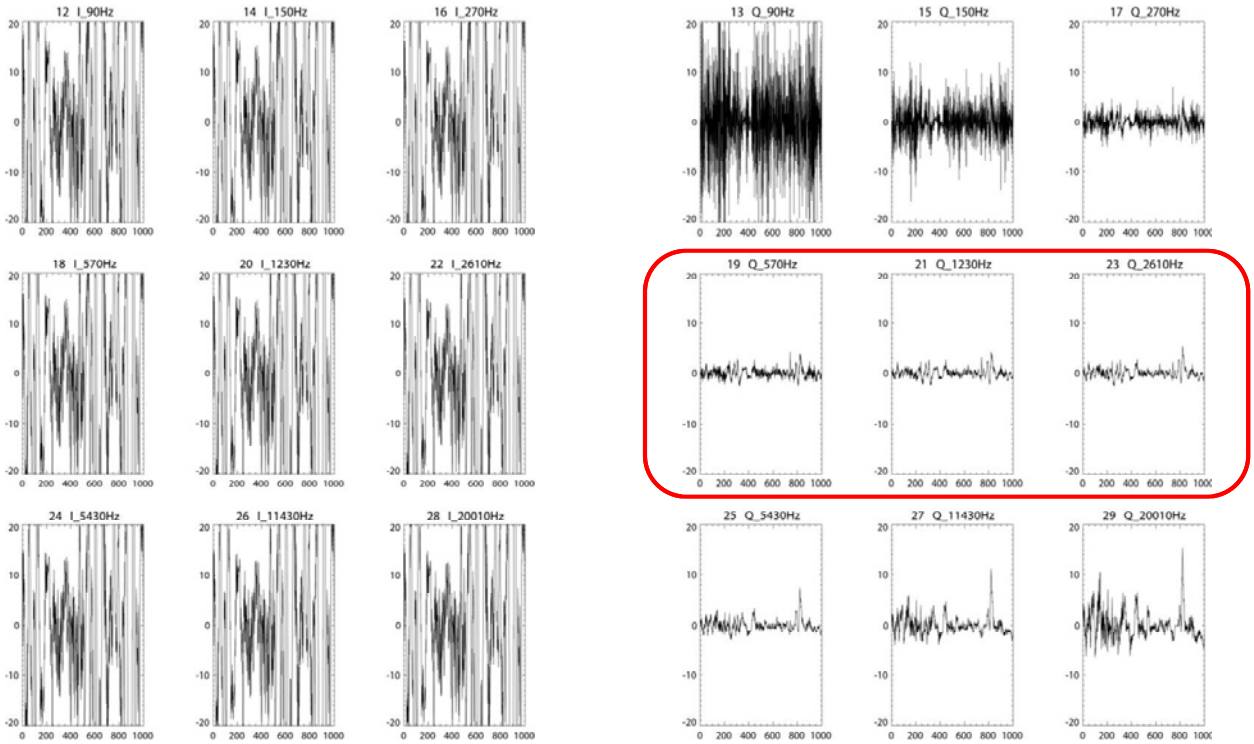

Figure 4-47 GEM-3 array, data down selection based on noise characteristics.

4.3.3.2. Inversion Approach

The inversion of GEM array data is based on a standard dipole model. The algorithm finds six (6) fitted parameters: x, y, z, phi, theta, psi, where x, y, z, are the target coordinates (m) and phi, theta, psi are the Euler angles (degrees). The associated best-fit betas, three polarizations for each frequency, are also recovered and values for the chi-squared error and coherence are calculated. Follow-on fits are made with betas constrained to match given values from a library. Associated chi-squared and coherence values are found for each library item, and ratios of (constrained coherence) / (un-constrained coherence) are calculated.

To avoid being trapped in local minima, unconstrained inversion operates in two stages. The first stage steps through fixed z values from ground surface down to 1.75m depth in 5cm intervals (Figure 4-48). At each z step, the best-fit target xy position is found using the "matrix" method in which elements of the response tensor are found through linear regression. This permits fast run times and experience has shown it is robust against local minima. No restrictions are placed on the tensor values: they may be positive or negative, even for quadrature data which are normally only positive. Each channel is treated independently, so each will have a different apparent target orientation.

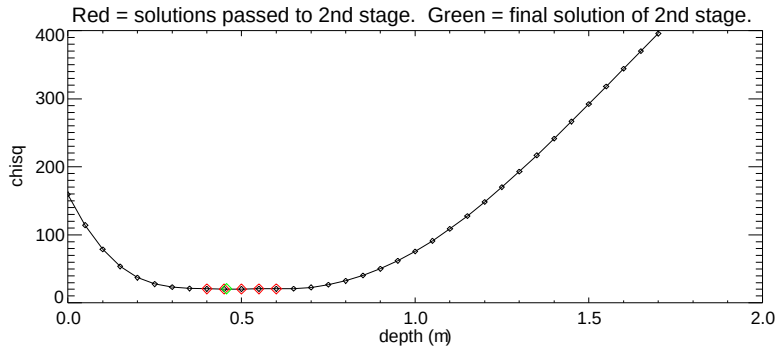

Figure 4-48 Example graph of the χ^2 error as a function of depth during the initial solver stage; GEM array data.

The 10 best solutions, judged by chi square value, are used as starting points in the 2nd stage. Before submitting these data, euler angles must be found. It was discovered that using arbitrary angles can lead to failure of the solver due to local minima, so a special optimization step is performed separately on each of the 10 solutions. In this step, "best-fit" Euler angles are found through minimization of off-diagonal elements in the response tensor, across all channels. Starting points for this optimization are the apparent Euler angles from each channel's tensor.

The second stage searches all 6 fitted parameter values: x, y, z, phi, theta, psi, through downhill simplex minimization. After cycling through all 10 of the start points from the 1st stage, the best-ever solution is saved.

It was found that making an adjustment to In-phase data improved performance, based on available ground truth. The adjustment consists in removing the local mean from inphase data at each measurement point: At each point, mean inphase across all channels is found and subtracted from inphase data at that point. Parameter search is then performed, and finally, best-fit betas are determined at the end through regression on the full unadjusted data set.

Summary of solver steps used for GEM-3 array data:

- Standard Dipole Magnetic Polarization Model
- First stage:
  - Step through Z (distance below array) in 5cm increments.
  - Time lag added as fit parameter to compensate for dynamic response.
  - Search target XY nonlinearly, find tensor elements linearly.
  - Find Euler angles to minimize off-diagonals across all gates.
  - Save 10 best fits judged by chi-square (different Z values & lags).
    These are start points for following stages.
- Second stage:
  - Search x, y, z, phi, theta, psi all non-linearly, find axial betas linearly.
  - Axial-symmetry not assumed.
- Third stage:
  - Library of fixed beta values from 21 UXO in GPO with high SNR.

- Search x, y, z, phi, theta non-linearly (axial symmetry imposed).
- Fresh fit with each library item using 10 restarts.
- Ratio of best library fit coherence / unconstrained fit coherence used in discrimination. This ratio is always < 1.

4.3.3.3. Labeled data – threshold selection

Classification of the GEM-3 array data was based on results shown in Figure 4-49. Here, we plot coherence ratio as a function of fit mismatch. We chose the coherence ratios instead of the χ^2 error ratios because is tends to produce better separation between TOI and non-TOI classes. The solid black line limits to the mean value of the coherence ratio for high SNR 4.2-inch mortars. The dashed line is shifted down from the mean by 10 standard deviations, normalized by variance. The decision metric is simply the distance from mean TOI response (solid black line), in units of coherence ratio (function of mismatch). Using these labeled data, we set the following thresholds (Figure 4-50):

Category 1: < -10
Category 2: -10 to -3
Category 3: fit error greater than 50%
Category 4: -3 to 0
Category 5: >0

Mitigating factors included the following: (1) if the fit depth was greater than 1m, then Category 2 or 4 based on coherence ratio, and (2) if the inversion failed, the anomaly was declared Category 3.

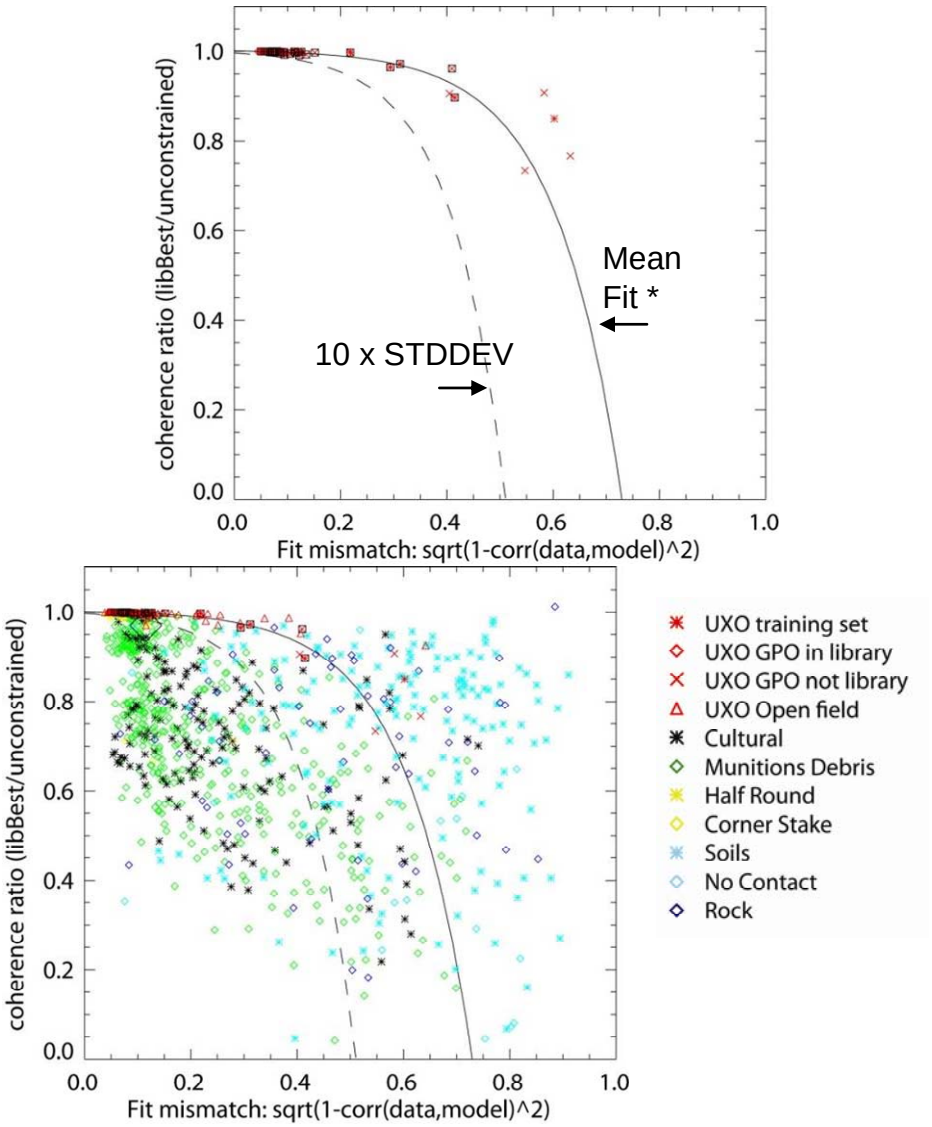

Figure 4-49 GEM-3 Array training data. Top – Response of 4.2-inch mortars from GPO. Bottom – Discrimination metrics for all training data.

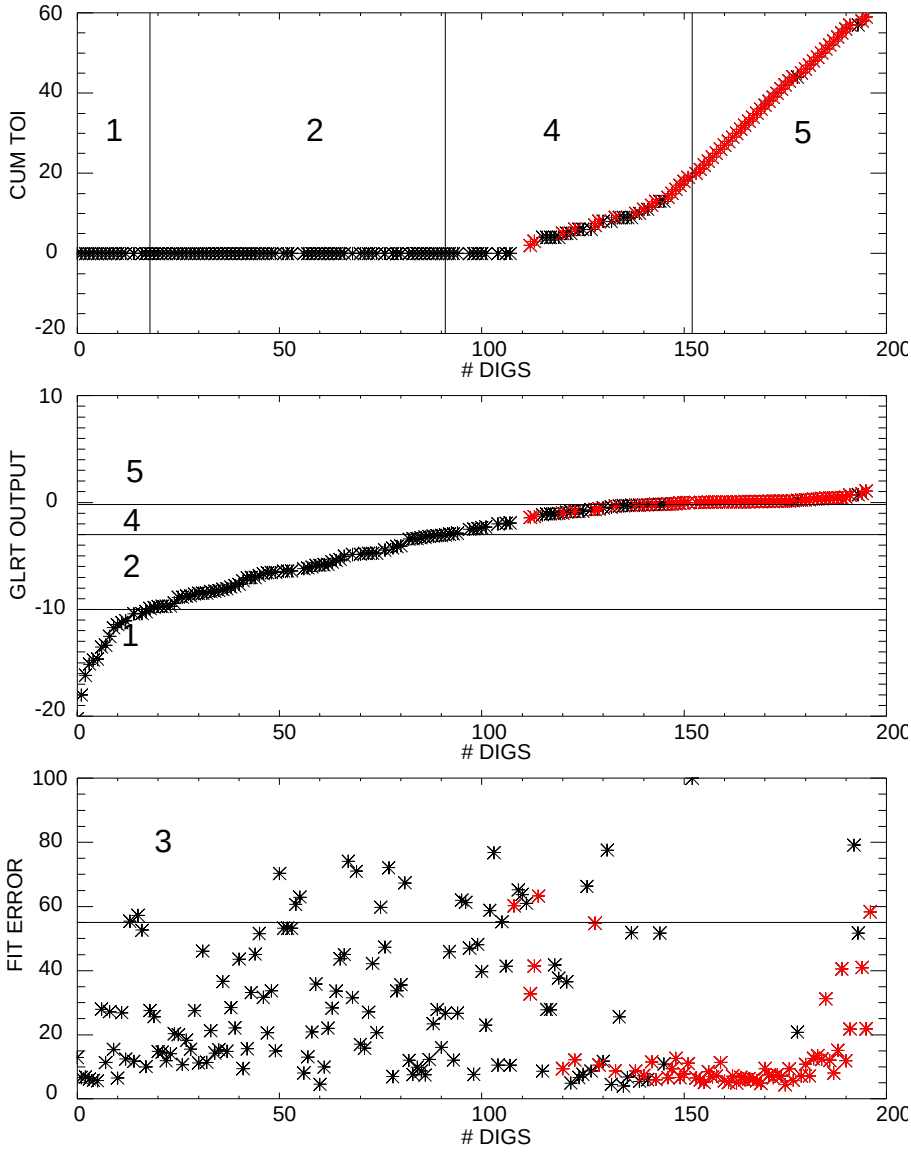

Figure 4-50 GEM-3 Array training data and selected thresholds.

4.3.3.4. Performance Scores from IDA

Scoring performances for the GEM-3 array analysis are reported in Table 4-12 and shown graphically in Figure 4-51. A ROC chart is shown in Figure 4-52.

Using the established thresholds, there was one False Negative. Anomaly #135 was declared high confidence clutter when in fact it was an emplaced 4.2-inch mortar. Anomaly #133 was declared Category 2 (low confidence clutter) but was also a seeded UXO.

Table 4-12 Performance Summary: GEM3 Array Constrained/Unconstrained Analysis

GEM-3 Array

	Cultural	Munition Debris	No Contact	Rock	Soil	UXO
1	104	317	5	17	21	1
2	4	44	0	5	15	1
3	18	37	11	23	97	1
4	1	20	0	5	7	38
5	0	5	0	0	4	78
TOTAL	**127**	**423**	**16**	**50**	**144**	**119**

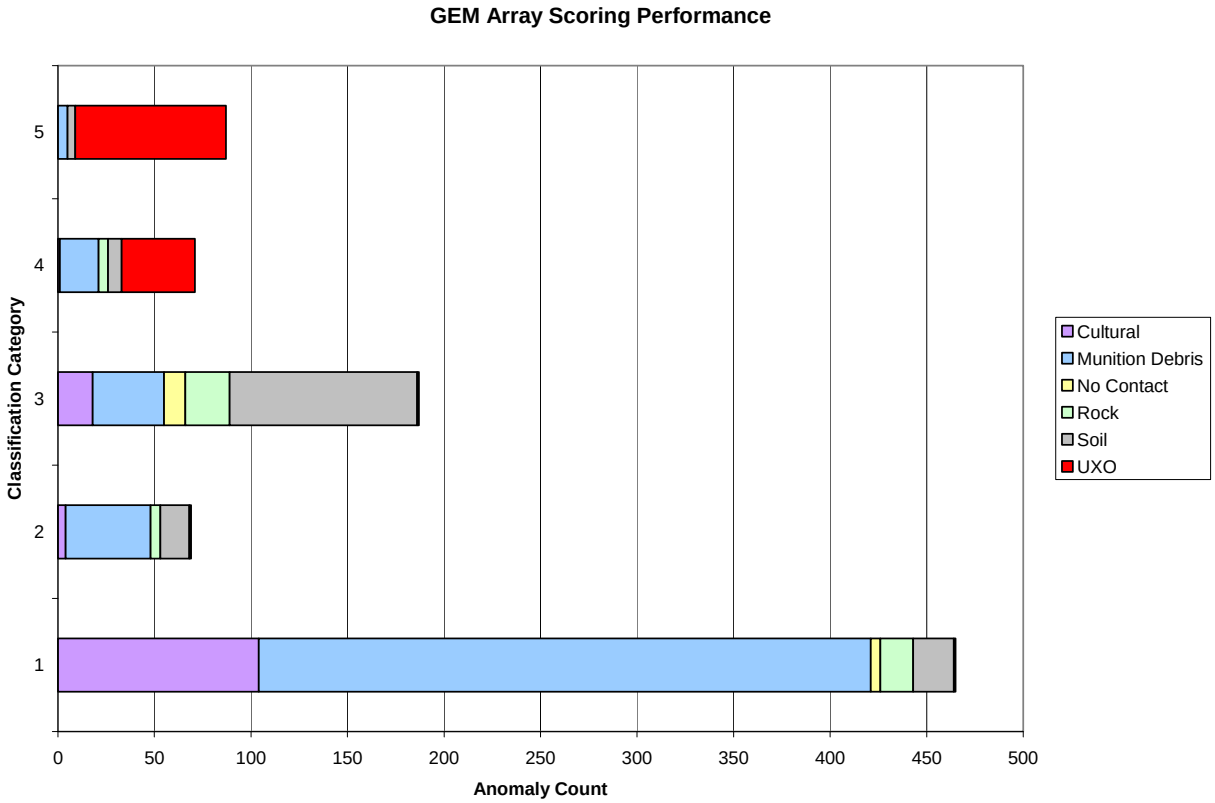

Figure 4-51 GEM-3 Array performance as a function of classification category.

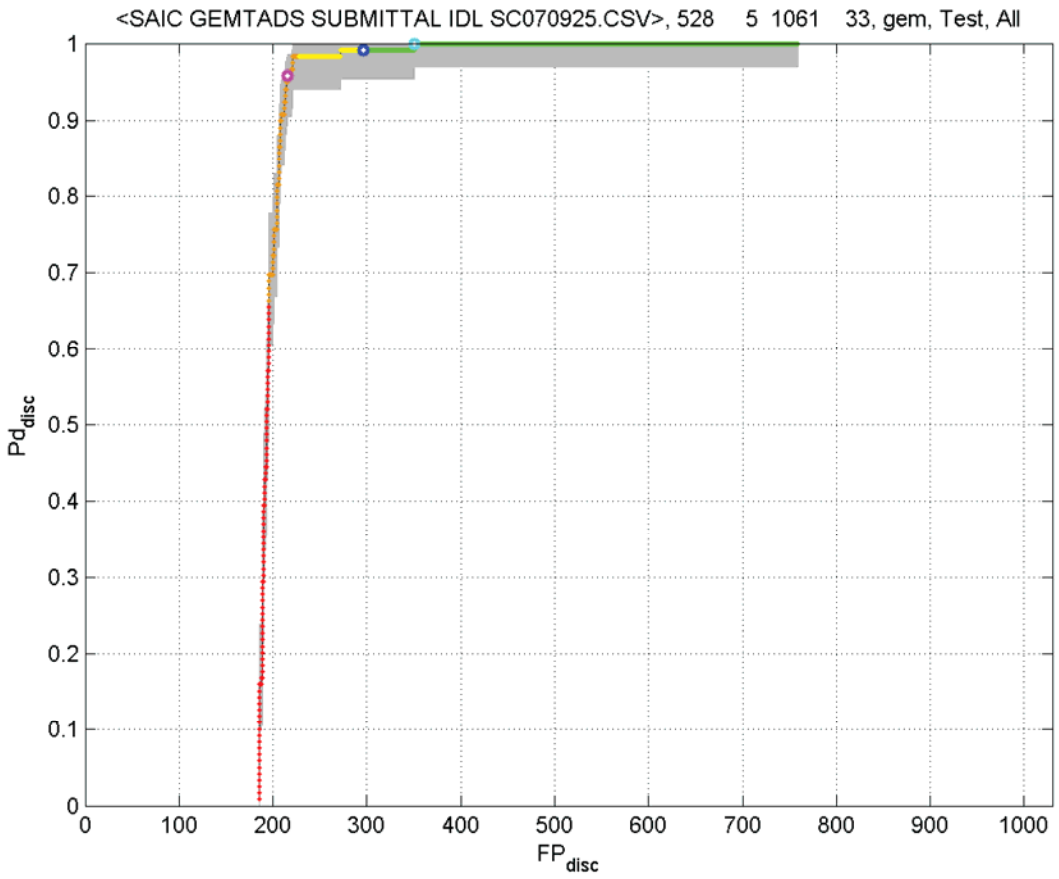

Figure 4-52 GEM-3 Array ROC chart; analyzed comparing library-constrained and unconstrained inversions.

4.3.3.5. Characterization Plots

The RMS error between the fitted and measured XY locations for seeded 4.2-inch mortars is 0.17m with a standard deviation of 0.10m. Figure 4-53 plots the distance between inverted and measured locations for UXO and clutter, segmented by discrimination ranking.

The RMS depth error for seeded 4.2-inch mortars is 0.15m with a standard deviation of 0.16m. Figure 4-54 plots the fitted depth versus measured depth for UXO and clutter, segmented by discrimination ranking.

Figure 4-55 plots the net polarizability for quadrature response at 570 Hz, for each of the 119 seeded 4.2in mortars. For the GEM-3 array data, the mean net polarizability was 2.555 with a standard deviation of 0.218. The corresponding COV is 0.097.

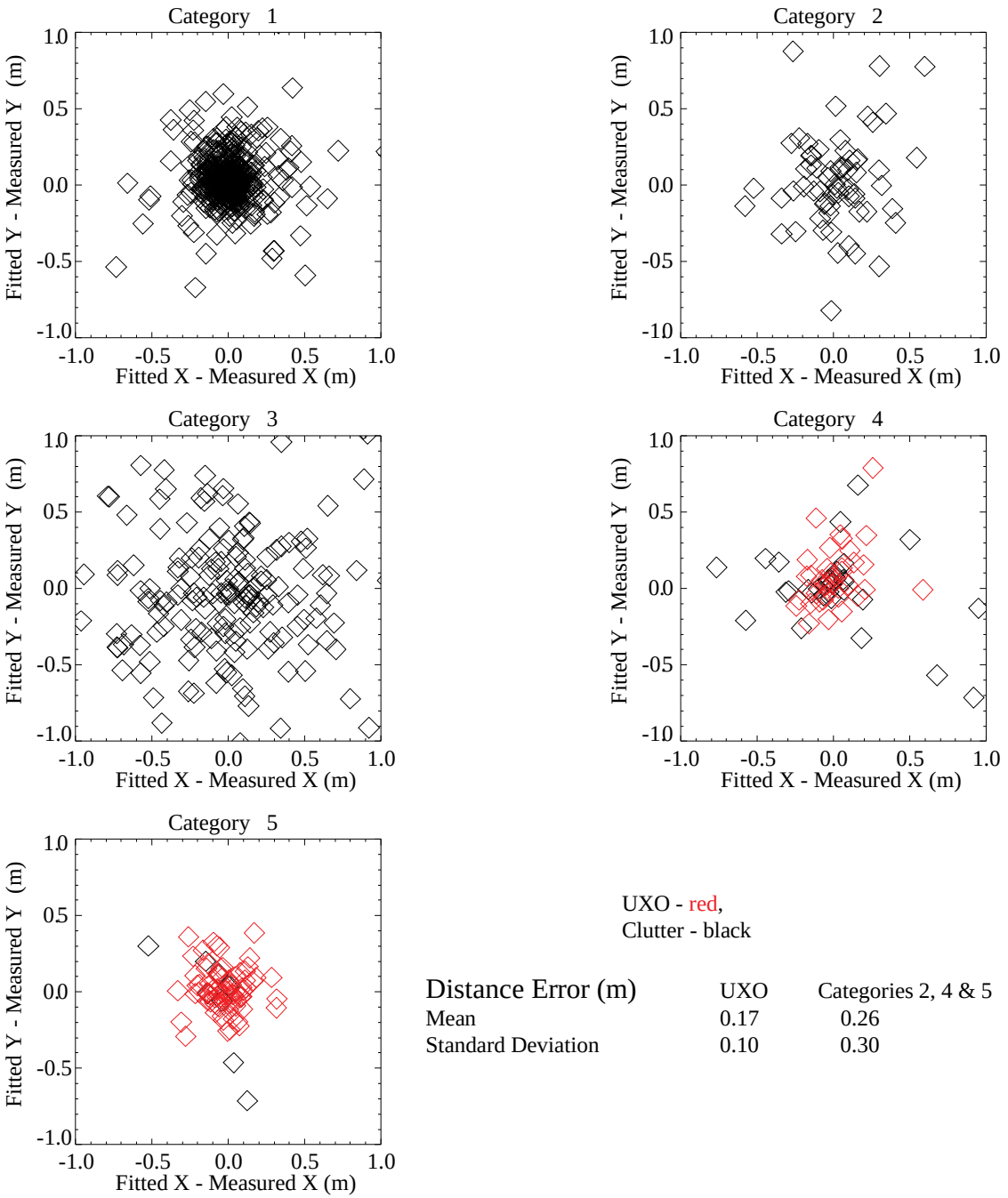

Distance Error (m)	UXO	Categories 2, 4 & 5
Mean	0.17	0.26
Standard Deviation	0.10	0.30

Figure 4-53 Differences between fitted and measured XY locations; GEM-3 array

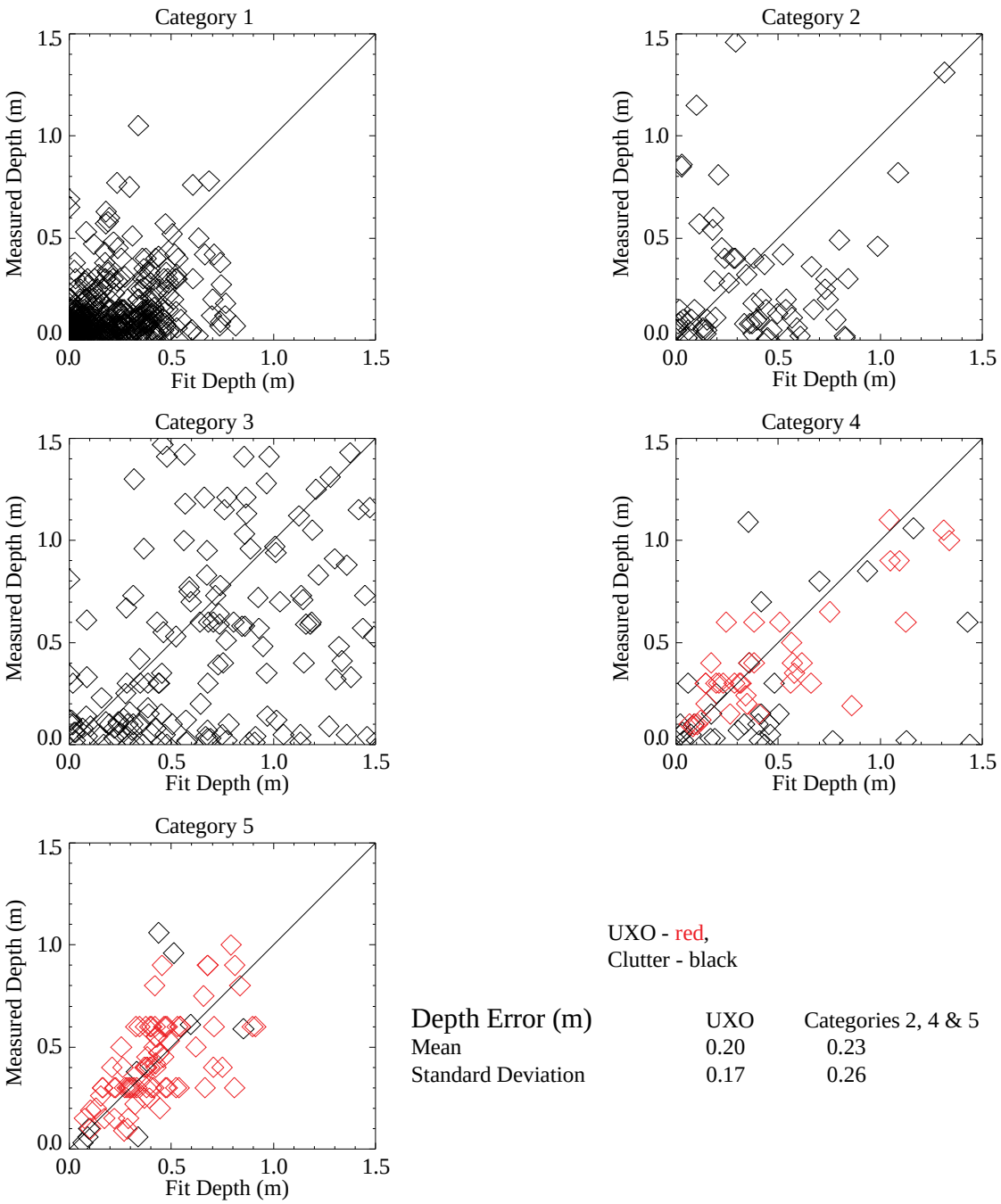

Depth Error (m)	UXO	Categories 2, 4 & 5
Mean	0.20	0.23
Standard Deviation	0.17	0.26

Figure 4-54 Fitted versus measured depth of burial; GEM-3 array

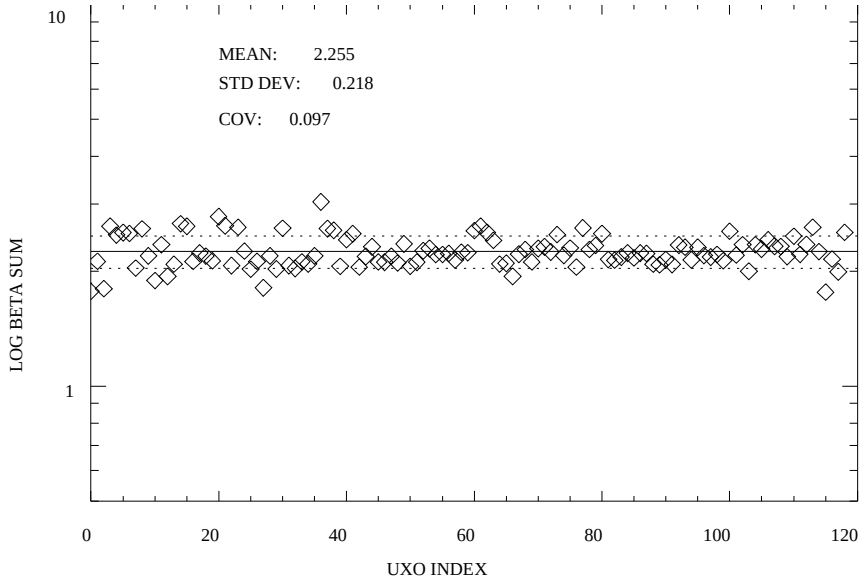

Figure 4-55 Raster of the Σβ, which is a measure of size, for 4.2in mortars, GEM-3 array. Dashed lines are ± one standard deviation.

4.3.3.6. Failure Analyses

Anomaly #135 was a seeded 4.2-inch mortar but was classified high confidence clutter (Category 1) using the constrained/unconstrained approach. A reexamination of the field data revealed that one pass of the array had elevation offsets relative to nearby transects (Figure 4-56). The corrupt elevation (z) readings gradually returned to normal after traveling 100m. The GEM-3 data were interleaved to increase spatial sampling. The poor z positioning of these transects of data altered the inverted polarizations such that it was not fit well using our library representing 4.2-inch mortars. Anomaly #133 was affected by the poor elevation data as well and was categorized low confidence clutter (Category 2).

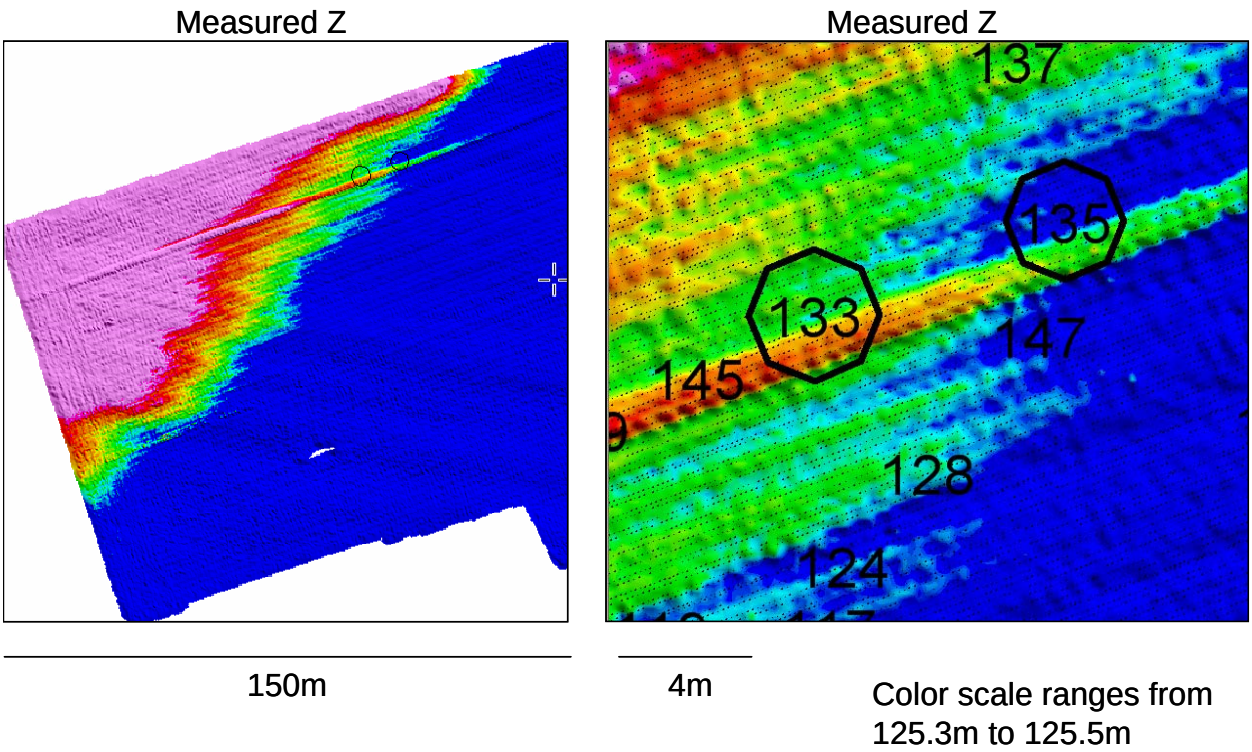

Figure 4-56 Contoured elevation data for GEM-3 sensor in vicinity of the single false negative (#135).

4.3.4 MAGNETIC ARRAY DATA

4.3.4.1. Data Presentation, Description, and Pre-processing

Data from the magnetic array (Figure 4-57) is shown in Figure 4-58 thru Figure 4-60. The circles identify anomalies selected for analysis by the ESTCP Program Office.

Figure 4-57 Magnetic array

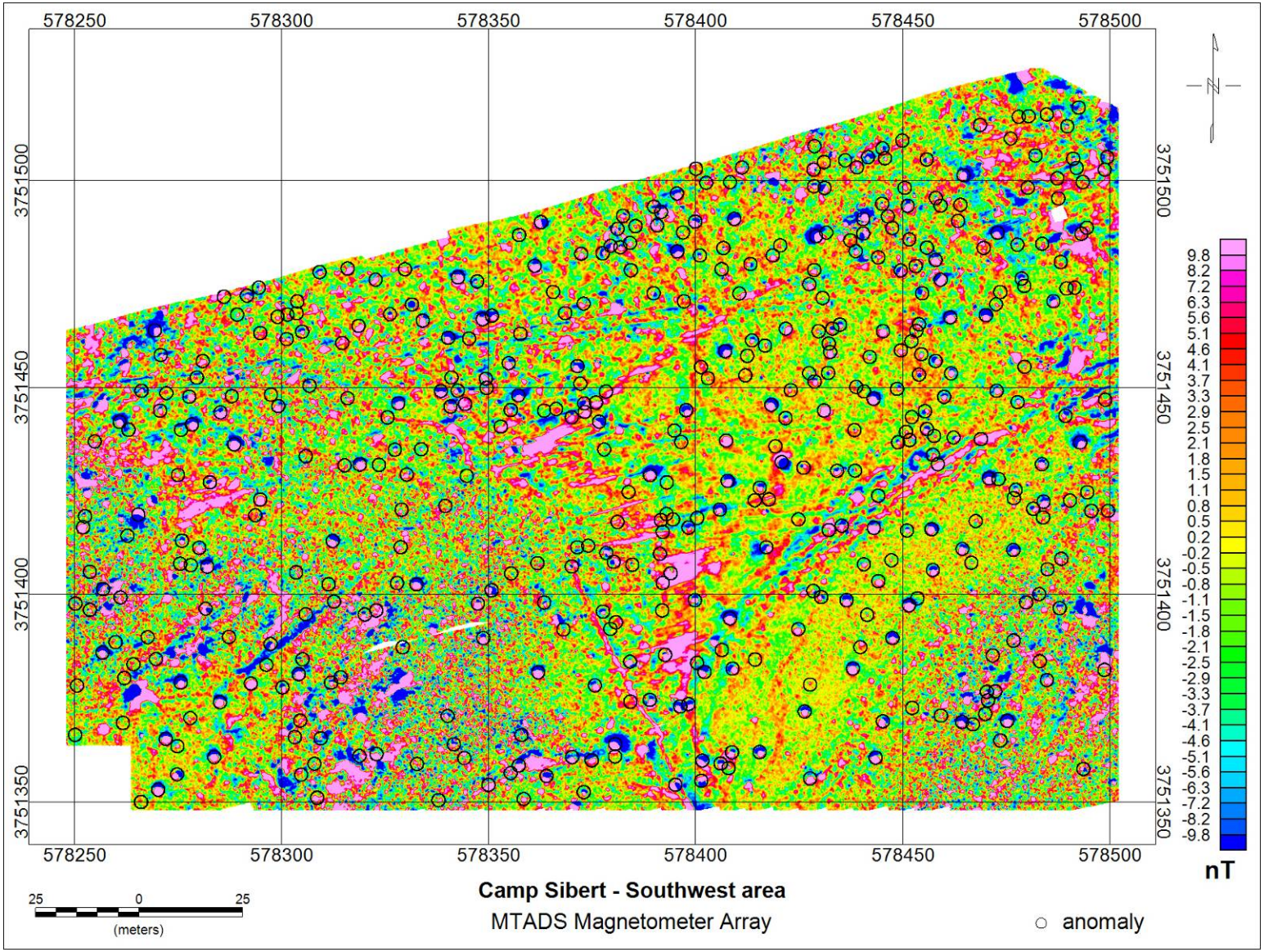

Figure 4-58 Magnetic array data; Southwest area.

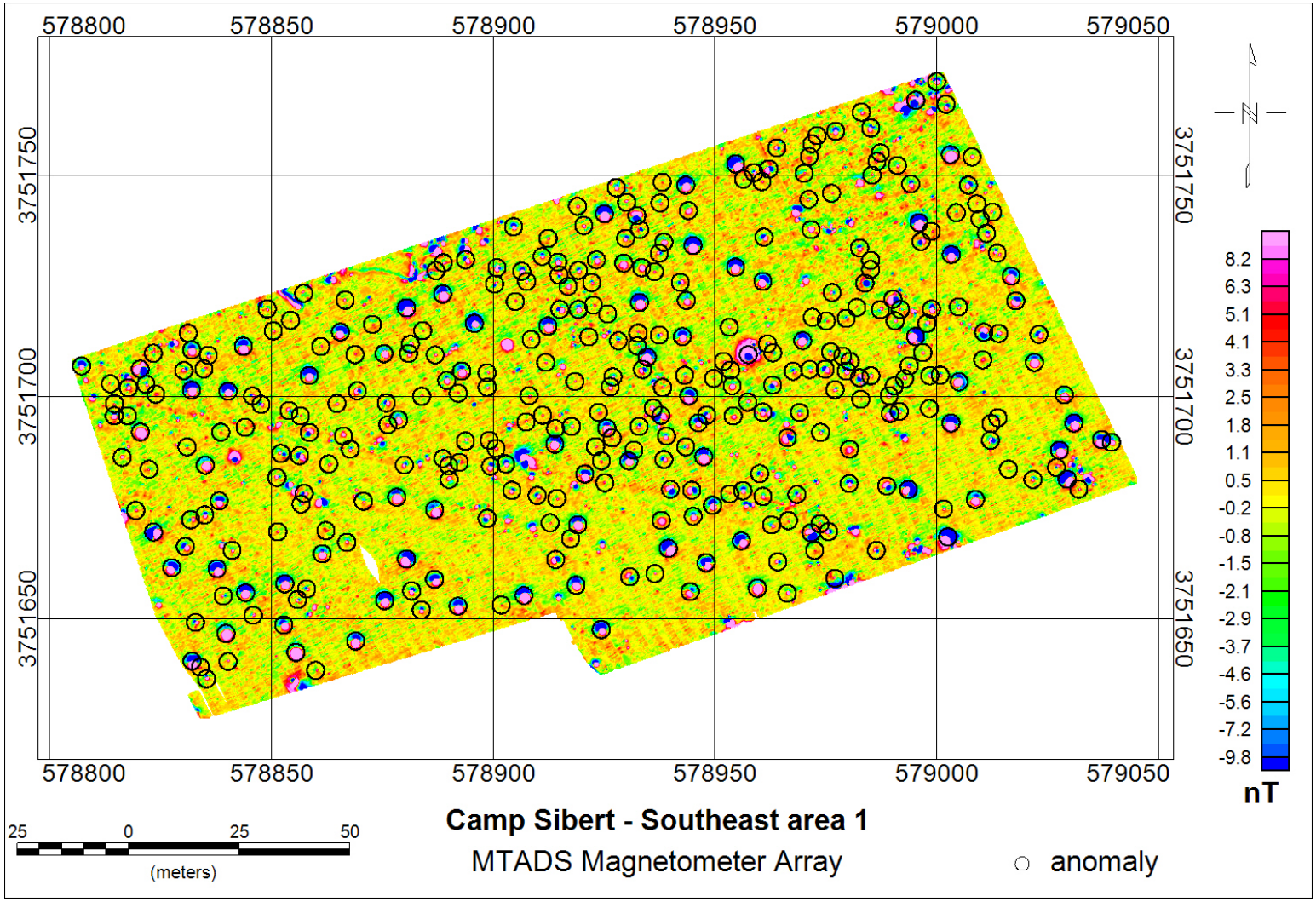

Figure 4-59 Magnetic array data; Southeast area 1.

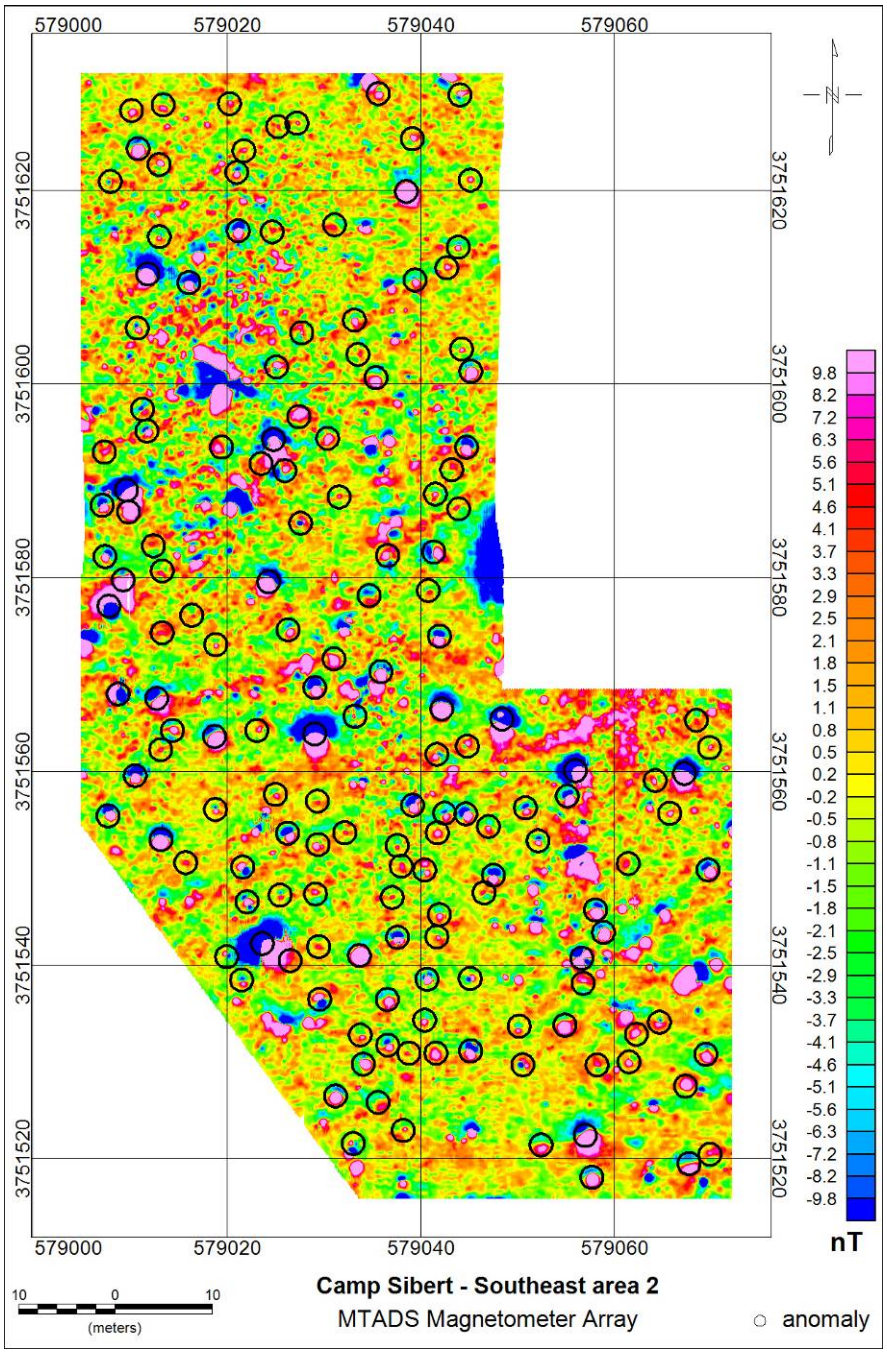

Figure 4-60 Magnetic array data; Southeast area 2.

4.3.4.2. Inversion Approach

The magnetic dipole model for this method inverts for the location (X_0, Y_0, Z_0), magnetic moment (radius of an equivalent sphere), and orientation angles (*declination and inclination*). The model used here first fits the shape of the footprint, then its magnitude. Initial guesses for the fit parameters are determined internally within the code based on the measured signature. The goodness of fit metric, ε, is the squared correlation of data and model. By definition, the dipole fit error metric is equal to $\sqrt{1-\varepsilon}$.

4.3.4.3. Labeled data – threshold selection

Classification of the magnetic array data was based on the apparent size (scaled magnetic moment). Figure 4-61 presents fitted results for all labeled data. In the figure, the data are prioritized according to apparent size and color coded according to the actual labels. Based upon these labeled data, we established the following thresholds:

Category 1: <0.055
Category 2: 0.055 to 0.069
Category 3: fit error greater than 60%
Category 4: 0.069 to 0.10
Category 5: >0.10

The threshold between categories 2 and 4 was set based on first UXO encountered. The thresholds between categories 1 and 2 and between 4 and 5 were set to accommodate observed uncertainty.

Mitigating factors included the following: (1) if the inversion failed, the anomaly was declared Category 3.

4.3.4.4. Performance Scores from IDA

Scoring performances for the magnetic analysis are reported in Table 4-13 and shown graphically in Figure 4-62. A ROC chart is shown in Figure 4-63.

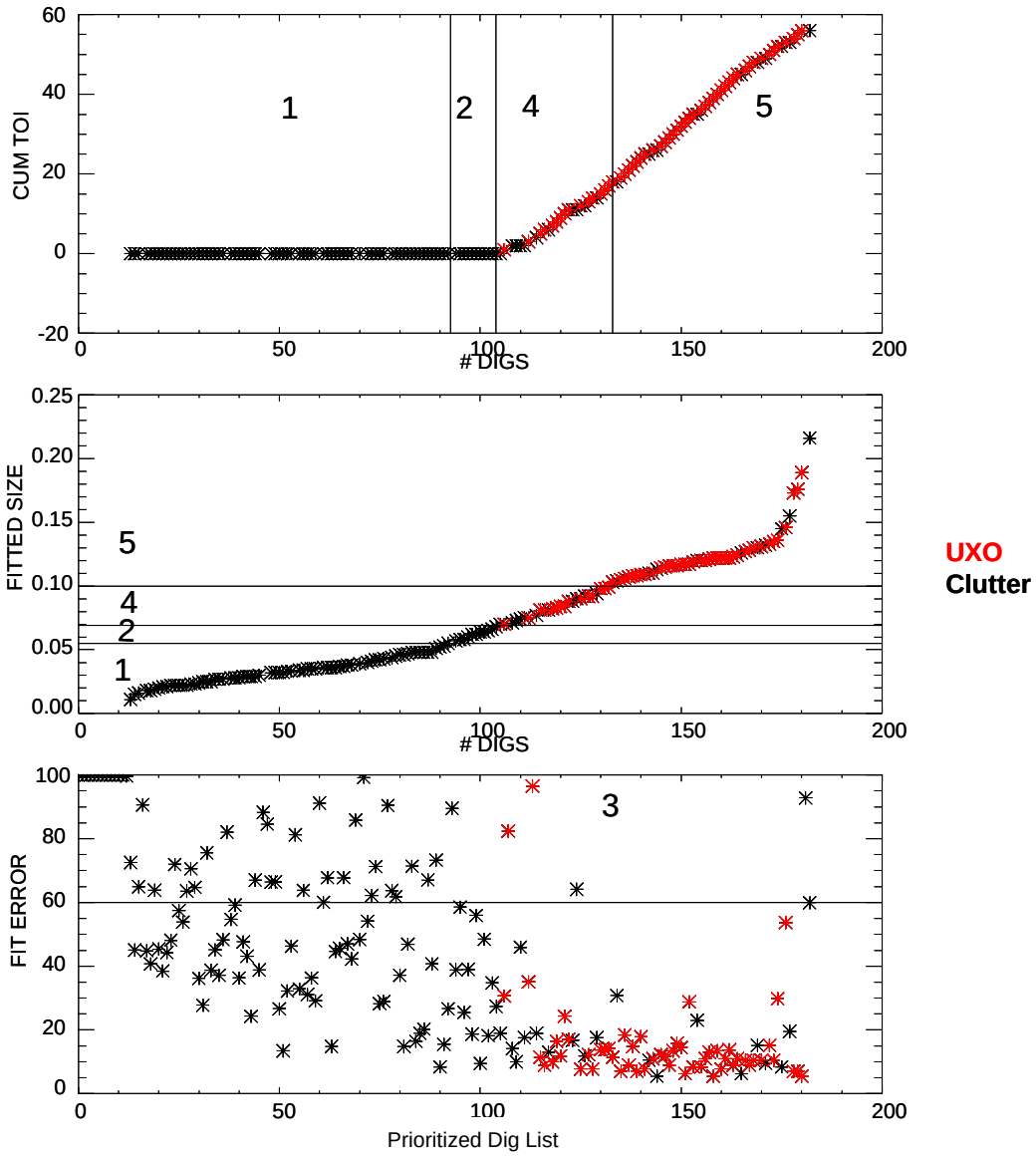

Figure 4-61 Magnetic array training data and selected thresholds; UX-Analyze analysis.

Table 4-13 Performance Summary Magnetic Array

MAG Array

	Cultural	Munition Debris	No Contact	Rock	Soil	UXO
1	60	258	2	18	22	0
2	4	41	1	3	12	3
3	35	63	2	42	56	0
4	1	33	0	3	15	45
5	1	23	1	2	8	70
TOTAL	**101**	**418**	**6**	**68**	**113**	**118**

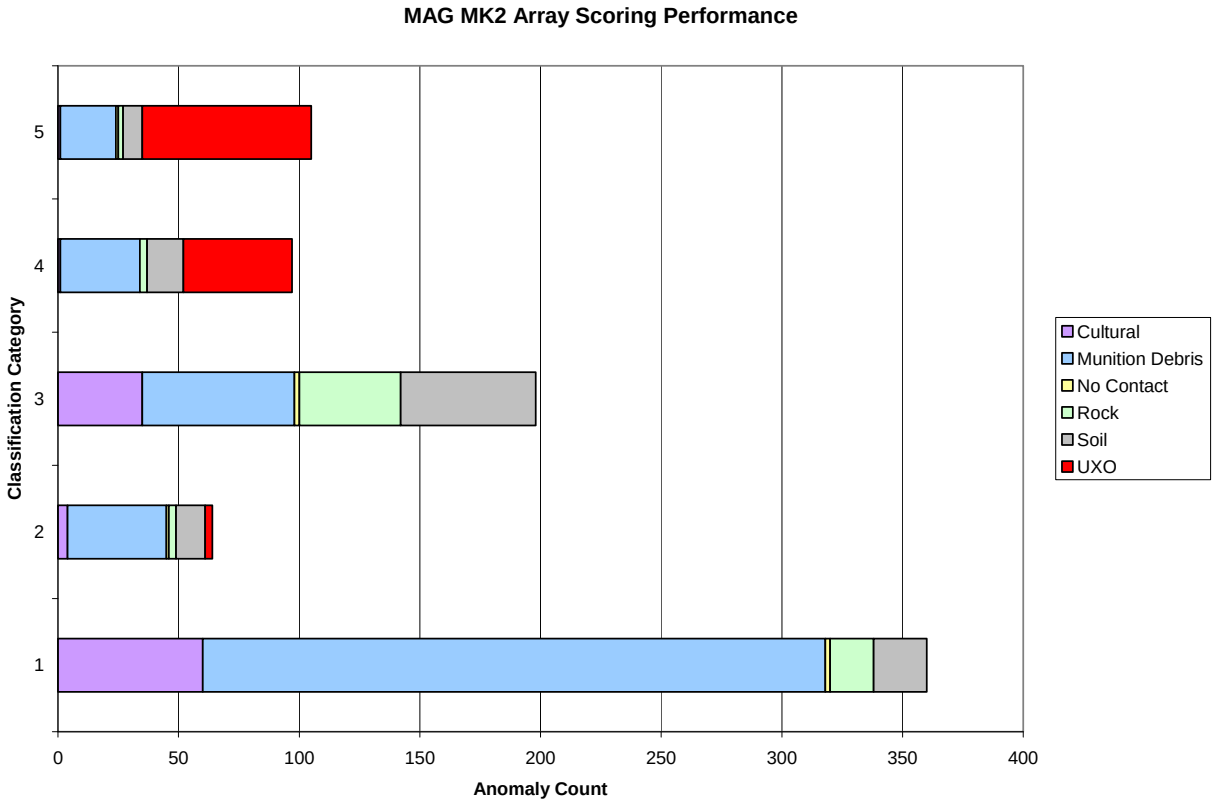

Figure 4-62 Magnetic Array performance as a function of classification category.

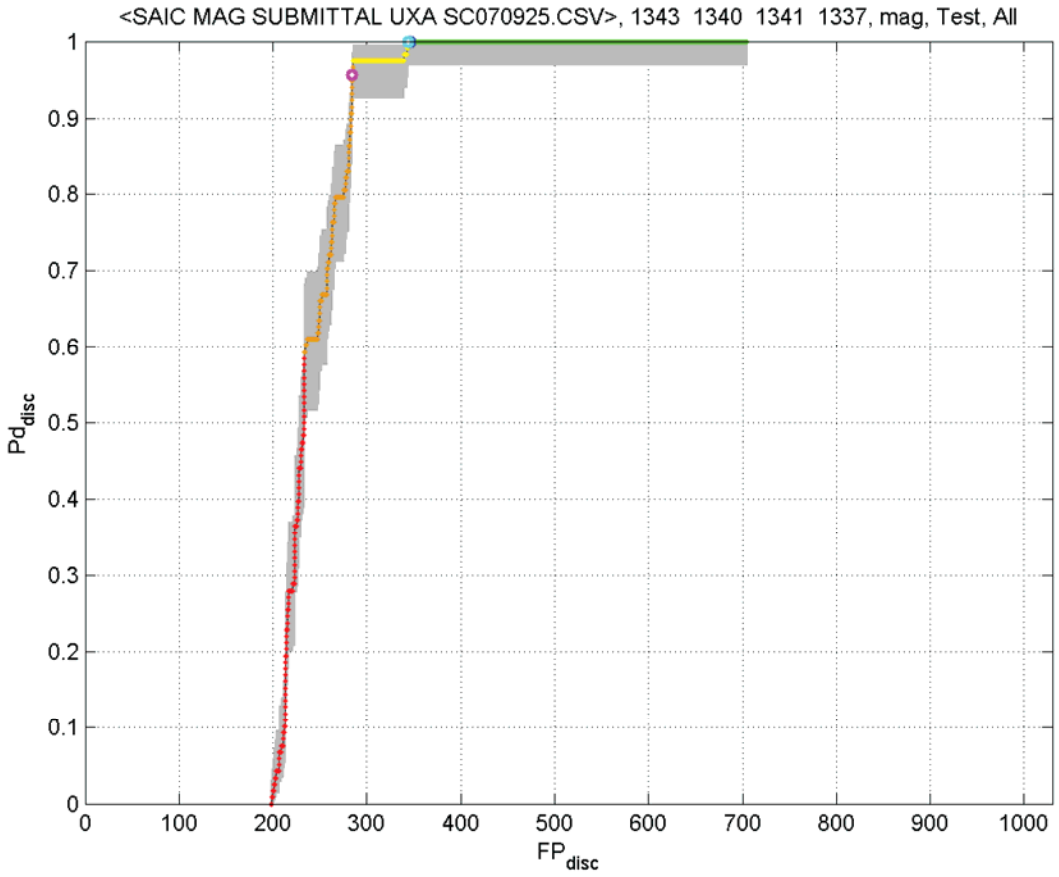

Figure 4-63 Magnetic Array ROC chart

4.3.4.5. Characterization Plots

The RMS error between the fitted and measured XY locations for seeded 4.2-inch mortars, based on magnetic array inversion results, is 0.14m with a standard deviation of 0.10m. Figure 4-64 plots the distance between inverted and measured locations for UXO and clutter, segmented by discrimination ranking.

The RMS depth error for seeded 4.2-inch mortars is 0.098m with a standard deviation of 0.12m. Figure 4-65 plots the fitted depth versus measured depth for UXO and clutter, segmented by discrimination ranking.

Figure 4-66 plots the fitted size, i.e., scaled magnetic moment, for each of the 119 seeded 4.2in mortars. For the magnetic array data, the mean fitted size was 0.105 with a standard deviation of 0.025. The corresponding COV is 0.24.

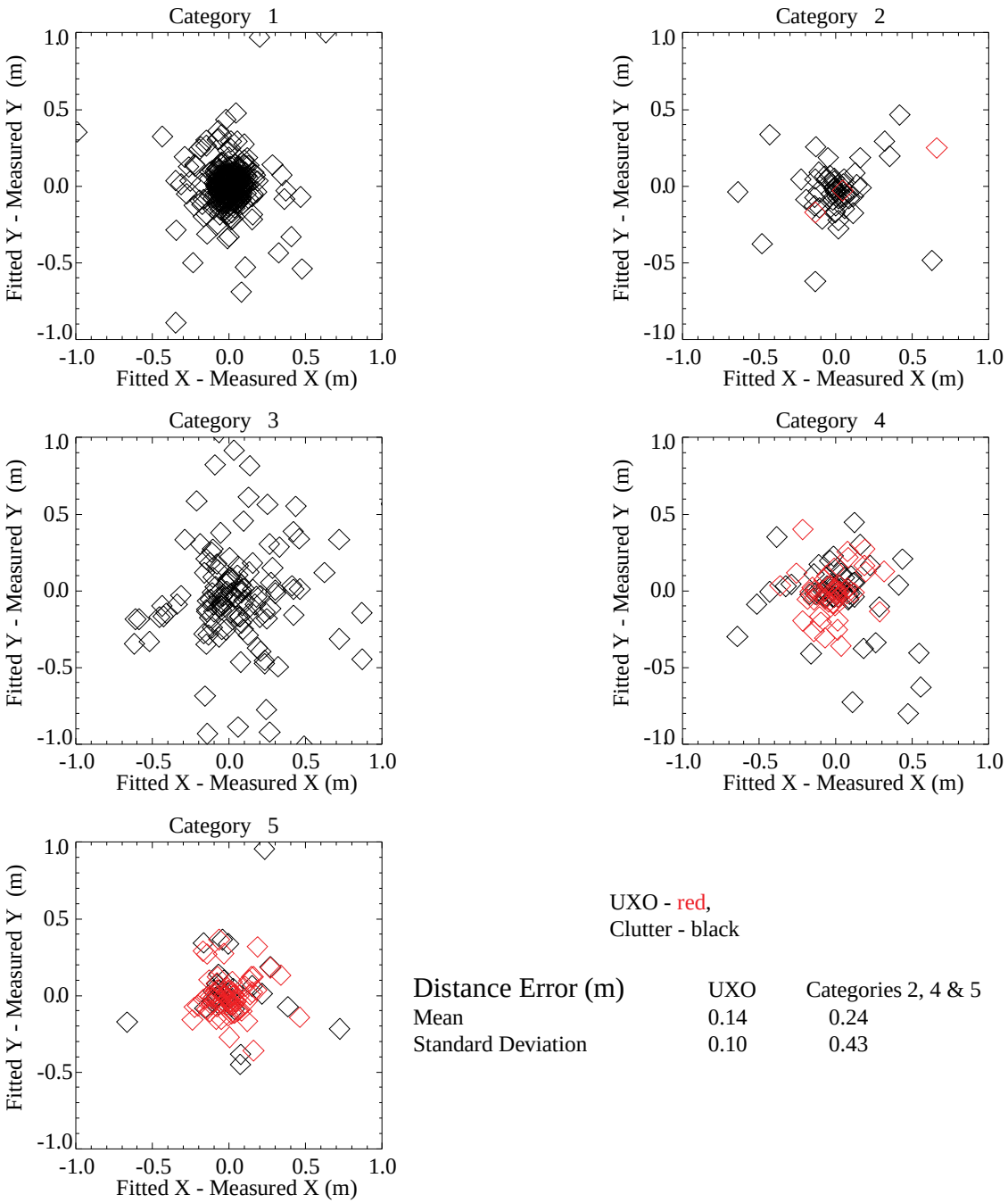

UXO - red,
Clutter - black

Distance Error (m)	UXO	Categories 2, 4 & 5
Mean	0.14	0.24
Standard Deviation	0.10	0.43

Figure 4-64 Differences between fitted and measured XY locations; magnetic array

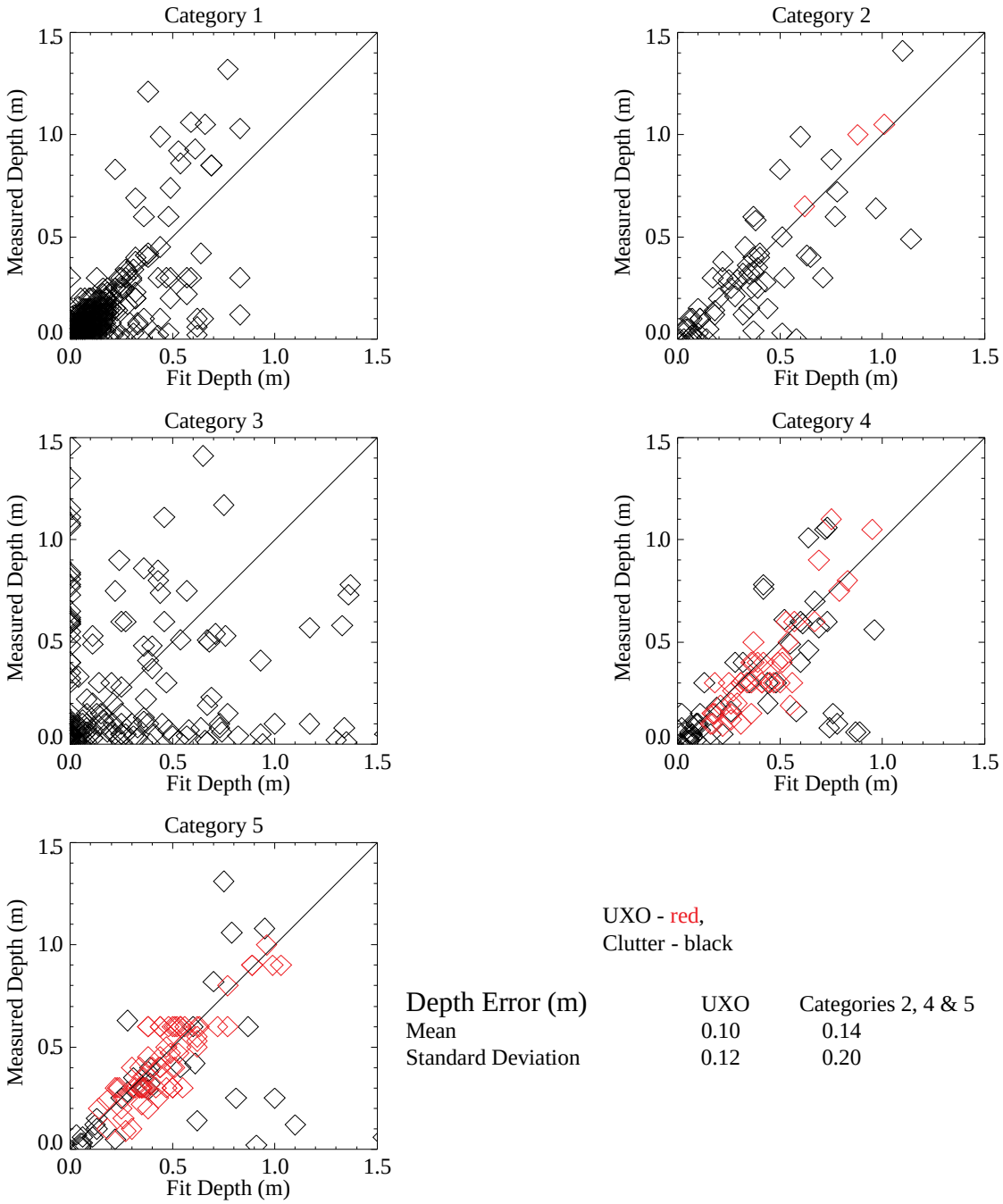

Depth Error (m)	UXO	Categories 2, 4 & 5
Mean	0.10	0.14
Standard Deviation	0.12	0.20

Figure 4-65 Fitted versus measured depth of burial; magnetic array

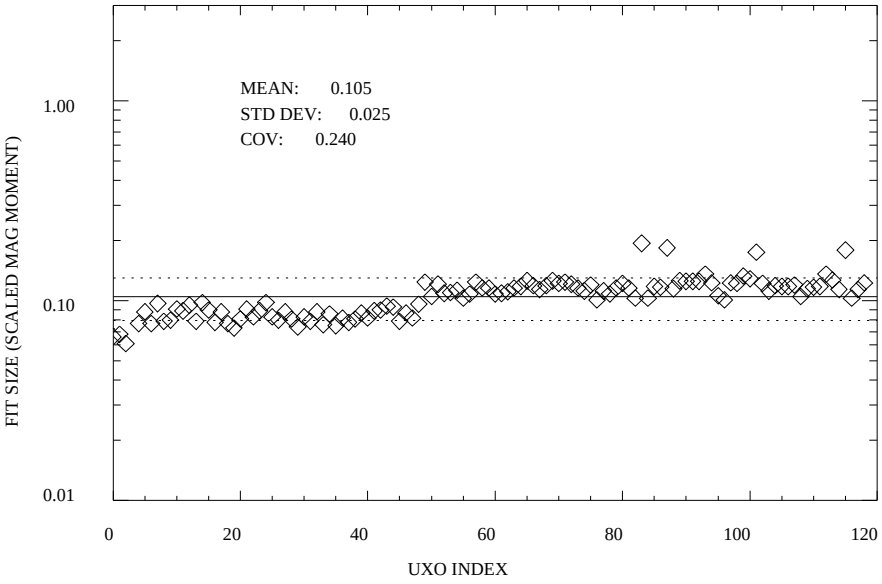

Figure 4-66 Raster of the fitted size for 4.2in mortars, magnetic array

4.3.4.6. Failure Analyses

Using the thresholds adopted for this analysis, there were no false negatives.

Anomalies 149, 170, and 197, all seeded 4.2-inch mortars were declared Category 2 based on inverted apparent sizes of 0.066, 0.068, and 0.061 (Figure 4-67; Figure 4-68). We refit each of these anomalies using different solvers and polygons during post mortem analysis and recovered similar model parameters.

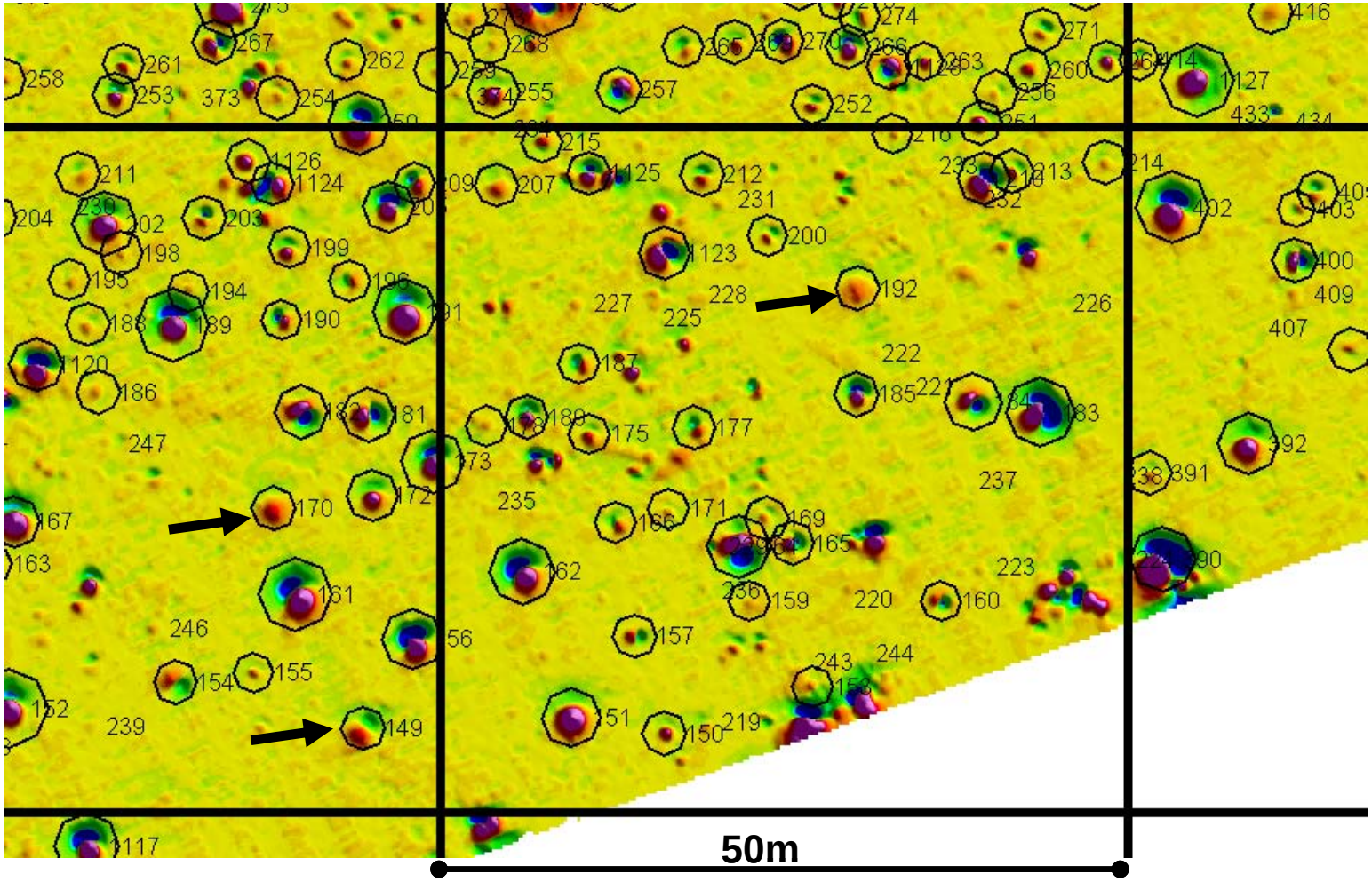

Figure 4-67 Color contour map of magnetic data. Arrows identify three seeded targets that possessed fitted sizes of less than 0.068 (Category 2 declarations). Color scale ±25nT.

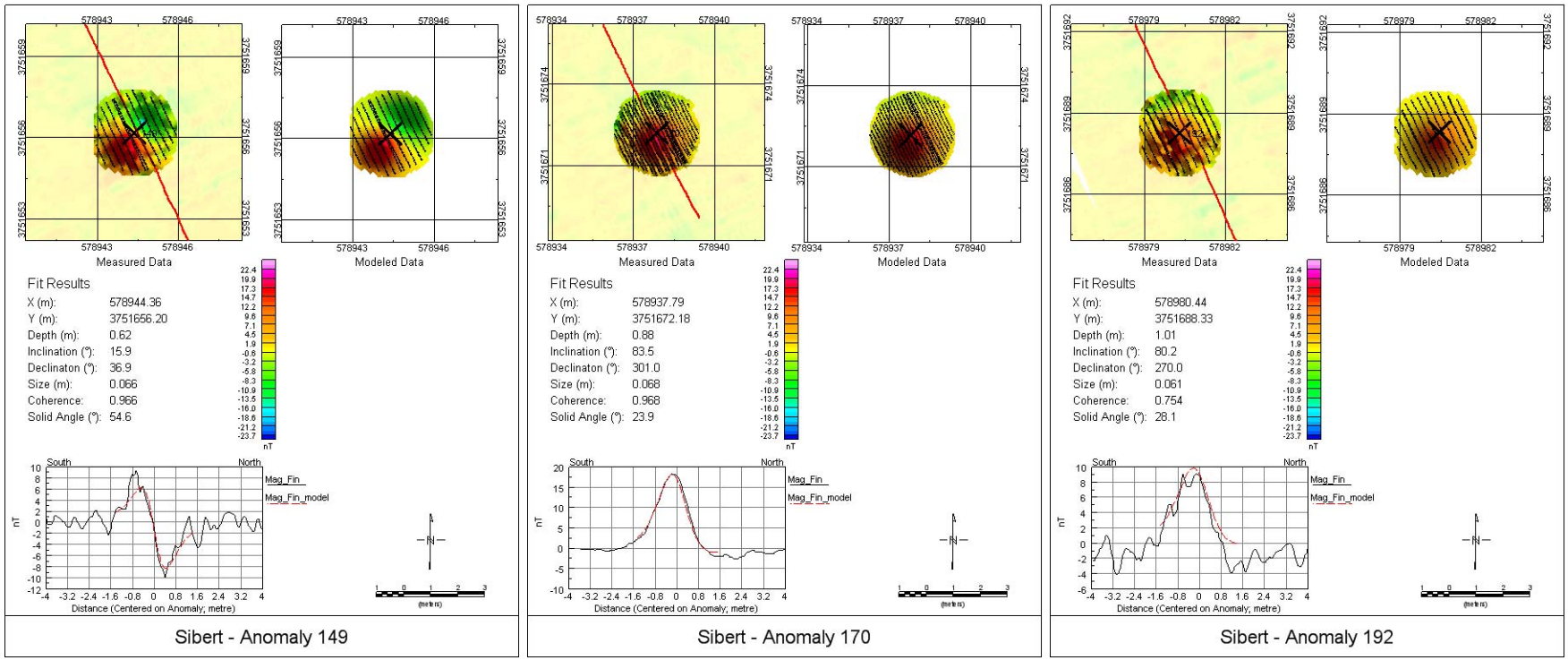

Figure 4-68 Anomaly plots showing inverted features and forward model for three anomalies 4.2-inch mortars that possessed apparent sized of less than 0.07 (Category 2).

4.3.5 COMBINED EM61 MK2 AND MAGNETIC ARRAY FEATURES

4.3.5.1. Overview

For the Combined Magnetic and EM dig list, we inverted the EM61 MK2 and magnetic array data independently, as described in Sections 4.3.1 and 4.3.4, and combined the features using conservative Boolean logic operators. In order to produce a combined ranking for targets surveyed by either one or both of the two systems, decision metrics from (i) EM only, (ii) magnetic only, and (iii) GLRT classifier output using magnetic size and EM coherence ratio as inputs, were involved in the final categorization.

It should be remembered that our magnetic-only categories were based solely on the inverted size. The EM only categories were based on the coherence ratio of the library-constrained fit versus the unconstrained fit. The EM decision metrics therefore are influenced by size and shape estimates. Based upon the labeled data, the EM classifications performed better than the magnetic. Because of this, slightly more confidence was given to the EM-only results in the event of different classifications. The combined category was based on the following Boolean rules:

1) if the anomaly was surveyed by only one instrument, adopt the corresponding category
2) if the anomaly was surveyed by both, then:
    a. if the EM only is high confidence UXO, then adopt the EM Category
    b. if EM-only and magnetic-only were each Category 3 or 4, then assign Category 4 (reduce the number of can't analyze declarations)
    c. otherwise, adopt the combined GLRT-assigned category.

4.3.5.2. Performance Scores from IDA

Scoring performances for the constrained versus unconstrained analysis approach are reported in Table 4-14 and shown graphically in Figure 4-69. A ROC chart is shown in Figure 4-70.

Table 4-14 Performance Summary Joint Magnetic & EM61 Array

JOINT MAG & EM61 ARRAYS

	Cultural	Munition Debris	No Contact	Rock	Soil	UXO
1	112	361	7	38	129	0
2	4	16	0	3	10	1
3	36	47	1	65	59	0
4	2	44	1	4	21	15
5	0	17	0	0	5	125

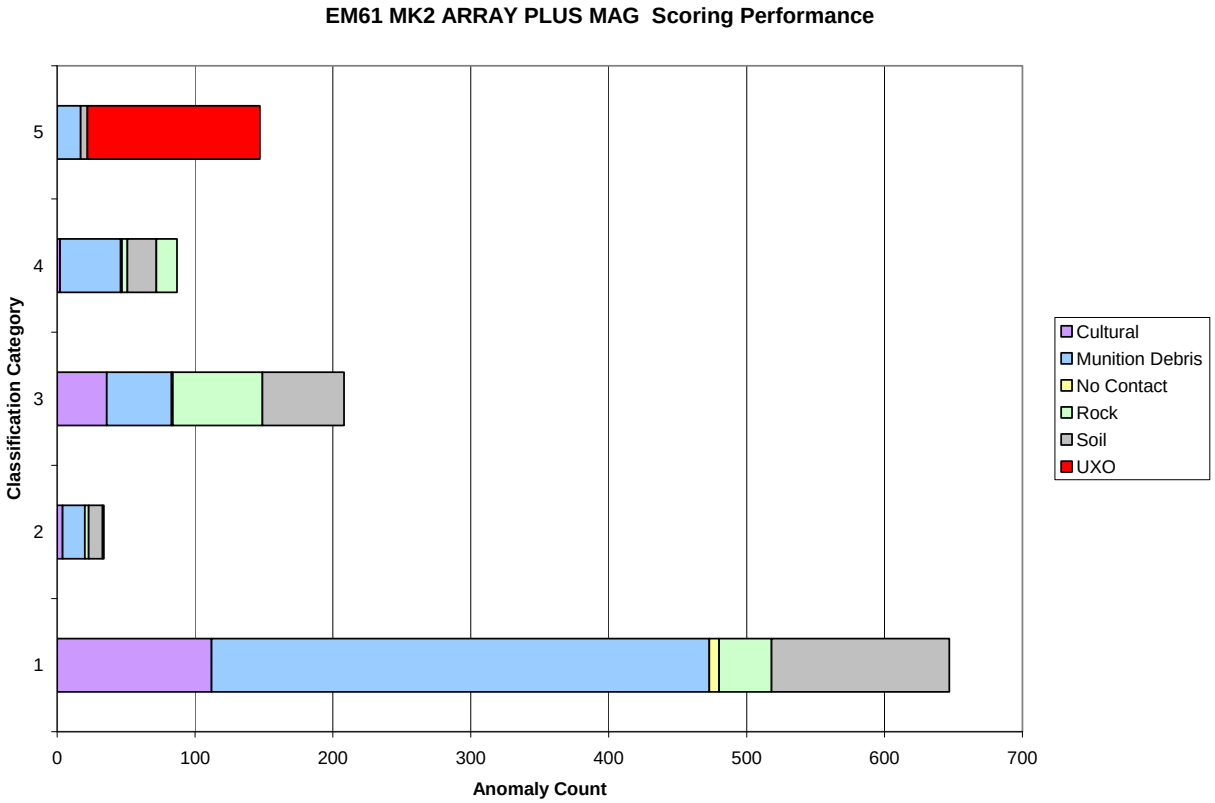

Figure 4-69 Magnetic Array performance as a function of classification category

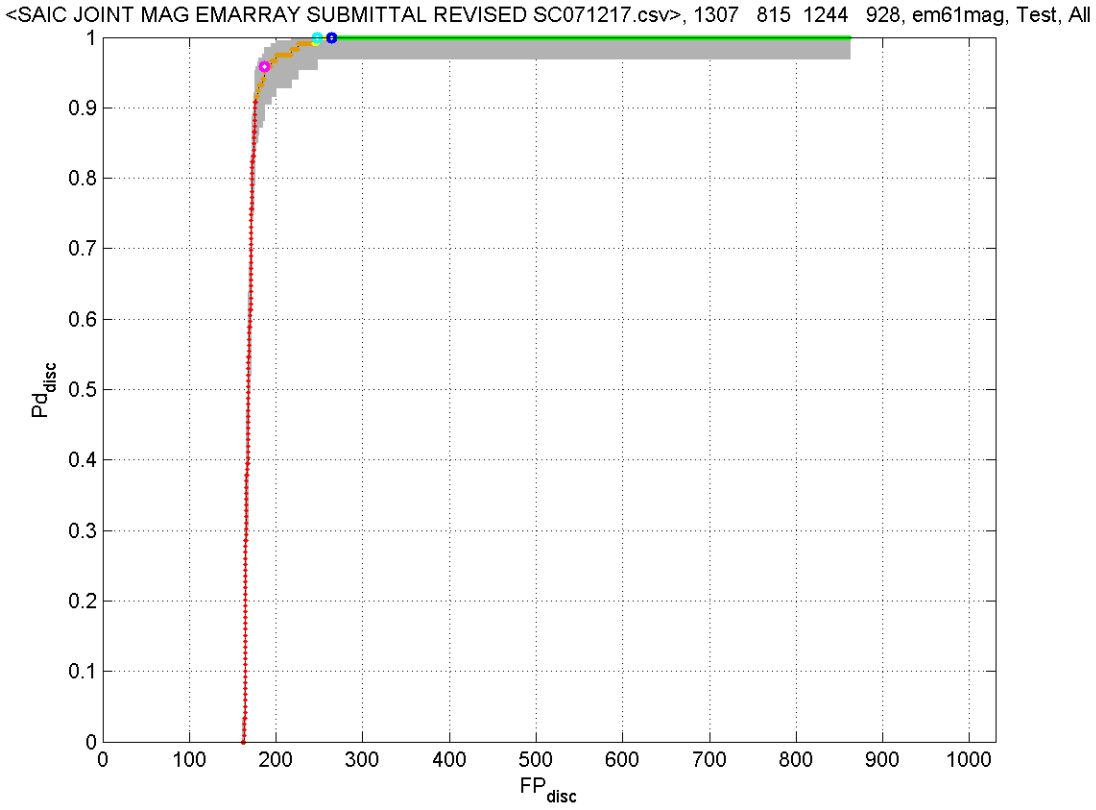

Figure 4-70 Magnetic Array ROC chart

4.3.5.3. Failure Analyses

Using the thresholds and logic adopted for this analysis, there were no false negative.

Anomaly #192 was a seeded mortar and was ranked Category 2. It was the last Category 2 target before Category 4. For this anomaly, the magnetic-only Category was 2, the EMI-only Category was 2, and the GLRT combined Category for this anomaly was 2. Anomaly #420, which was a false negative failure of the EM61 MK2 array only processing (§4.3.2.1) due to positioning errors, was not a failure in this analysis because the magnetic-only analysis classified it as a Category 4 based on apparent size.

4.4 In-air Clutter Measurements

After the excavations were complete, 803 clutter items were re-numbered (to protect their identity) and shipped to Blossom Point by the Program Office (Table 4-15). Basically, the idea was to collect data in a controlled setting in order to collect extremely high-quality data that could be used to establish discrimination bounds for this collection of UXO and clutter. By recording signatures for each object individually, at optimal coil-target separations, the in-air controlled tests inherently removed all positioning errors, eliminated any possible overlapping signatures, eradicated motion noise, and did away with any soil response.

Time-domain EMI data were collected using the G&G Science array developed under funding from MM-0601 (Figure 4-71). It consists of 25 transmit (Tx)/receive (Rx) pairs arranged in a 5x5 fixed-separation grid. For these tests, we used the central 9Tx coils and recorded the decay, using all 25Rx coils, from 0.04msec to 25msec. We performed dipole inversions for all signatures to obtain principal axis polarizabilities (approximately 5% were too small to produce decent inversion results). The data are of excellent quality. Fits for an example mortar and large, medium, and small clutter are shown in Figure 4-72 through Figure 4-75 respectively.

The net polarizability, defined here as $\Sigma\beta i$ for t = 0.04-0.06 msec (Figure 4-76), indicates that perfect discrimination is possible for this distribution of UXO and clutter using only size estimates. As shown in the figure, the 4.2in mortar target strength is clearly larger than any clutter item.

Table 4-15 In-air TEM measurements of Sibert clutter

Camp Sibert	Half-shell	63
	Base plate	91
	Nose frag	97
	Misc clutter	552
	Total	**803**

Figure 4-71 The prototype time domain EMI (TEM) sensor developed under MM-0601 was utilized to measure responses of all Sibert clutter.

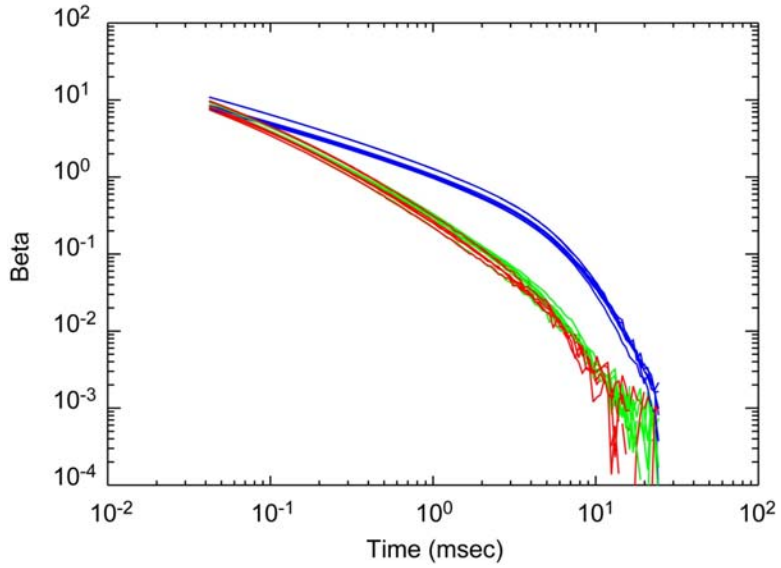

Figure 4-72 Principal axis β decay curves for 4.2in mortar (seed target 42-073). Six different location/orientation combinations.

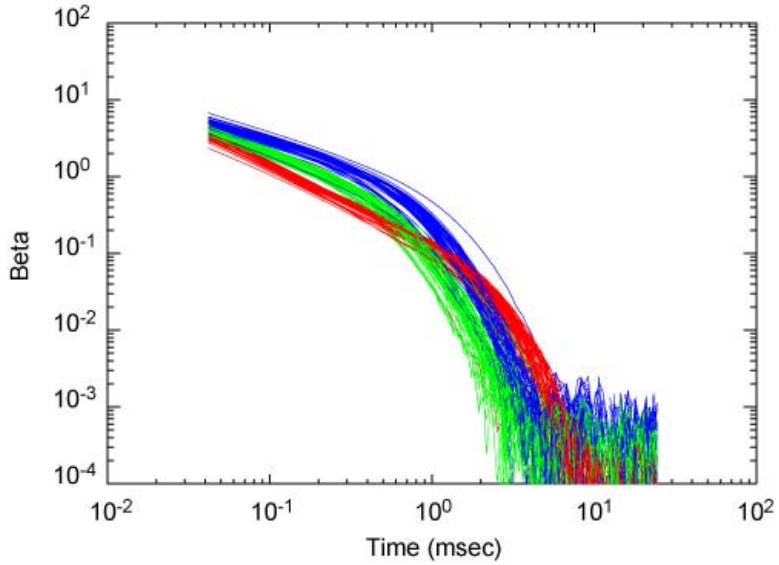

Figure 4-73 Principal axis β decay curves for large clutter (half shells)

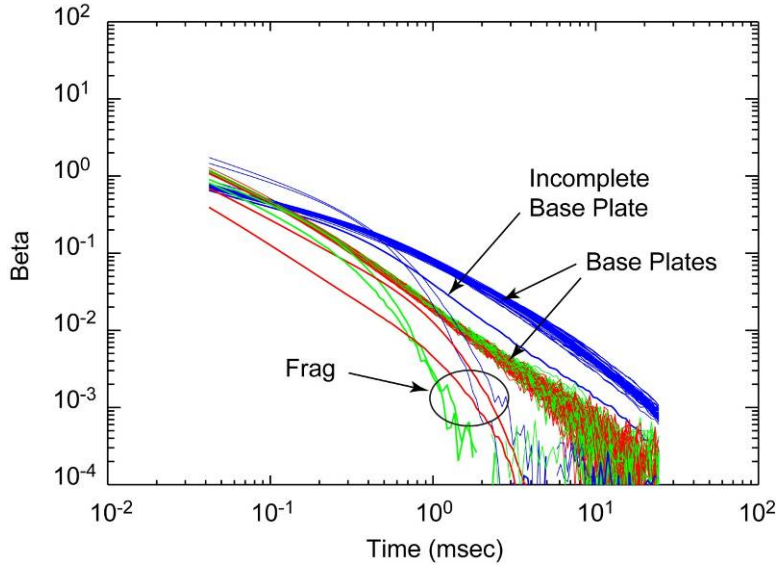

Figure 4-74 Principal axis β decay curves for medium clutter (base plates, etc.)

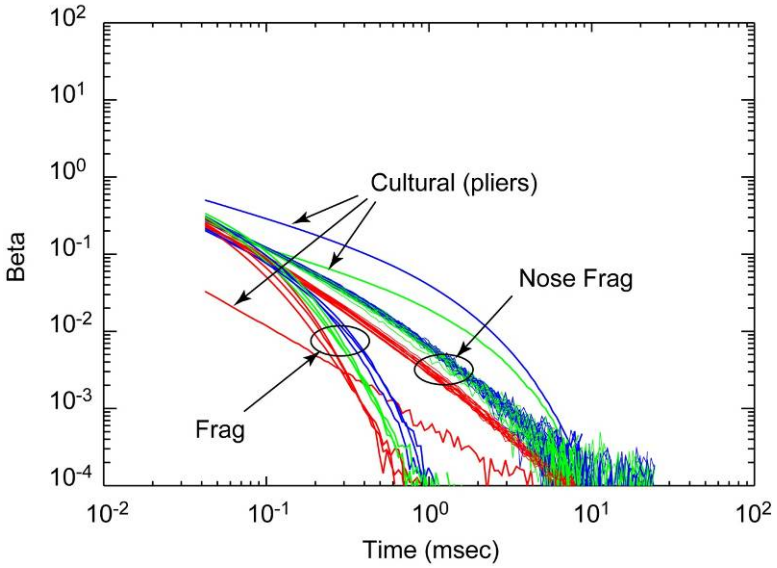

Figure 4-75 Principal axis β decay curves for small clutter

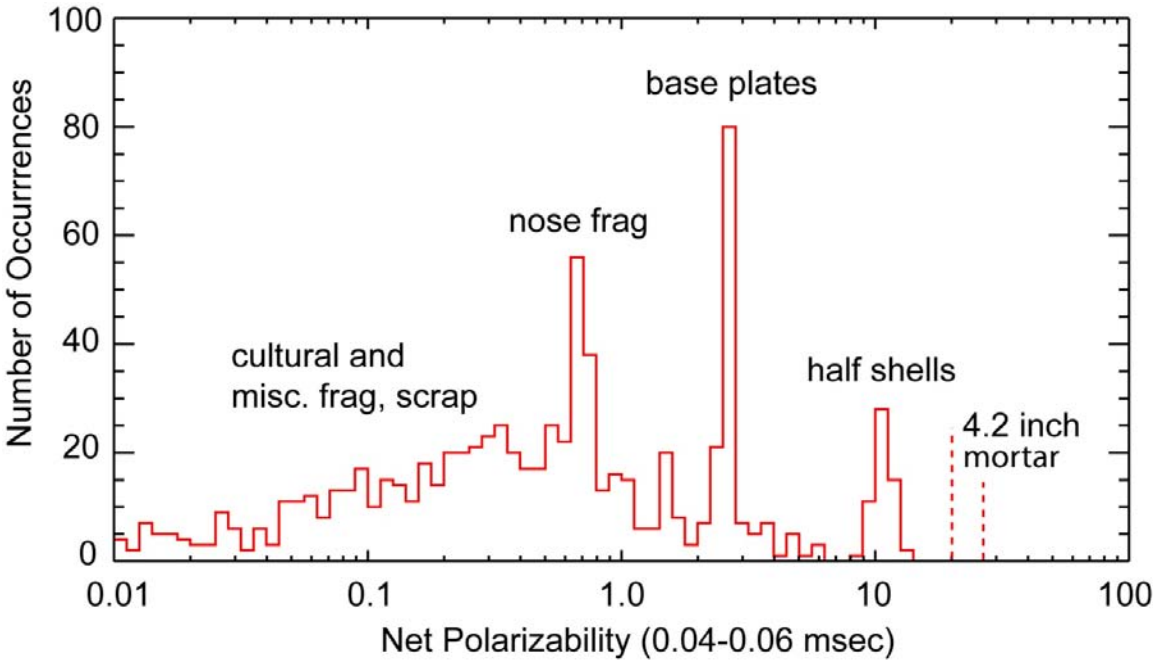

Figure 4-76 In-air target strength (net polarizability, Σβi for t = 0.04-0.06 msec) suggests perfect discrimination is possible for this collection of TOIs and clutter. The 4.2-inch mortar target strength is clearly larger than any clutter item

5. Discussion

We were provided magnetic and/or EMI data and target selections (ID, XY), and were asked to discriminate between native clutter objects and 4.2in mortars, whether seeded or native (no native 4.2in mortars recovered). Because 4.2in mortars generally produce high SNR responses, the primary problem became one of discriminating the mortars that were deeply buried and therefore possessed broad, low-amplitude responses that could be masked by geology. Data shown in Figure 5-1 illustrates the issue. The circles in the figure identify the seeded 4.2in mortars. As shown here, not all of the high amplitude anomalies are caused by 4.2in mortars and, conversely, not all of the small amplitude anomalies are clutter. Our objective was to identify as many clutter objects as possible without misclassifying any 4.2in mortars.

Figure 5-2 shows photographs of items recovered during the demonstration. The largest clutter items were the half shells, which were presumably created when the 4.2in shell casings split open at impact.

Anomalies were selected by the Program Office based on thresholds. The thresholds were set to be one-half of the observed sensor-dependent magnitude for 4.2in mortars buried at their maximum (11x) depth. Because of this selection method, the number of anomalies identified for analysis varied across data types (Figure 5-3).

The EM61 cart data possessed variable time lag that degraded the fitted results (Figure 5-4). To alleviate this problem, we added a time lag parameter to the solver used for the EM61 cart data.

We processed and classified each data type independently and did not compare results. Because of the size difference in the TOI versus clutter at this site, however, a significant fraction of the targets were identified as high confidence clutter regardless of data type or classification approach (see Category 1; Figure 5-5).

As discussed in §4, we based our classifications on (i) the estimated size or (ii) fit ratios using a library that consisted only of 4.2in responses. The second approach inherently includes size and shape information.

Performance results for size based classifications of magnetic and EMI data are shown in Figure 5-6. Although both approaches performed well (Table 4-4 and Table 4-6), the EMI-based results had fewer Can't Analyze declarations and better separation between classes than the magnetic (as visually observed by the slope of the curve as well as AUC of 0.97 for EMI versus 0.91 for magnetic).

We analyzed the EM61 array twice. Different inversion routines and classification schemes were used. As detailed above, one approach performed a non-linear simultaneous inversion for all model parameters and based the classification on apparent size. The second performed a multi-step inversion that involved stepping through z, non-linear and linear searches, and

schemes to avoid local minima. The classification metric for the second approach involved comparisons of fit quality of unconstrained versus library constrained inversions. The approaches were indeed quite different. The performances, however, are strikingly similar (Figure 5-7). No significant differences in the ROC curves are apparent with the notable exception that the library-based approach had one false negative (failure). Because the library-based approach incorporates size and shape information (in the form of the library), it is more sensitive to glitches in the data. Our post-mortem analysis revealed that the false negative was indeed caused by a GPS data problem that went unnoticed during analysis.

A performance comparison of cart versus array deployment methods for the EM61 MK2 sensor shows minor differences in the shape of their respective ROC curves (Figure 5-8). There were, however, differences of significance. First, the cart data classified 9 TOIs as Can't Analyze (Category 3) due to large fit errors. Second, the cart-based analysis had one false negative failure.

A conceptual model useful for framing the problem is to divide the ROC curve shown in Figure 5-9 into three areas; (A) can't analyze, (B) analyzed-and-dig, and (C) analyzed-but-do-not-dig. Clearly, our objective is to (i) reduce the number of 'can't analyze' declarations, (ii) reduce the number of analysis failures in the 'analyzed-and-dig' category, and (ii) quantify the residual risk in the 'analyzed-but-do-not-dig' space.

With regard to the 'analyzed-and-dig' category, our post mortem analysis revealed that some of the failures, and many of the near failures, were caused by spatial registration problems. We discovered problems with the measured GPS elevation and timing lags (Figure 5-10).

Excluding the EM61 cart data, the sources of the 'Can't Analyze' declarations turned out to be small fragments, scrap metal, no contact, or soil. These anomalies were characterized by low amplitude responses and small spatial footprints and were not, therefore, well characterized by our models (Figure 5-11, Figure 5-12).

As shown in §4.4 In-air Measurements, the 4.2in mortars had target strengths that were clearly larger than any of the clutter. In other words, based on size estimates alone, these in-air measurements suggest perfect discrimination is possible for this distribution of UXO and clutter. Figure 5-13 compares the net polarizability of the in-air measured responses to the EM61 array field data. For field data, the β spread results in overlap between UXO and clutter. Geolocation errors are a likely factor in the observed 30% RMS β spread. In Figure 5-14, we approximated the β error using the mortar distribution and used it to smear out the in-air distributions. After accounting for β spread, the in-air and EM61 array field data have similar distributions for net polarizabilities > 0.1. Differences for weak targets ($\Sigma\beta < 0.1$) are consistent with increasingly poor fit quality and inability to classify.

In summary, it is possible to separate 4.2-inch mortars from native clutter found at this site using geophysical data acquired in survey mode:

1. Size-based decisions worked fairly well. Over 43% of the targets were rejected as 'high confidence clutter' without failure using size-based decisions.
2. GPS positioning errors caused the classification failures for the EM61 array and GEM-3 array data. The single false negative in the EM61 cart analysis was caused by a poorly defined spatial footprint.
3. In-air target strengths of 4.2-inch mortars are larger than any clutter item, indicating that perfect discrimination is possible, for this set of UXO and clutter, using systems that mitigate or eliminate positioning errors and motion noise.

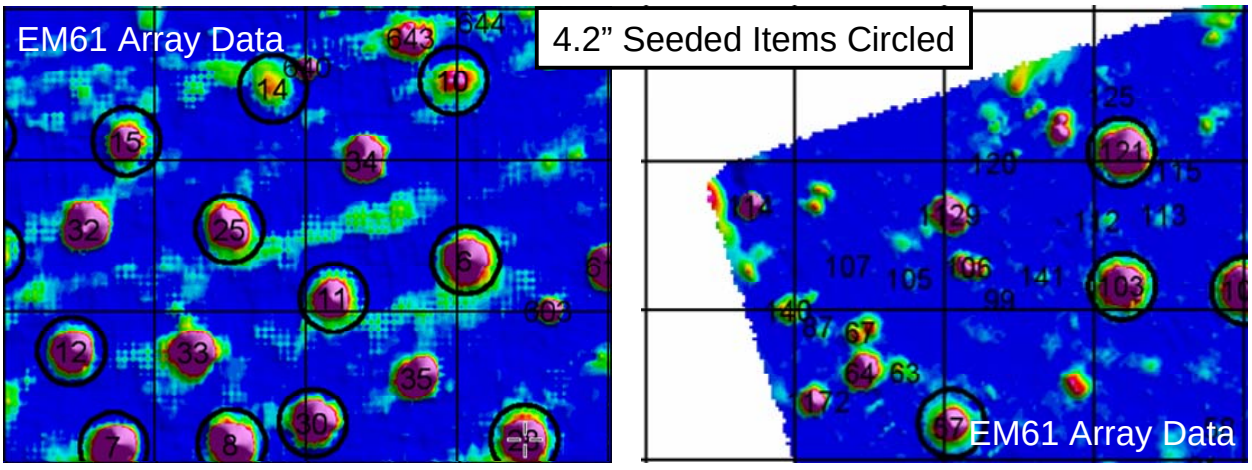

Figure 5-1 EM61 MK2 array data from the geophysical prove out (left) and southeast 1 area (right)

Figure 5-2 Photographs of objects recovered from the Sibert demonstration area

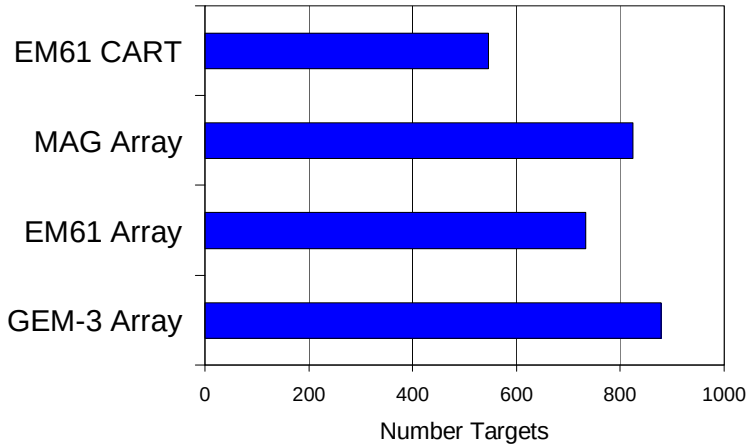

Figure 5-3 Number of anomalies identified varied across data sets

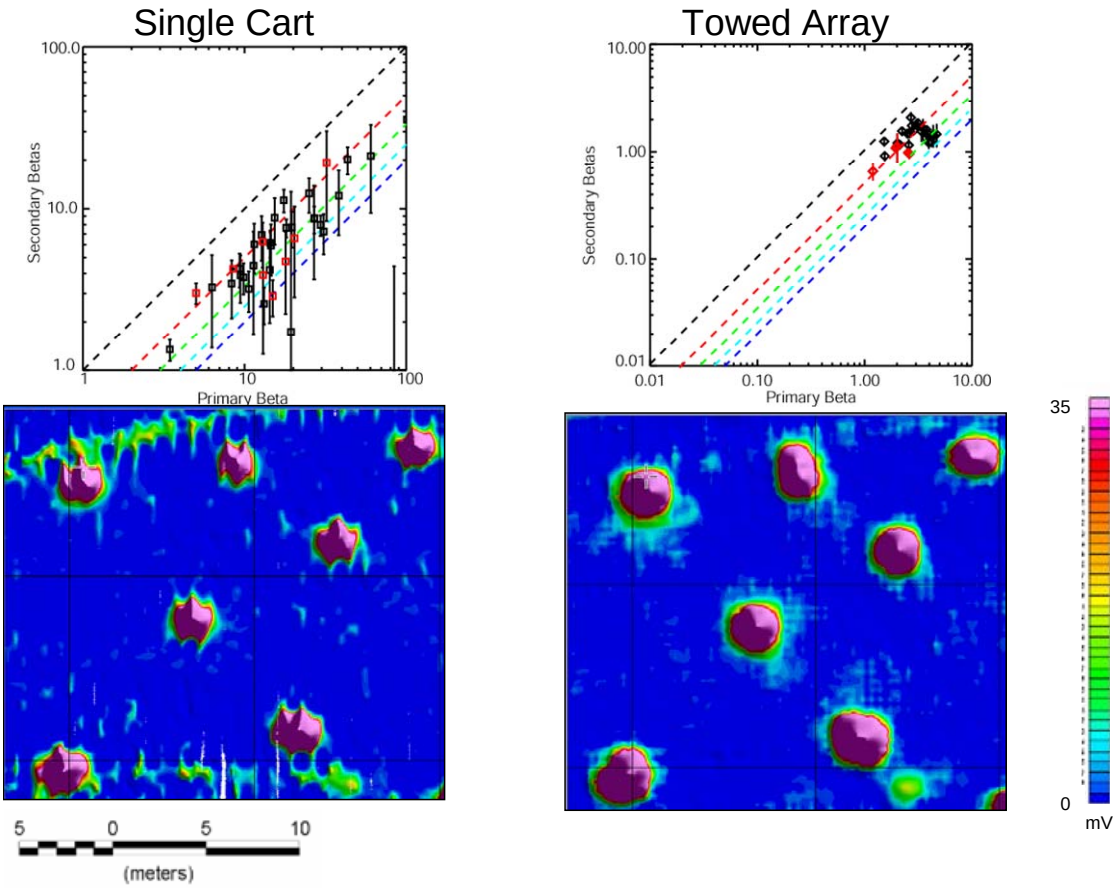

Figure 5-4 EM61 MK2 data from the geophysical prove out area for the cart (bottom left) and array (bottom right). As observed in the fitted results (top), the array produced a tight clustering of polarizations (black is UXO and red represents half shells) but the cart did not. To fix this problem, we added a time lag parameter to the cart solver.

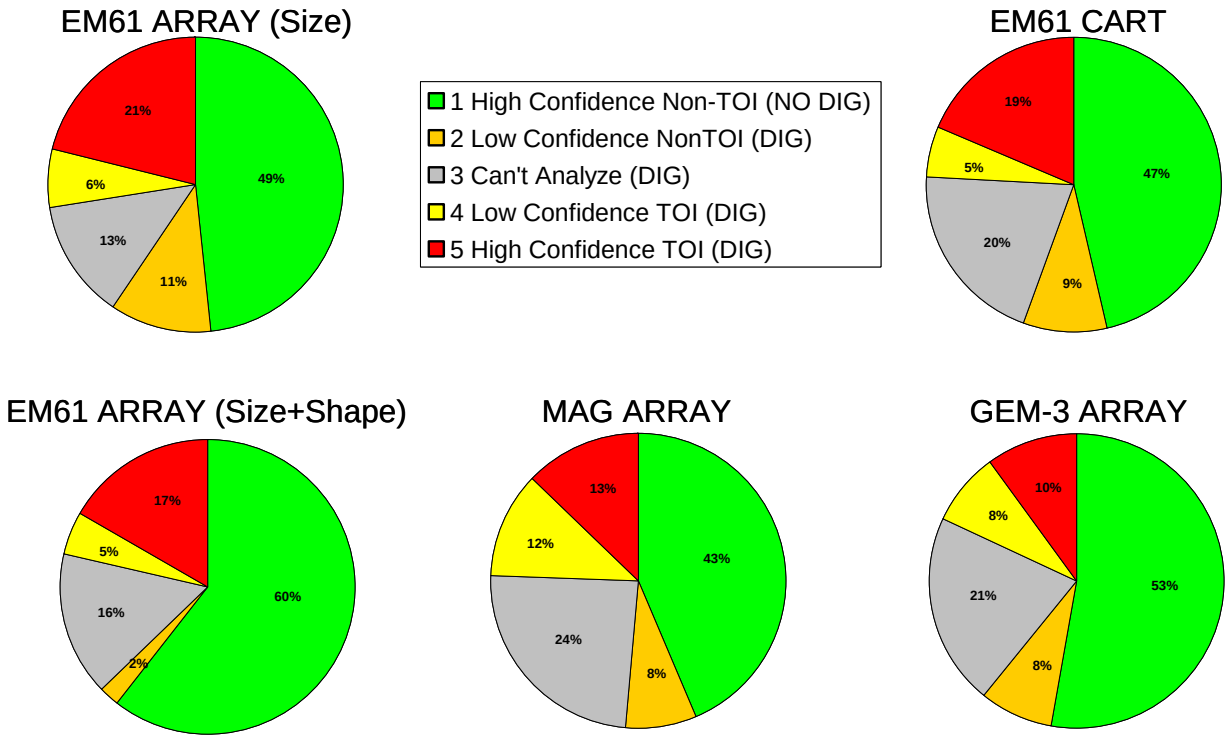

Figure 5-5 Comparison of classification results

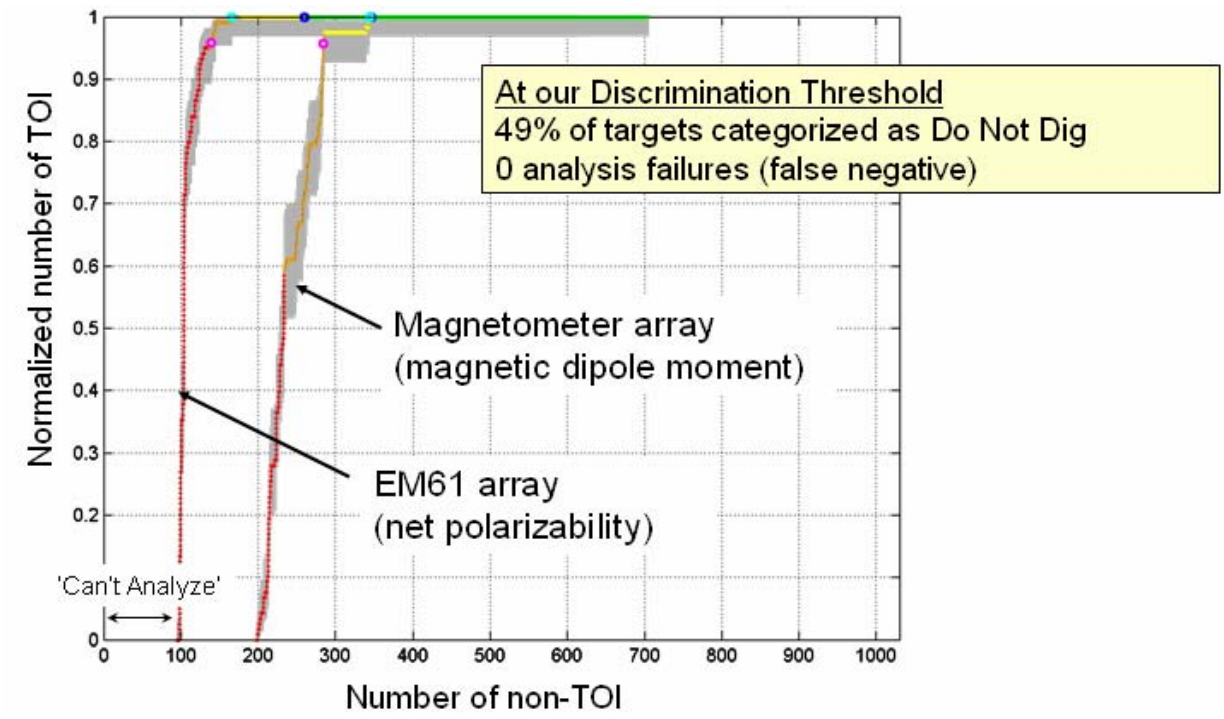

Figure 5-6 Performance comparison of size based classification for magnetic and EMI array data

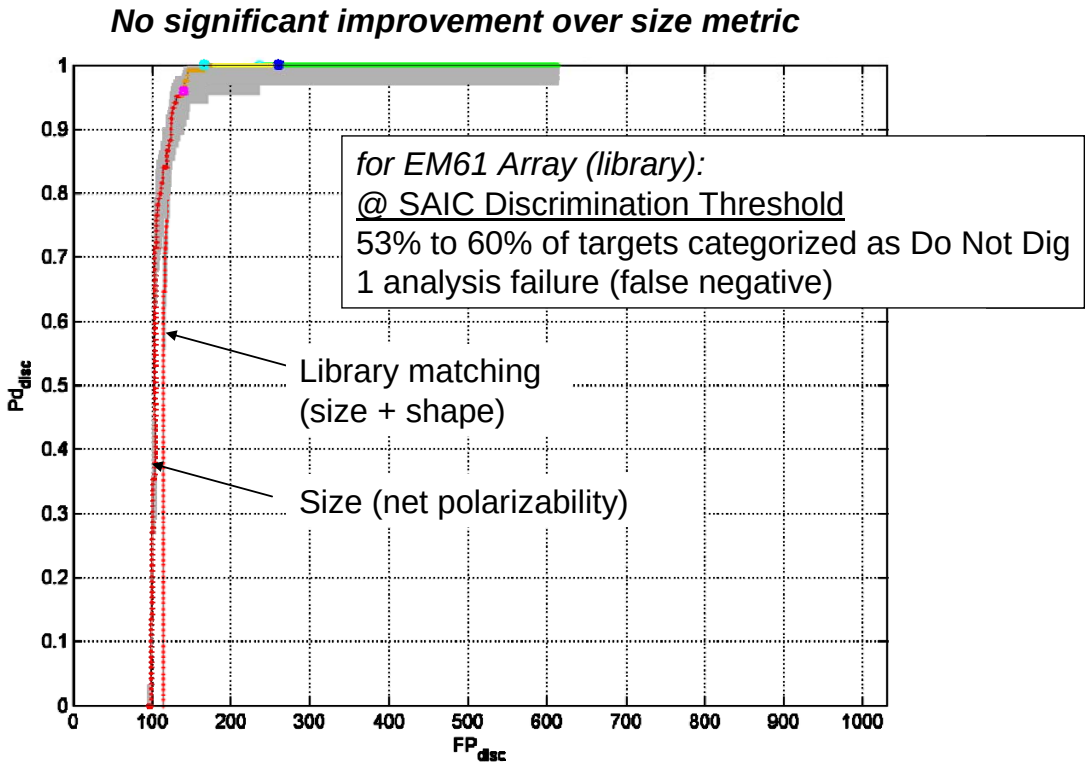

Figure 5-7 Performance comparison of size- versus library-based classification for EMI array data

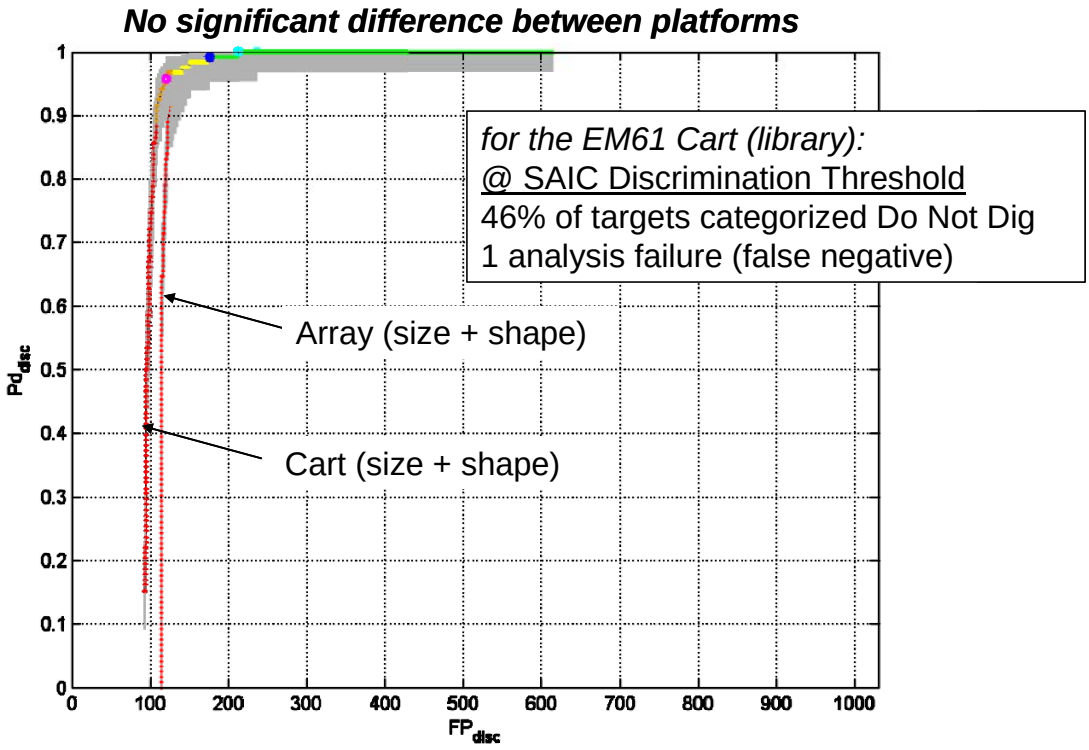

Figure 5-8 Performance comparison of cart versus array EMI data

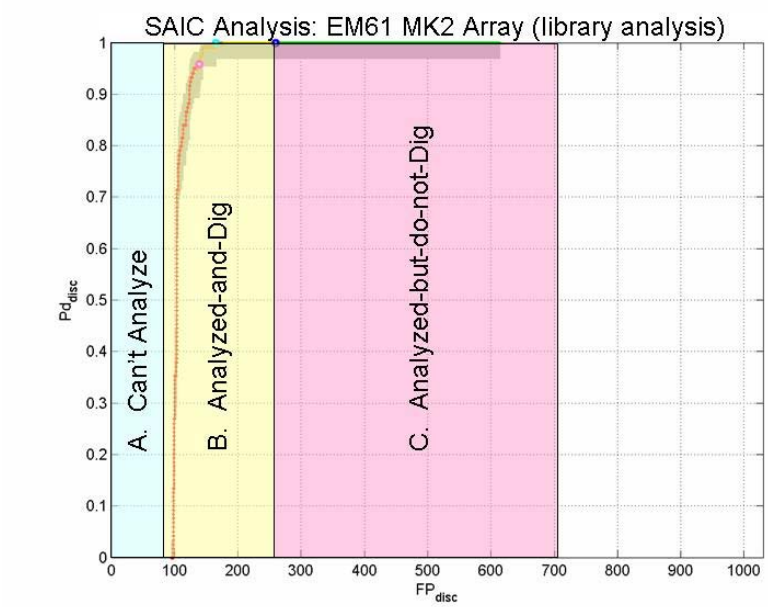

Figure 5-9 The ROC curves can be divided into three conceptual domains

- bad GPS positions
- system timing errors
- data acquisition system limitations

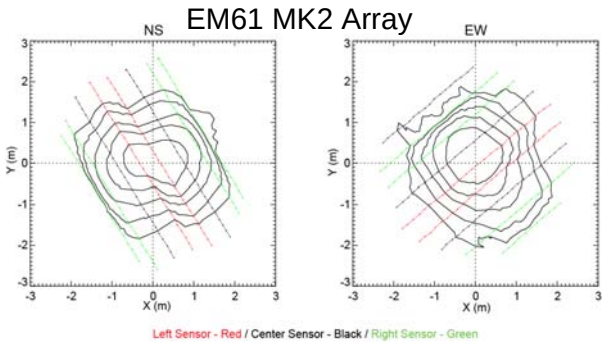

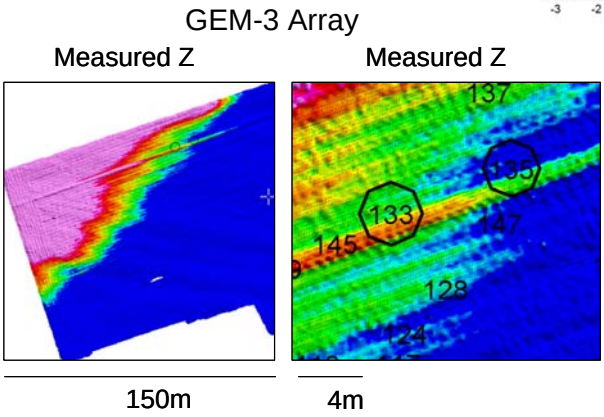

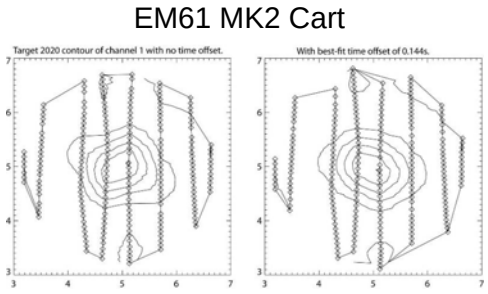

Figure 5-10 A post mortem failure analysis revealed that sources of analysis errors were caused primarily by GPS errors

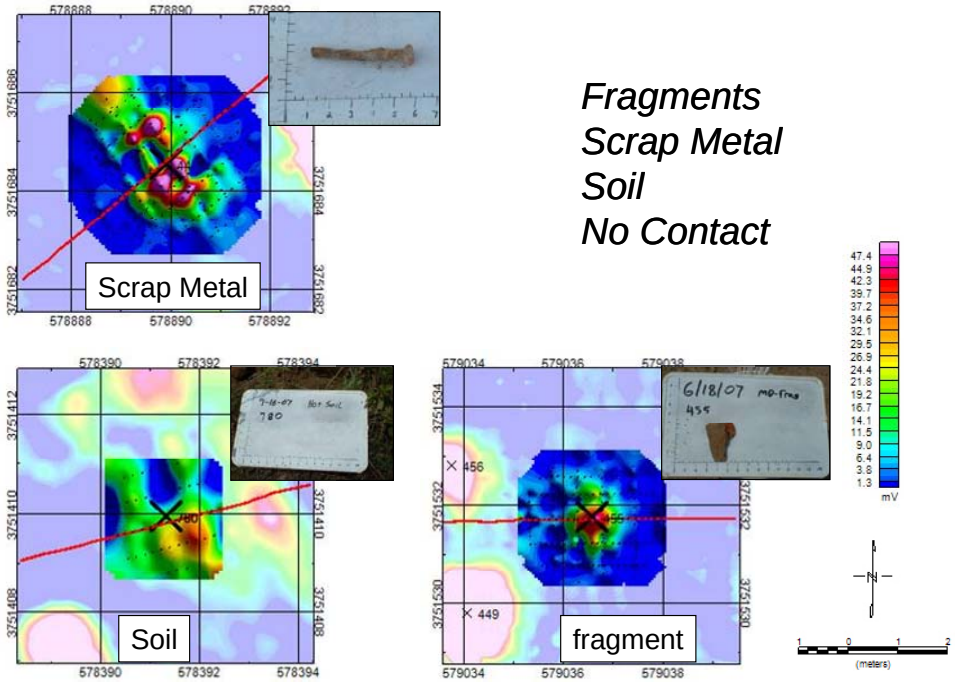

Figure 5-11 Example EMI anomalies classified Can't Analyze (Category 3)

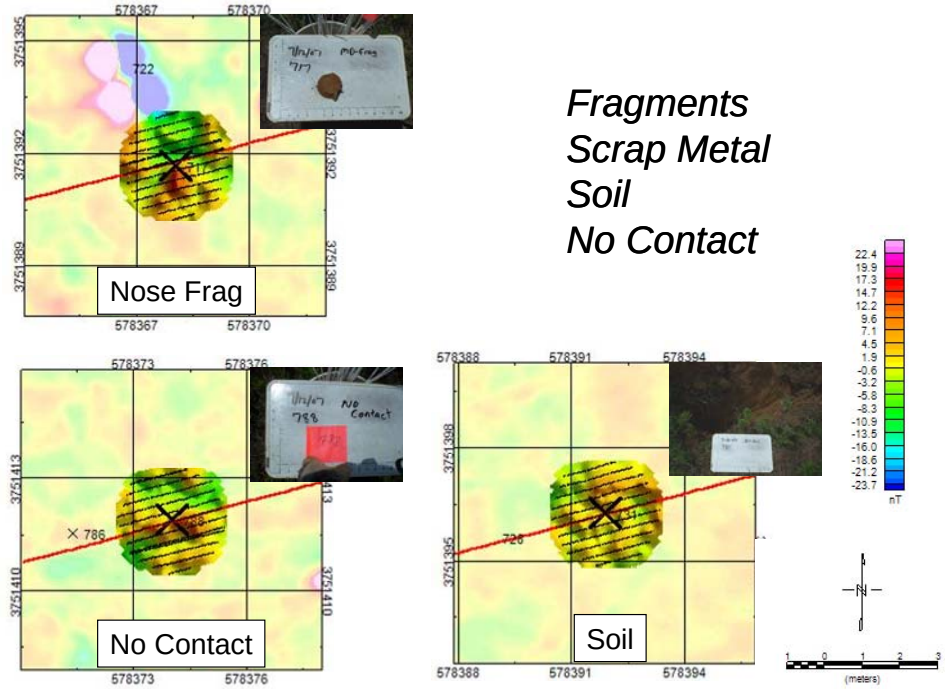

Figure 5-12 Example magnetic anomalies classified Can't Analyze (Category 3)

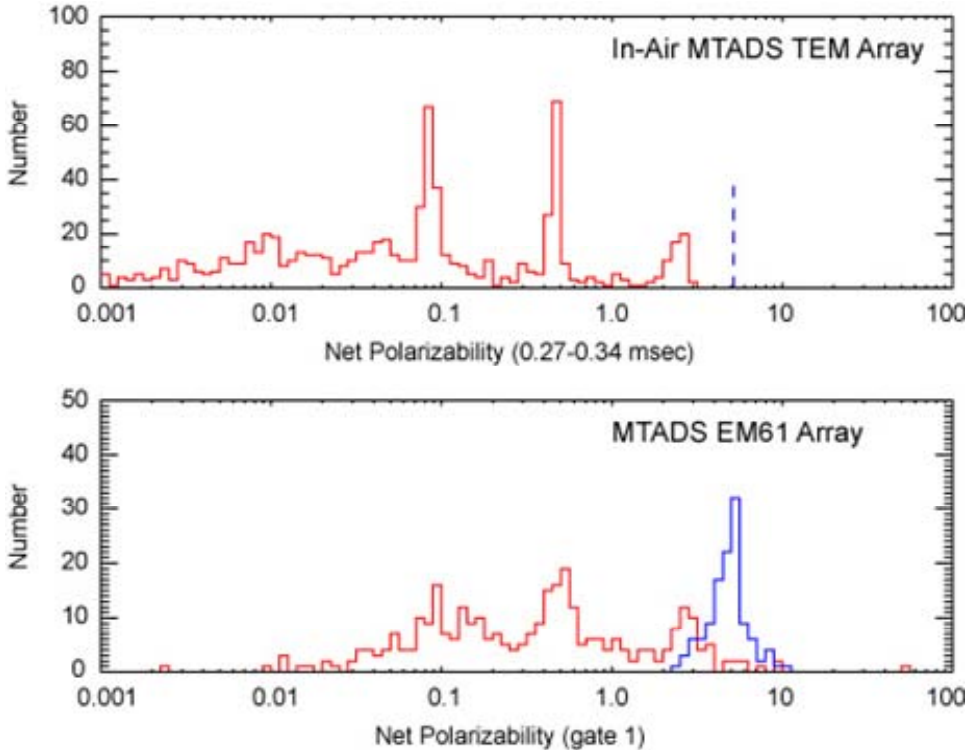

Figure 5-13 Net polarizabilities for in-air versus EM61 array field data

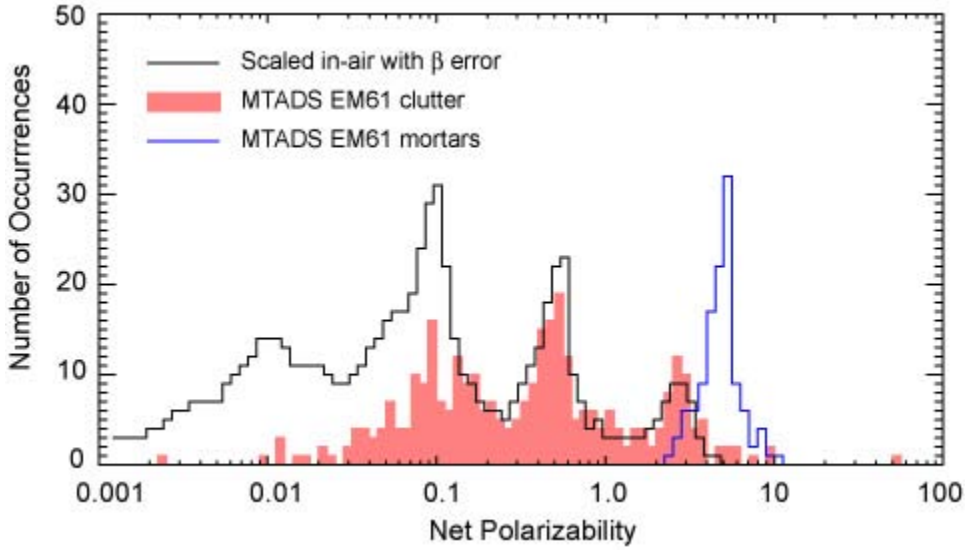

Figure 5-14 After accounting for b spread, the in-air and EM61 array field data have similar distributions for net polarizabilities > 0.1.

6. Cost Assessment

6.1 Cost Reporting

Cost categories for the overall ESTCP Discrimination Pilot Program include mobilization, field survey, data analysis, demobilization, and reporting. Cost categories for this data analysis demonstration are data analysis and reporting.

The data analysis phase consists of a number of distinct and sequential operations. The operations include pre-processing, anomaly extraction, characterization (inversion), classification, and documentation. The hours and costs were tracked throughout the demonstration and are shown in Table 6-1. The reported costs assume an average labor rate of $115 per hour.

The magnetic array data required the fewest number of hours and lowest cost per target. The EM61 Cart data required more pre-processing than the EM61 array data because it was collected in a number of small grids with overlapping turns instead of large sorties without overlaps and because the organization of the delivered data required more manipulation than did the array data. TheEM61 array data analyzed with our IDL solver required more time during the characterization phase than that required by UX-Analyze because the IDL routine does a much more thorough job of avoiding local minima and has numerous restarts and significantly more logic loops.

Table 6-1 Cost Summary

Cost Summary	Hours	Cost	Number of Targets	Cost per Target
Pre-Demo Testing Prep	650	$ 74,750		
EM61 Cart	108	$ 12,420	671	$ 18.51
MAG Array	66	$ 7,590	1007	$ 7.54
GEM-3 Array	94	$ 10,810	1077	$ 10.04
EM61 Array (UX-Analyze)	84	$ 9,660	908	$ 10.64
EM61 Array (IDL Solver)	126	$ 14,490	908	$ 15.96
Demonstration Report and Meetings	300	$ 34,500		
Total	1428	$ 164,220	4571	

6.2 Cost Analysis

6.2.1 Cost Basis

The cost basis for this demonstration is the labor hours spent characterizing, classifying, and documenting the discrimination results.

6.2.2 Cost Drivers

The primary cost driver for this technology is the amount of time spent processing and interpreting each anomaly. If targets are isolated, leveled, and of high data quality then the cost is driven by inversion times and time spent making the classification decision. If a lot of preprocessing is required to identify spatial footprints, to remove turnarounds, to recognize database problems, or to re-level the data, then the cost is driven by these later factors and the inversion time becomes much less important. For the most part, the data collected at Sibert had anomalies that were isolated.

7. Implementation Issues

7.1 Regulatory and End-user Issues

The ESTCP Program Office established an Advisory Group to facilitate interactions with the regulatory community and potential end-users of this technology. Members of the Advisory Group include representatives of the US EPA, State regulators, Corps of Engineers officials, and representatives from the services. The ESTCP staff worked with the Advisory Group to define goals for this Program and developed Project Quality Objectives. As the analyzed data from the demonstrations become available, the Advisory Group assisted in developing a validation plan.

8. References

1. “Report of the Defense Science Board Task Force on Unexploded Ordnance,” December 2003, Office of the Under Secretary of Defense for Acquisition, Technology, and Logistics, Washington, D.C. 20301-3140, http://www.acq.osd.mil/dsb/reports/uxo.pdf.

2. "Shape-Based Classification and Discrimination of Subsurface Objects Using Electromagnetic Induction," Thomas H. Bell, Bruce Barrow and Nagi Khadr, Proceedings of the International Geoscience and Remote Sensing Symposium, Seattle, Washington, July 6-10, 1998.

3. "Model-Based Characterization of EM Induction Signatures for UXO/Clutter Discrimination Using the *MTADS* Platform," Bruce Barrow and H. H. Nelson, Proceedings of the UXO Forum 1999, Atlanta, Georgia, May 25-27, 1999.

4. *Electrodynamics of Continuous Media*, L. D. Landau and E. M. Lifshitz, Pergamon Press, New York, 1960.

5. *Detection and Identification of Visually Obscured Targets*, C. E. Baum (Ed.), Taylor and Francis, Philadelphia, 1999.

6. Bell, T., 1997, “Looking for a perfect match: Model-based characterization fits data to UXO signatures,” Ordnance and Explosives Environment, 4(2), April-June 1997, p. 5.

7. Barrow, Bruce and H. H. Nelson, 1998, “Collection and Analysis of Multi-Sensor Ordnance Signatures with MTADS,” Journal of Engineering and Environmental Geophysics, 3(2), 1998, pp. 71-79.

8. Won, I. J., Dean A. Keiswetter and Thomas H. Bell, 2001, “Electromagnetic Induction Spectroscopy for Clearing Landmines,” IEEE Transactions on Geoscience and Remote Sensing, 39(4), 2001, pp.703-709.

9. Barrow, Bruce and H. H. Nelson, 2001, “Model-Based Characterization of EM Induction Signatures Obtained with the MTADS EM Array,” IEEE Transactions on Geoscience and Remote Sensing, 39(6), 2001, pp. 1279-1285.

10. Bell, Thomas H., Bruce J. Barrow and Jonathan T. Miller, 2001, “Subsurface Discrimination Using Electromagnetic Induction Sensors,” IEEE Transactions on Geoscience and Remote Sensing, 39(6), 2001, pp. 1286-1293.

11. Bell, Thomas, Bruce Barrow, Jonathan Miller and Dean Keiswetter, 2001, “Time and Frequency Domain Electromagnetic Induction Signatures of Unexploded Ordnance,” Subsurface Sensing Technologies and Applications, 2(2), 2001, pp. 152-175.

12. DiMarco, R. and B. Barrow, 1996, “A Comparison of Magnetic Survey Methods,” UXO Forum 1996.

13. Nelson, H., 2003, “Frequency-Domain EMI Sensor Array for Use with MTADS,” SERDP/ESTCP Symposium & Workshop - Partners in Environmental Technology.

9. Points of Contact

ESTCP

Anne Andrews	Program Manager, MM	Tel: 703-696-3826 Fax: 703-696-2114 anne.andrews@osd.mil
Katherine Kaye	Program Assistant, MM	Tel: 410-884-4447 Fax: 703-478-0526 kkaye@hgl.com

SAIC

Dean Keiswetter	Project Lead	Tel: 919-653-0215x103 Fax: 919-653-0219 keiswetterd@saic.com
Tom Bell	Quality Assurance Officer	Tel: 703-413-0500 Fax: 703-413-0512 Thomas.H.Bell@saic.com
Jonathan Miller	Data Analyst	Tel: 703-413-0500 Fax: 703-413-0512 millerj@saic.com
Bruce Barrow	Data Analyst	Tel: 703-413-0500 Fax: 703-413-0512 barrowb@saic.com
Tom Furuya	Data Analyst	Tel: 919-653-0215x104 Fax: 919-653-0219 furuyat@saic.com